Search for anomalies in cosmic air showers measured with the Surface Detector of the Pierre Auger Observatory

von

Anna Friederike Nelles

Diplomarbeit in Physik

vorgelegt der
Fakultät für Mathematik, Informatik und Naturwissenschaften
der
Rheinisch-Westfälischen Technischen Hochschule Aachen

im April 2010

angefertigt am

III. Physikalischen Institut A

Erstgutachter und Betreuer

Prof. Dr. Thomas Hebbeker
III. Physikalisches Institut A
RWTH Aachen

Zweitgutachter

Prof. Dr. Martin Erdmann
III. Physikalisches Institut A
RWTH Aachen

Contents

List of Figures

Outline

Studying cosmic air showers has been a fruitful field of particle physics for about a century. Since the discoveries of Victor Hess and Pierre Auger many experiments have tried to clarify details about origin, composition and propagation of cosmic rays. One of the most recent experiments is the Pierre Auger Observatory in Argentina, whose data has been the basis of this work.

This diploma thesis aims at providing a model-independent approach towards the study of cosmic air showers. According to the current understanding extensive air showers are caused by atomic nuclei accelerated to the highest energies by astrophysical objects. However, in recent literature various theoretical models predict cosmic air showers to be caused by particles not predicted by the Standard Model of Particle Physics or to produce such exotic particles in interactions in the shower development. Since the variety of propositions is too large to check each model independently, this thesis follows the idea to systematically search for any kind of significant deviation from the expectations given by the Standard Model. Thereby events will be identified that are interesting for further model-dependent studies.

The approach itself and its applications are described in the first chapter of this thesis. In order to follow such a model-independent approach it is necessary to have an overview of the current models of cosmic air showers, which is given in the second chapter. Exotic Models are shortly touched upon but since the approach is model-independent the models are not discussed in depth. Afterwards, the relevant characteristics of the detector are described as well as the chain of reconstruction used by the Pierre Auger Collaboration. Having covered this, different aspects of model-independent approaches and their results are explained. Possible deviations are studied in the geometry of air showers, chapter 5, in the characteristics of stations rejected by the reconstruction, chapter 6, and in the quality of the reconstruction algorithm itself, which is presented in chapter 7. Following this, the thesis is concluded by summarizing the results and discussing points of further interest.

1. Introduction and Methodological Approach

At the Pierre Auger Observatory extensive air showers induced by cosmic rays of energies up to 10^{20} eV are measured. These air showers are the consequence of interactions of primary particles and atomic nuclei at energies that no collider experiment has been able to reach so far, thus offering opportunities to search for *new physics* in the data-set. Concerning this new physics it is hard to keep track of all theories. Over the years of studying cosmic air showers various models have been developed about what physical effects or yet unknown particles could possibly be observed at energies this high. Giving an overview of all theories already proves difficult. In order to reduce the number of theories possible, each theory has to be ruled out by experimental evidence. All models have to be tested independently in order to exclude them or at least set limits on their validity. For some even this cannot be done since the predicted signatures would not differ from extensive air showers according to the current understanding.

Given the amount of models it is quite possible to overlook a new effect when testing each model independently. There is certainly not enough capacity to really test each model. What models are tested depends on many factors and not always the most promising ones are tested. One could even say that sometimes the ones that are most *fashionable* are tested. Furthermore, there might be new physics that has not been predicted at all. Consequently, a model-independent search could be a solution to prevent the omission of features that lead to an exotic signature.

The idea to use a model-independent approach in such a situation is certainly not new. In many experiments at colliders model-independent approaches were and are used to look for new physics, for instance at Tevatron [1], [2], at HERA [3] or at LEP [4]. The methods might be different in detail but the general approach is always similar. Starting from all known particle interactions an expected signature for an experiment is calculated, mostly based on Monte Carlo simulations. This expectation is then compared to the measurements of a detector. By means of mathematical methods deviations between the two distributions can be found. In other words, they identify a signal in the background of known interactions and are therefore independent from model-predictions for new signals. Some of those searches have indeed reported deviations according to their model-independent expectation [5]. However, new physics could afterwards not be confirmed so far by a specific model-dependent search. New results of a model-independent analysis are expected from the CMS detector at the LHC [6].

In experiments concerning cosmic air showers, however, model-independent searches were never prominently applied, probably due to the fact that there is not yet a complete and profoundly understood model of the nature of cosmic rays comparable to the Standard Model of Particle Physics. Literature suggests that one is well on the way to establish a Standard Model of Cosmic Rays [7], but not all aspects are yet agreed on. Details of this common understanding will be discussed in chapter 2.

After all, model-dependencies are an issue in air shower and cosmic ray physics. Especially in questions of an absolute calibration of energies of air showers or the estimation of the composition of the primary particles by means of Monte Carlo simulations, model dependencies influence the results. Concerning these aspects the dependency on models cannot be eliminated soon. Also, overall model-independent approaches prove to be not easily applied and are currently not prominently used in experiments concerning cosmic air showers.

So what could a model-independent approach look like concerning the data of the Pierre Auger Observatory? A model-independent approach will always look for deviations in the data from an expectation. As a standard model of cosmic air showers is yet to be completed, features need to be found that are well understood and required for the standard approaches with respect to all uncertainties. From those features a standard expectation can be defined. This is obviously not comparable to a full Monte Carlo simulation of the predictions, which is not yet available in cosmic rays physics, but it should be able to identify crucial features.

As will be discussed in chapter 2, there are certain features that can be considered to be necessary for all air showers to have. There is first of all a certain compactness in position and timing needed for an event to even be considered an air shower. Furthermore, the lateral spread of particles from an air shower will always show similar characteristics. Starting from these general features, one can go further into detail and define criteria of quality that will describe a *standard shower* and that will enable us to distinguish any *non-standard shower*. This is, of course, an iterative process as long as defining the standard has not been completed. This iterative idea will be followed throughout this thesis.

Such a model-independent analysis will first of all lead to a better understanding of the data and the detector. Usually most deviations will be due to effects caused by either the detector or the reconstruction. These effects need to be identified, studied and included in the model of expectation. After all major technical effects have been excluded, deviations possibly existing in physics will be found. The more precise the expectation is the better the limit on the deviations will be that can be found.

Still, one has to keep in mind that having found non-standard showers is not equal to a discovery of any kind. A deviation can only hint at events that need to be carefully checked. It is well possible that a deviation will again lead to an identification of not fully understood effects of the detector itself or incorrect predictions resulting from the Standard Model. A model-independent approach will only identify classes of events that are interesting for model-dependent searches. Re-checking those classes with searches that are optimized for a certain signature will enable to set limits

on respective models. This ensures that more models will be tested to explain an effect than would have been tested if only model-dependent approaches had been conducted. Therefore a model-independent approach is a tool to find not completely understood events of possibly new physics, as well as a cross-check or control mechanism to identify whether the data and its reconstruction are well understood.

2. Cosmic Rays

Cosmic Rays are particles that reach the earth from outside the earth's atmosphere. There is a flux of many kinds of particles. Overall there are ionized atoms, neutrinos, electrons, positrons and of course photons, not listing all possibilities. Even though the first cosmic radiation was already discovered in 1912 many characteristics are still subject to intense research.

The energy spectrum of cosmic rays reaches over many decades of energy up to about 10^{20} eV with a decrease in flux following a power-law. The Pierre Auger Observatory has been built in order to increase information about cosmic rays at the highest energies. In this energy regime above 10^{18} eV cosmic rays are often referred to as *Ultra High Energy Cosmic Rays*, UHECR. Due to the very low flux there is not yet a complete picture about the origin and propagation of these cosmic rays as their detection is experimentally challenging. So far UHECRs have only been

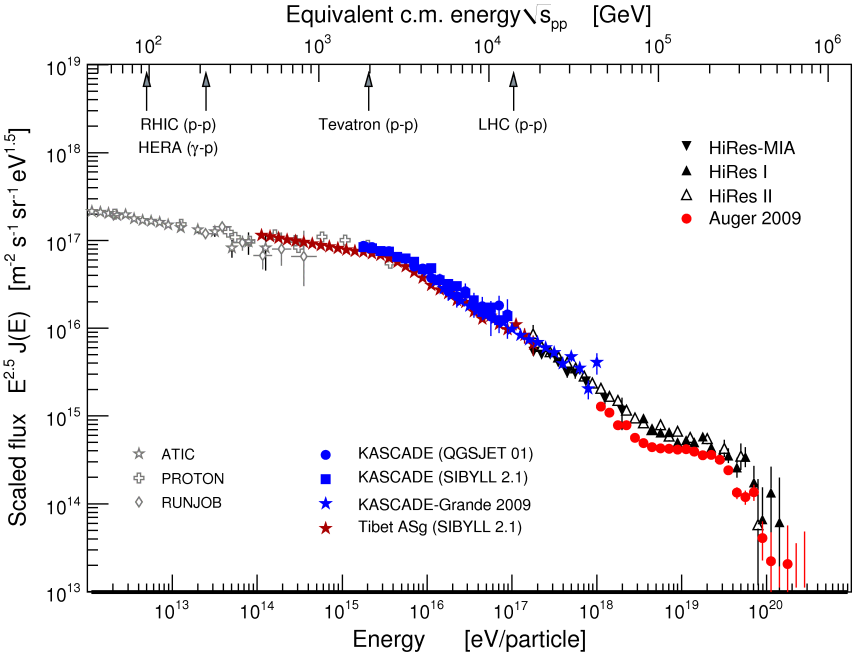

Figure 2.1: Spectrum of highest energy cosmic rays as measured with different experiments. The gray markers represent direct measurements of flux above the atmosphere, while the other data was taken at ground level. The energies are compared to energies from recent collider experiments. Update from [8]

measured by detecting the results of their interactions in the atmosphere, thus they have never been detected directly. In figure 2.1 some of the latest results of the flux at high energies are presented. The figure shows that flux decreases according to a power spectrum $dN/dE \propto E^{\gamma}$. At the characteristic steepening, *the knee* at 10^{15} eV the spectral index changes from -2.7 to -3.1. At even higher energies further features in the spectrum can be observed, usually referred to as the *ankle region*. The reasons for these changes in the spectral index might be a change in composition or change of sources.

In this chapter the current knowledge about UHECRs will be presented. Standard models will be described as well as alternative approaches touched upon in order to gain some insight into the current development.

2.1 The Origin of Ultra High Energy Cosmic Rays

The existence of Ultra High Energy Cosmic Rays (UHECR) has been a controversial field of study. As their flux is very low large detectors are required to measure even a few events per year. Earlier cosmic ray detectors were small and reported only one or two events in this energy regime. Also, it has been and still is largely unknown what mechanisms can create particles of such high energies. After having studied UHECRs for some time now it was agreed on something like a Standard Model of Cosmic Rays. Especially in regimes of lower energy this model describes the data quite well. Still, one has not yet agreed on a model for the origin of the particles having the highest energies. The most common models describe the particles as iron or hydrogen nuclei, *Hadronic Cosmic Rays*, but there are also models that claim that cosmic rays at these energies can only originate from yet unknown particles, therefore we speak of *Exotic Origins* [9].

2.1.1 Hadronic Cosmic Rays

In lower energy regimes it is known from direct measurements that Cosmic Rays are mostly fully ionized atoms. Their composition corresponds to the composition of the matter in the universe and they are accelerated in stars and their dynamic magnetic fields [10]. At higher energies the picture is no longer this clear. If we consider also UHECRs to be ionized atoms the first question that arises is what mechanisms and sources can accelerate the particles to these energies.

Charged particles are accelerated in electromagnetic fields. As not all is yet known about the galactic magnetic fields and magnetic fields in astrophysical objects many discussions about sources of acceleration have to be based on theories. It is believed that in objects such as supernova remnants, radio galaxies or active galactic nuclei magnetic fields of large strength and shock waves exist that are able to accelerate charged particles to the necessary energies [11]. In the shock acceleration (2nd order Fermi acceleration) particles interact with the magnetized diffuse shock fronts in and around astrophysical objects and gain energy. A dimensional argument can be established that relates the characteristics of such an astrophysical object to the

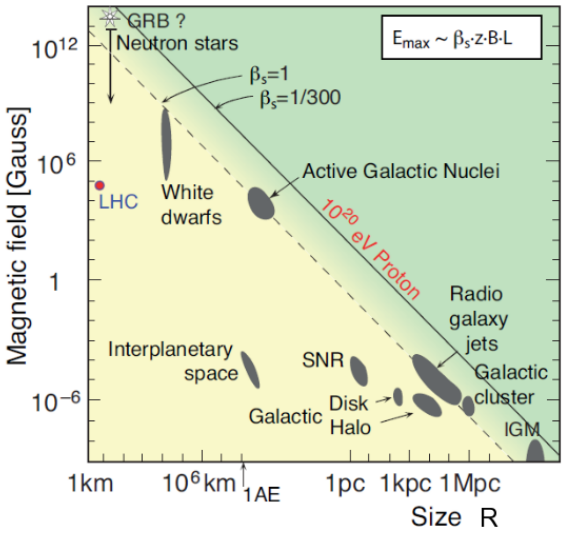

Figure 2.2: This plot shows an overview of the possible sources of acceleration of UHECRs. On the axes the strength of the magnetic fields and the size of the source are given as they determine the maximum energy. Different maximum energies are indicated by lines through the plot. This plot is often referred to as the "Hillas Diagram", adapted from [8, 13]

energy a particle can gain from it [12]. The following equation therefore constraints the possible sources:

$$\left(\frac{B}{\mu G}\right)\left(\frac{R}{kpc}\right) = 2\left(\frac{E}{10^{18}eV}\right)\frac{1}{Z\beta} \tag{2.1}$$

The magnetic fields B of an object need to be strong enough to confine the particle within its circumference with radius R. Furthermore, the characteristic velocity βc of the shocks that scatter the particles defines the ability to accelerate particles to the highest energies E. This restriction leaves only some candidates for the acceleration of UHECRs [7]. A graphical interpretation of equation 2.1 is shown in figure 2.2.

It can therefore be concluded that there are only few possible types of sources of hadronic UHECRs. Adding to this, the cosmic rays have to propagate from their origin to the earth through intergalactic space. It has been discussed whether an energy loss could prevent the particles from reaching the earth being still at the highest energies. Shortly after the discovery of the Cosmic Microwave Background Radiation (CMB) it was pointed out that cosmic rays would interact with the photons and lose energy. At a threshold energy of 10^{18} eV pair production is enabled.

$$p + \gamma_{CMB} \longrightarrow p + e^+ + e^- \tag{2.2}$$

The protons as cosmic rays will lose about 0.1% of their energy per interaction.

At a threshold of about $10^{19.6}$ eV the additional process of photo-pion production will set in, which will result in a loss of energy of up to 20% per interaction.

$$p + \gamma_{CMB} \longrightarrow \Delta^+ \longrightarrow p + \pi^0 \tag{2.3}$$
$$\longrightarrow n + \pi^+ \tag{2.4}$$

The latter effect is known as the *GZK-cutoff* as proposed by Greisen, Zatsepin and Kuzmin in 1966 [14, 15].

Therefore it is predicted that almost no cosmic rays should be measured at energies above this energy. However, if there are sources of UHECRs in close distance to the earth an observation could be possible. If cosmic rays are heavier nuclei those will be photodisintegrated into protons during propagation. As iron is the element with the highest nuclear binding energy, it will be the heaviest component of the cosmic rays from the standard model. Concerning propagation, only iron nuclei could propagate longer distances at the highest energy due to their lower gamma factor. Still, the propagation distance is limited. [16]

The knowledge about the galactic and extragalactic magnetic fields which will influence the propagation of UHECRs is also incomplete. The strength of the galactic field is reasonably well established by measurements in certain regions. The overall structure, however, is still under debate. Most of the knowledge about the magnetic field of our galaxy is based on observations of other galaxies. Overall, it is agreed that the magnetic fields will not be able to restrain particles of this energy within our galaxy and that UHECRs must be of extragalactic origin, if there are no sources very close to the earth [17].

Thus, according to the current standard model, UHECRs consist of iron nuclei or protons that have been accelerated in extragalactic objects and propagate through the interstellar medium towards earth.

2.1.2 Exotic Origins

In contrast there are lots of theories that suspect UHECRs to be caused by other particles, mostly unknown and undiscovered, thus referred to as *Exotics*.

The number of theories for more exotic candidates is vast. Some less exotic models claim UHECRS to be neutrinos (ν) or photons (γ). In models of acceleration in astrophysical objects neutrinos and photons are often taken into account. It is known that supernovae emit neutrinos. In addition, Gamma-ray Bursts (GRB) have been observed that emit spectacular amounts of γ in a very short time. Those two astrophysical objects have also been considered for the acceleration of hadronic UHECRs. Thus ν and γ are possible candidates.

Furthermore, it is argued that neutrinos from very distant sources might annihilate with relic neutrinos at the Z-resonance. This would lead to *Z Bursts* that could be observed as extremely high energy cosmic rays. An observation of such bursts will limit the mass of relic ν and could explain events above energies of 10^{20} eV [18].

The main principle of theories known as top-down scenarios for air showers is the claim that an unknown very heavy particle instead of a light but very highly accelerated particle will interact with the earth atmosphere and cause an air shower. Alternatively, such a particle might decay in the vicinity of earth into very high energetic particles from the Standard Model. The characteristics of these theoretical particles are individually very different.

As cosmologists have argued that the universe needs to consist of a large amount of yet unknown *dark matter* many theories concerning this phenomenon have been developed. Dark matter will only interact weakly and has never been observed directly, but due to cosmological constraints on the expansion of the universe and the gravitational behavior of galaxies there is strong evidence for its existence [19]. From those theories it has been deduced that so called *Super heavy dark matter* (SHDM) should also be able to cause extensive air showers. SHDM is expected to be found everywhere in the galaxy, with a high density in the galactic halo. As the earth traverses through the galaxy particles will interact with nuclei from the earth's atmosphere [20].

Another model for cosmic rays has been derived from cosmology. It is believed that the Big Bang at the beginning of the universe should have left very heavy relics. In the symmetry-breaking phase transitions in the early universe so-called *Topological Defects* could have formed, which are stable until they are disintegrated in a collapse or an annihilation [21]. This will result in very massive X particles that can decay into known particles. Thus, when such a decay takes places near earth it could look like an extensive air shower. Examples for models describing such defects are cosmic strings or magnetic monopoles [22].

Also in the early universe small *Primordial Black Holes* (PBH) with masses well below the self-gravitational collapse limit may have formed. As discussed also in collider physics numerous processes compatible with standard cosmological scenarios and standard particles can explain their formation. If such a PBH evaporated it could produce a cascade of particles at a 10^{20} eV threshold, thus again looking similar to a cosmic air shower from standard model particles [23].

The theory of supersymmetry also offers alternative explanations for UHECRs. Even though there is no direct evidence for the existence of supersymmetric particles it is one of the theories that is hoped to be confirmed at the Large Hadron Collider (LHC). If for example the *Minimal Supersymmetric Standard Model* (MSSM), which is the minimal extension to the Standard Model, is confirmed, the number of possible particles will more than double [24]. Due to the yet unexplained and partly inconsistent observations of UHECRs many groups proposed supersymmetric particles to cause the extensive air showers. As it is unknown but proposed to be the cause of air showers, such a supersymmetric particle was named U, *UHECRon* [25]. It is argued that is has to be strongly interacting, due to the structure of showers that have been observed. Also, it has to be stable or at least long lived and very massive as it has never been detected in collider experiments. Furthermore, it is likely to be neutral as it then would not be affected by the Cosmic Microwave Back-

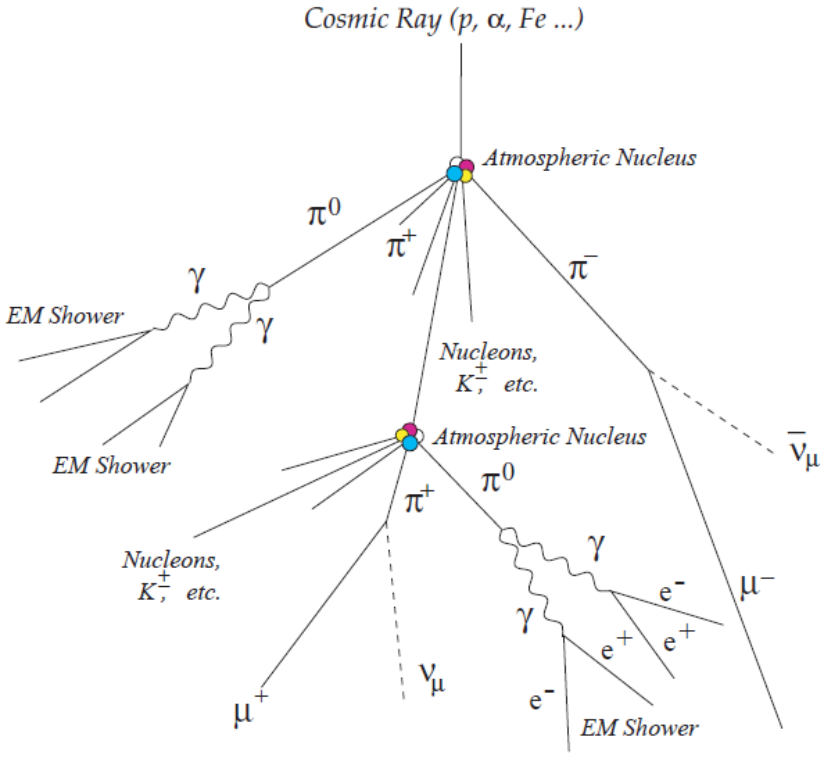

Figure 2.3: The schematics of an air shower caused by a primary hadronic particle. Hadronic subshowers as well as electromagnetic subshowers are shown. Adapted from [28]

ground (CMB). As the possibilities of forming such a particle in supersymmetry are manifold many different signatures and reactions could be possible [26].

Many of these models have in common that the theoretical particles will decay with a typical signature. These signatures often include large amounts of photons and neutrinos, which are searched for in model-dependent searches.

Lastly, it should be mentioned that the confirmed results concerning the nature of cosmic rays will set limits on a lot of other theories, such as Lorentz violation [27] in the development of showers at the highest energies.

2.2 The Development of Cosmic Air Showers

As already discussed UHECRs have never been detected directly. Only the products of their interaction with the earth's atmosphere can be measured. Even if the primary particles are part of the Standard Model of Particle Physics, the relevant interactions at energies this high have never been explored at collider experiments. Therefore there is quite some uncertainty about the development of an air shower and what reactions, even exotic ones, might take place.

2.2.1 Standard Model Air Showers

An air shower contains many interactions of particles from the reactions of the primary cosmic ray with atomic nuclei of the atmosphere. In the first interaction a primary particle will scatter inelastically with an atom in the atmosphere, e.g. a nitrogen atom. The atomic nuclei will fragment at these energies and pions $\pi^+, \pi^-$and π^0 will be produced. As shown in figure 2.3 the neutral pions will then form an electromagnetic cascade consisting of electrons e^-, e^+ and photons γ. The charged pions will form a hadronic cascade; interacting again with other nuclei, generating kaons, protons and other hadrons and finally decaying into muons μ^+, μ^- and neutrinos $\nu_\mu, \bar{\nu_\mu}$.

The process of a hadronic particle interacting in the atmosphere can be described in an analytic *Heitler Model* [29], [30]. The thickness of the atmosphere is converted into splitting lengths that are related to radiation lengths of electrons and interaction lengths of pions. It is found that the maximum size of a shower is proportional to the primary energy and that the depth of the shower maximum also depends on the primary energy. Also, the number of muons from a shower will be about 25 times as high as the number of electrons at sea level.

The model can be further refined by using full Monte Carlo simulations estimating the particle content of the shower at ground level. However, since many effects such as the fragmentation rates and the pion multiplicity are not yet fully understood, the simulations cannot make exact predictions. Air shower experiments have in fact contributed to the improvement of simulations of hadronic interactions by measuring the particle content of showers with regard to the energy of the primary particle [31].

2.2.2 Exotic Models concerning the Shower Development

As the energies of primary cosmic rays have not yet been reached in collider experiments, there is a lot of space for theories to predict yet unknown particle reactions in air showers. In fact, reactions that are expected to take place in the LHC should also take place in the first interactions of an air shower. Interesting for the shower development are only those reactions that could create a signature that will be visible in the particle content at ground level. Any non-standard particle that will decay with no significant signature into particles from the standard model will not be detectable at ground level. Knowledge about such reactions could contribute to better understand the shower development but will itself not be obtained in air shower experiments.

Some reactions are thought to produce a significant signature, thereby influencing the form and characteristics of an air shower. An example of such a signature can be caused by *Mini Black Holes*. In general scenarios that claim a TeV-scale gravity, ultra high energy cosmic neutrinos will produce black holes in the earth's atmosphere, leading to anomalously large rates for quasi-horizontal hadronic showers. Also, a signature known as *double-bang* i.e. a second cascade in an air shower, is considered to be possible from reactions producing mini black-holes. How distinct such a second bang could be depends on a lot of parameters characterizing such a model [32, 33].

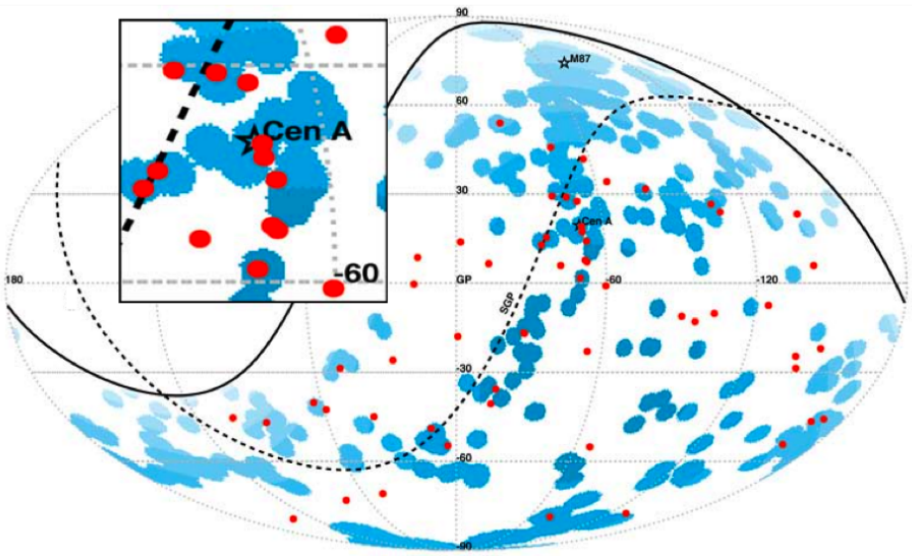

Figure 2.4: The figure shows an Aitoff projection of the celestial sphere in galactic coordinates. The red dots indicate events above 55 EeV that have been measured with the Pierre Auger Observatory. The blue areas are possible sources from the VCV catalogue. The strength of the blue colour is drawn according to the exposure of the detector. Taken from [34]

2.3 Results from the Pierre Auger Observatory

The Pierre Auger Observatory was built in order to gain further knowledge about the nature of UHECRs and extensive air showers. As data has been taken since 2004 there are already results constraining certain models of UHECRs.

The energy spectrum obtained with the combination of Surface and Fluorescence Detector shows a strong suppression of flux above the energy of $4 \cdot 10^{19}$ eV at a confidence level of 20σ [35]. This supports the hypothesis of the GZK-cutoff that has been predicted for high energetic particles as a result of interactions with the cosmic microwave background. Still, the effect could also be related to a change of the shape of the average injection spectrum at the sources of cosmic rays [36].

Furthermore, information on the mass composition of the air showers has been gathered. By comparing the depth of the shower maximum as measured with the Fluorescence Detector with predictions from Monte Carlo simulations one is able to draw conclusions concerning the mass composition. Usually showers from heavier primary particles will develop higher in the atmosphere. In general the measurements do not agree with neither a composition of purely protons nor purely irons. But there is the tendency that the mixed composition contains more iron the higher the energy of the shower is [37].

Concerning the origin of UHECRs many studies have been conducted. The most prominent is a comparison of the arrival directions of Auger events with an energy above 55 EeV with known positions of Active Galactic Nuclei (AGN) from the Veron-Cetty-Veron (VCV) catalogue [38]. Of 44 events 17 are correlated with objects from

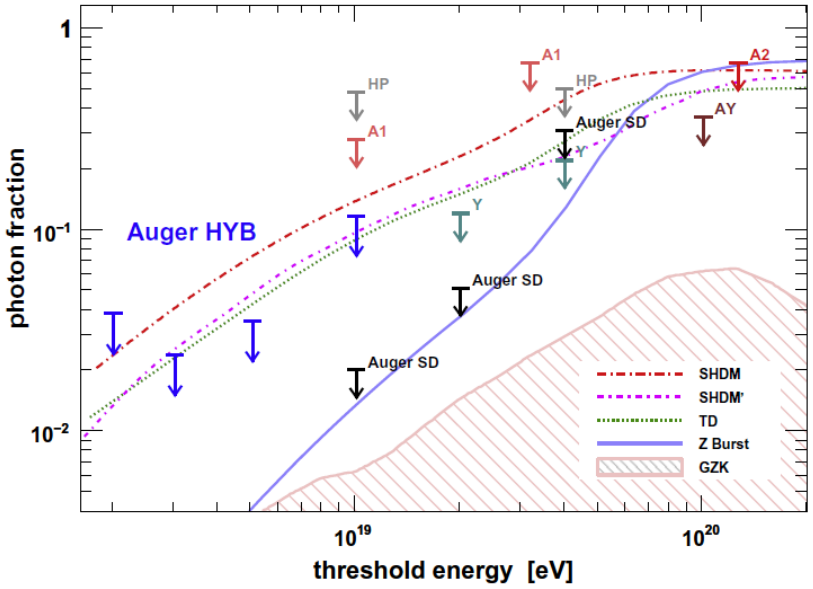

Figure 2.5: Shown are the limits that have been obtained concerning the photon content of UHECRs. The fraction of photon showers is plotted against the threshold energy. As many exotic scenarios require a high photon content this also limits models such as Super Heavy Dark Matter (SDHM), Topological Defects (TD) and Z Burst. Some photon content is expected from GZK processes. Taken from [39].

the VCV catalogue, which has a probability of less than 1% to occur by chance if the events were part of an isotropic distribution. Especially an excess was measured in the region of Centaurus A, which is a dense region of possible sources. It has to be noted that the VCV catalogue does not contain a complete list of all possible sources. Overall it has been concluded that more data is needed in order to make further progress in identifying the sources of UHECRs [34]. The events and their arrival directions are shown in figure 2.4.

The Pierre Auger Collaboration has also set limits on the more exotic models. Many top-down scenarios for UHECRs require a relevant fraction of UHECRs to be photons, γ. By setting limits on the γ-fraction some models could already be excluded as shown in figure 2.5. Therefore models that require a large amount of γ seem unlikely according to the most recent results [41].

Also limits on the diffuse flux of ultrahigh energy neutrinos, ν_τ, have been obtained [40]. The results are shown in figure 2.6. The most recent upper limits have almost reached the predicted flux of GZK-ν that is expected from the decay of pions from the GZK-effect. Therefore, exotic models requiring decays into ν_τ have become less likely.

By identifying that the arrival directions of UHECRs are anisotropically distributed and establishing correlations with astrophysical objects all top-down scenarios for UHECRs have become less likely. Nevertheless, it has to be kept in mind that it is assumed that for example dark matter follows the general distribution of matter in the

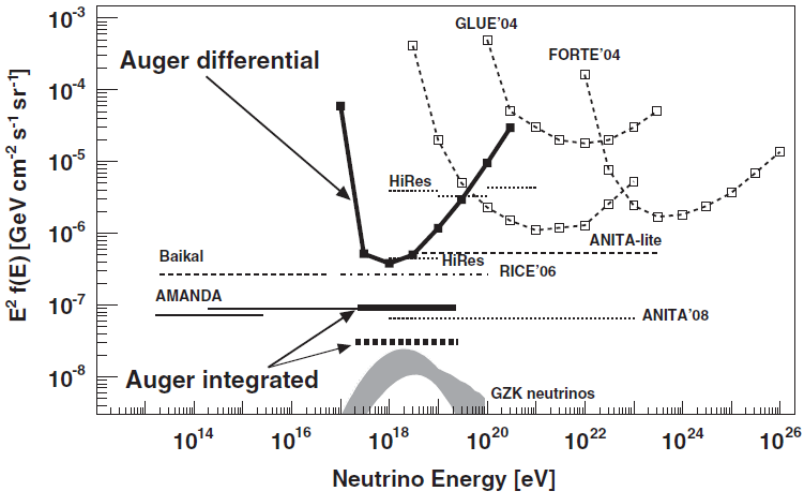

Figure 2.6: The upper limits for the diffuse flux of tau neutrinos are shown. The excluded flux scaled with the energy is plotted against the energy of the neutrino. The solid lines represent the worst case concerning systematic uncertainties. Similar to the expectation about photons, some flux is expected to originate from GZK processes. Taken from [40].

universe. As more possible astrophysical sources are also found in regions of higher density of matter a correlation does not necessarily exclude top-down scenarios.

Therefore it can be concluded that some progress has been made to increase our knowledge about UHECRs. But as there are still open questions about the origin and the nature of these particles further investigations will have to be pursued.

3. The Pierre Auger Observatory

The southern part of the Pierre Auger Observatory is located in the province of Mendoza in Argentina. Near the city of Malargüe the Observatory covers an area of over 3000 km^2. The Observatory consists of different detectors, all aiming to study cosmic air showers of energies above 10^{17} eV. Its location on the southern hemisphere provides a field of view that includes the galactic center. A second site is planned to be built on the northern hemisphere in Colorado, USA.

The Observatory combines different techniques to detect cosmic air showers. This enables a cross-calibration between the experimental methods and therefore offers the unique opportunity to gain further knowledge of cosmic rays. One of the main parts of the Observatory is the Fluorescence Detector that detects the fluorescence light of nitrogen particles excited by particles from a cosmic air shower in the atmosphere. The second important part is the Surface Detector, which is an array of about 1600 water-Cherenkov detectors that directly measure secondary particles from the cascade of a cosmic air shower. In addition, there are different further experiments and enhancements to the Observatory that will exploit both improved and new techniques of air shower detection.

3.1 The Fluorescence Detector

The Fluorescence Detector (FD) consists of four sites named Los Morados, Coihueco, Loma Amarilla and Los Leones, each equipped with six telescopes overlooking the

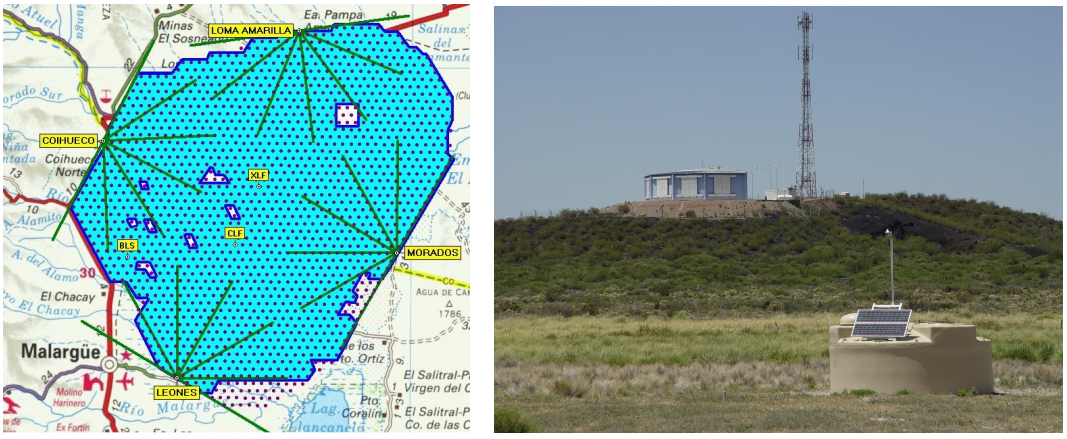

Figure 3.1: The Pierre Auger Observatory, Geographic Location and View of Detector

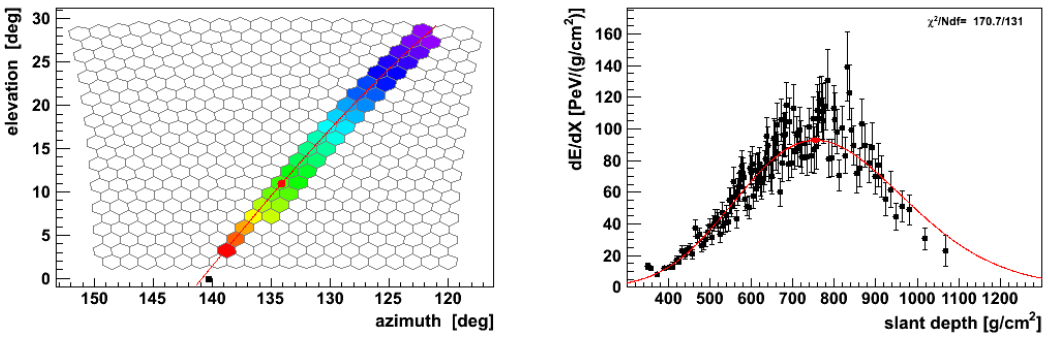

Figure 3.2: Illustration of Event 6834623 recorded with the Fluorescence Detector. The left side shows the trace of triggered pixels on the telescope. The timing information is coded in color. On the right side the profile of the shower is depicted. In units of atmospheric depth the energy loss is drawn, which shows the development of the shower in the atmosphere. In the regime of the highest energy loss, near 750 g/cm^2 the shower reaches its maximum.

array of the Surface Detector. This method of detection allows to observe the path of the air shower in the atmosphere by means of the ultra-violet fluorescence light emitted by de-exciting nitrogen molecules. Detecting cosmic air showers by their fluorescence light has the advantage that the atmosphere can be used in a calorimetric way. For a shower to reach the ground it has to cover about eight hadronic interaction lengths and 20 radiation lengths, thereby losing a large amount of its energy. The number of photons emitted by the nitrogen molecules is proportional to the energy loss of the shower. The conversion factor *fluorescence yield* is well known from laboratory measurements. Thus, the FD measurements provide quite accurate measurements of the energy of the shower [42].

The fluorescence light is collected with 24 Schmidt telescopes. Every telescope is equipped with 440 photomultiplier tubes (PMTs), each having a field of view of 1.5° per pixel. This results in an overall field of view of about 30° x 30° per telescope and 180° x 30° for each of the four telescope sites as depicted in figure 3.1. In each telescope the light is collected by a spherical mirror with an area of 12 m^2 after having passed an only UV-transparent aperture. An example of an event detected by the FD is shown in figure 3.2.

Since it is a prerequisite for the exactness of the measurement to detect all and only the fluorescence light, the FD can only operate in cloudless and moonless nights. Therefore it has a duty-cycle of only 13%. Also, a continuous monitoring of the weather is neccessary. The light detected depends on the atmospheric conditions, for instance pressure or temperature. Also aerosols in the atmosphere can lead to additional scattering of the light before it can be detected. In general the FD is not completely robust against environmental influences, which are therefore carefully measured and considered in the reconstruction of FD events.

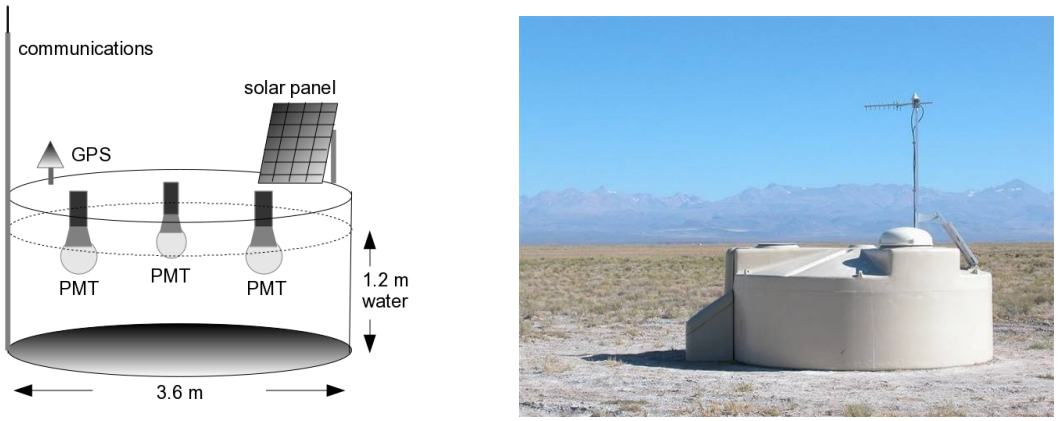

Figure 3.3: The left side shows the schematics of a Surface Detector station as shown on the right side.

3.2 The Surface Detector

The Surface Detector (SD) operates almost independently from environmental conditions, thus having a duty-cycle of 100%. It consists of a hexagonal grid of water-Cherenkov detectors with a spacing of 1500m. Each station is designed to detect particles from the cascade of a cosmic air shower. The minimum energy needed for a shower to be detected with the SD is about 10^{18}eV. Above these energies the flux of cosmic rays is expected to be much smaller than one shower per square kilometer per hour. Therefore such a large detector is needed to gain sufficient statistics.

3.2.1 Detection Mechanism

Particles traversing with a speed higher than the speed of light in the respective medium emit *Cherenkov light*. In a certain energy regime the Cherenkov light emitted by a particle is directly proportional to its track length [43]. As discussed in chapter 2 air showers consist mainly of muons, electrons and an hadronic component. The muons from the shower are in fact in this energy regime and consequently the Cherenkov light can be used for detection. The electromagnetic component of the shower only emits certain amounts of Cherenkov light, thus can be detected but their signal cannot be directly converted.

The particles of the shower also emit Cherenkov light in the atmosphere, which can also be used by the Fluorescence Detector. The threshold energy that a particle needs to have in order to emit Cherenkov light depends on the refraction index n of the media and it is $E_{th} > \sqrt{1 - 1/n^2}$. As the refraction index for water is $n = 1.33$ as opposed to air having only $n \approx 1.0003$ the Cherenkov effect is more distinct in water since the threshold is a lot lower. Furthermore, enclosed detectors have a full 24-hour duty-cycle, which is the main advantage of the Surface Detector.

As the SD is only able to sample the particle content of the shower on the ground the energy of the shower cannot be measured directly. There is only a rough correlation between the number of particles measured in SD stations on the ground and the

energy of the primary particle. Therefore a cross-calibration between the FD, which is believed to enable a rather accurate energy measurement, and the SD is used [44]. Air showers measured in both detectors are known as *Hybrid events*. For an event to be a Hybrid it does not need a full reconstruction in both detectors. Those events are called *Golden Hybrids* and are used to define a calibration procedure. Without this calibration, measurements of the energy from the SD would have to rely on Monte Carlo simulations for the particle content on the shower, which introduces large uncertainties.

3.2.2 Electronics, Communications

Every local station of the Surface Detector is able to operate and detect secondary particles completely autonomously. It consists of a 1.5 m high cylindrical tank with a base of 10 m^2 filled with purified water. The 12 m^3 of water are contained in a Tyvek^{TM} liner to prevent any form of contamination that might affect the well-known characteristics of the water. The Cherenkov photons that are emitted by particles from an air shower crossing the tank are detected by three photomultiplier tubes (PMT), Photonis XP 1805PA/1. The signals of these PMTs are read out by 10 bit Flash Analog to Digital Converters (FADC) at a rate of 40 MHz. Thus each bin of the FADC has a width of 25 ns and consists of 0-1032 channels. An example of signals measured as a FADC trace is shown in figure 3.4.

The signal data from a shower is sent by the local station on request to the Central Data Acquisition System (CDAS). This will only take place in a predefined time slot [45]. As shown in figure 3.3 every station is equipped with a radio unit for data-transmission and its own energy supply via a solar panel and a battery. A GPS unit enables a precise timing information for every event. The array of the SD is divided into four areas of communication, i.e. every station belongs to a predefined communication tower to which the data is transmitted. The communication towers are located near the position of the FD buildings.

3.2.3 Trigger

The local station does not send every recorded signal to the CDAS. Due to atmospheric muons a high background is expected. In order to reduce the rate of data transmitted to CDAS to events of high energy, every station has a programmable logical device installed to implement the first hardware based triggers. The signals are measured in units of VEM, Vertical Equivalent Muon, which are equivalent to the light deposited by a central vertically through-going muon. This is a common unit for air shower experiments. The method of calibrating the signal in this unit will be discussed in detail in section 4.

The first trigger level which is implemented, called T1, can be achieved in two ways; the Time-over-Threshold (TOT) and the Threshold trigger (Thr). The TOT requires 13 FADC bins out of 120 to have measured signals higher than 0.2 VEM in coincidence of two PMTs. Alternatively, a three-fold coincidence of PMTs with a signal of 1.75 VEM is needed, which is adequate for horizontal air showers (Thr). All events that have passed the TOT criteria are then directly promoted to the second

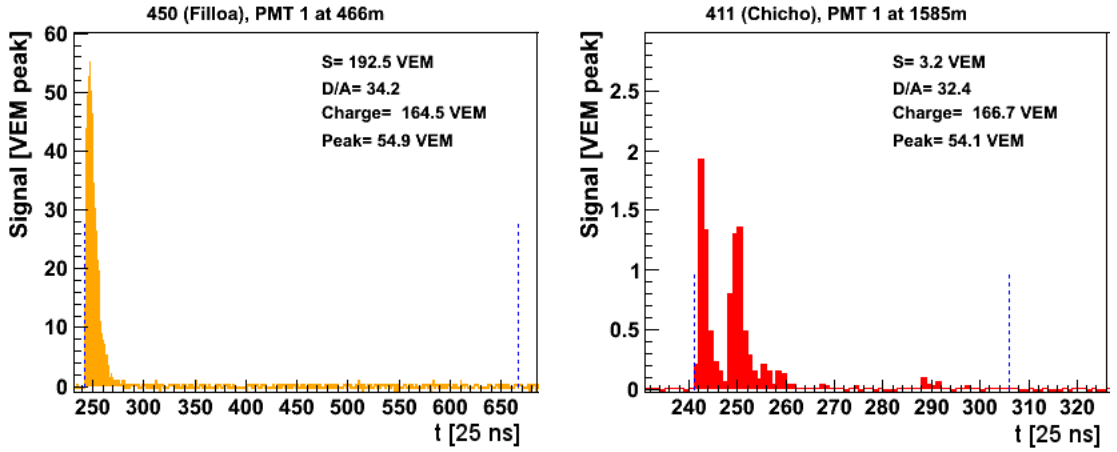

(a) Station closest to shower core **(b)** Station in some distance to shower core

Figure 3.4: An example of signal traces belonging to event 1915292. Shown are the entries of the Flash Analog to Digital Converter (FADC) bins calibrated in Vertical Equivalent Muons (VEM). A signal in a station close to the shower core is dominated by large entries caused by the muonic and electromagnetic component of the shower. Therefore individual particles cannot be distinguished. Further out, single muons can be identified.

trigger level T2. For the signals having meet the Thr criteria an additional three-fold coincidence of 3.2 VEM is needed in order to be promoted to T2. The arrangement of the triggers is affected by hardware needs. The usage of those first two triggers reduces the rate of events to about 20 Hz per station, which can be handled by the communication devices of the stations.

The stations constantly send all T2 triggers to the CDAS where subsequently a third trigger level T3 is formed. It is tested whether a coincidence of 3 stations all having sent a TOT can be found within a time window of 60 μs. Of those stations two have to be neighbours while one can be a second closest neighbour. Again there is an alternative especially implemented for rather horizontal showers. It requires a four-fold coincidence of stations with any type of T2 within a maximum distance of six kilometers.

If a valid T3 is formed, CDAS sends a request to every station in a distance of up to nine kilometers from the T3 to read out and transmit the data. On this request the stations send the necessary information in a predefined time slot. In detail 768 FADC bins are read out, whereas 100 bins are before the trigger to enable baseline and background studies. T2 that have not formed a T3 are stored for a short time on the local disk but are removed once new T2 signals are recorded [46].

This entire trigger mechanism determines the energy limit of the detector. Since a shower has to be detected in at least three stations with a signal of more than 1.75 VEM, it needs to have a certain energy to be spread as far as the area between three stations. Due to the hexagonal grid this energy limit depends on the exact position of the shower core and thus the distance to the next station. A shower hitting in

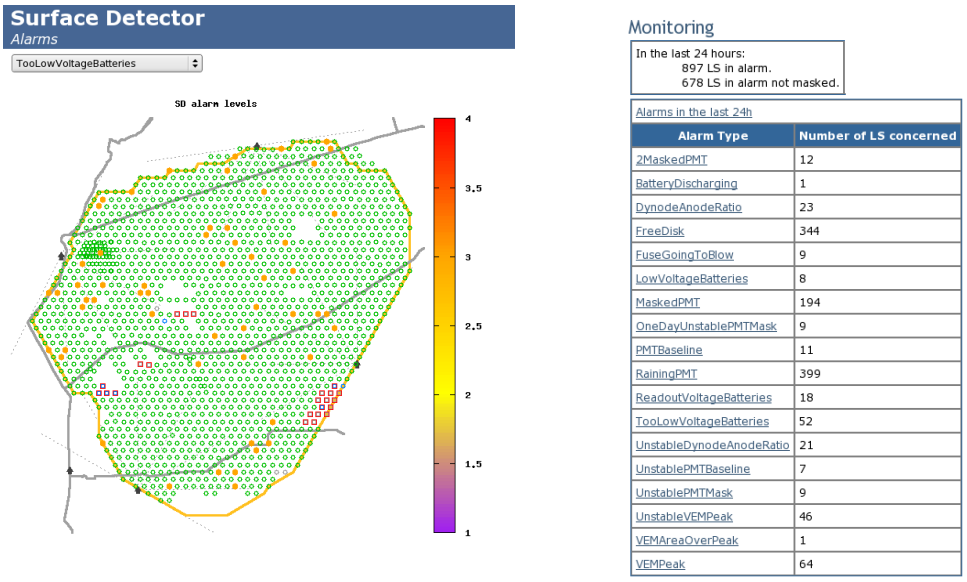

(a) Array Alarm Overview **(b)** Alarm History

Figure 3.5: Exemplary data from the Auger monitoring system for the Surface Detector. In a database every single station as well as the entire array can be called and the alarm signals and errors can be viewed. All maintenance conducted is also recorded; taken from [48]

between three stations has a higher probability to be detected than a shower that is centered on a station. At about $3 \cdot 10^{18}$ eV the Surface Detector has an efficiency near 100% [47].

3.2.4 Monitoring

While the Fluorescence Detector needs an intense atmospheric monitoring to guarantee a good quality of data as well as technical monitoring, the Surface Detector is more or less independent from environmental conditions. It only requires little environmental monitoring and technical monitoring, but the latter in a non-negligible amount. As the Surface Detector has been built in a continuous process since 2004, it was most important to keep track of which station was active and taking data. Once a station is active it has to be monitored whether it keeps on being fully functional.

For this purpose every 10 minutes all stations send monitoring data, including information about batteries, the PMTs, disk space etc. to CDAS, which is then stored in an extensive database. All issues concerning the hardware are marked and will be followed up by the local technicians. The CDAS also monitors the amount of T2 triggers sent by the station. In case of a considerable decrease in triggers the station is also marked as there could be an unidentified issue that could corrupt the data. If at a period in time too many issues occur, this period will be flagged as *bad period*. Data from this period will not be used for calculations of flux, spectrum and other analyses that need the full acceptance. Consequently the monitoring database provides a complete overview of the performance of each local station [49].

The main environmental monitoring that is needed for measurements with the SD is the monitoring of temperature and pressure. Since the density of the atmosphere influences the spread of the shower and thus the trigger probability, these effects have to be accounted for. Overall a 10% seasonal modulation of the event rate is observed, mostly affecting the low energy range [50]. Monitoring this effect and implementing it into the reconstruction improves the energy systematics of the SD.

3.2.5 Further Development

The spacing of 1500 m of the Surface Detector has the advantage that a huge area can be covered at a reasonable sampling rate. Still, this spacing sets a limit on the lowest energy detectable as a minimum of three stations have to be triggered in order to be able to reconstruct the event and showers of lower energy have a smaller lateral spread than this distance. Consequently, reducing the spacing will reduce the energy limit. This is done in the so called *Infill*. Additional 23 stations were deployed, each in between two existing stations from the Surface Detector, thus reducing the spacing of the grid to 750 m. This lowers the energy threshold to about $3 \cdot 10^{17}$ eV, which is about a decade lower than the regular SD limit. The measurements with the infill can help to further understand the lateral distribution of particles from the air showers on the ground, as a higher sampling rate produces more detailed information [51]. Especially near the core of the shower the lateral distribution is largely unknown.

The additional stations are deployed in combination with buried muon counters as part of the AMIGA extension (Auger Muons and Infill for the Ground Array)[52]. Those counters will also increase knowledge about the distribution of particles on the ground, especially the muon content of the shower since buried counters will no longer measure the electromagnetic content of the shower as it has been stopped in the ground above the counter.

3.3 Further Extensions

In general, there is a unique opportunity to develop and install further detectors for extensive air showers in combination with the regular detectors at the Observatory. Using different techniques to measure the same shower enables to cross-calibrate and improve the knowledge about detection techniques and the shower itself.

The High Elevation Auger Telescope (HEAT) uses the same technique as the FD. The main difference is the field of view. The HEAT telescopes can be tilted and therefore cover a field of view above the regular FD telescopes. Showers of energy below the acceptance of the FD telescopes are known to develop higher in the atmosphere and will therefore be detectable by the HEAT telescopes [53]. Due to the tiltable construction the telescopes are also able to measure in coincidence with the regular FD telescopes and hence offer the opportunity to develop new detection methods for FD telescopes.

Furthermore, it is possible to detect cosmic air showers by the pulse-shaped electromagnetic signals that the charged particles within the shower emit in the earth's

magnetic field. For this purpose the AERA (Auger Engineering Radio Array) is currently deployed at the southern site of the Observatory. After having successfully tested this detection method with a small set-up in 2006 in coincidence with the Surface Detector, 160 antennas will soon be able to further exploit the possibilities of detecting cosmic air showers in the radio frequency band [54].

4. The Reconstruction of Events from the Surface Detector

The data of the Surface Detector as well as the Fluorescence Detector is collected by the Central Data Acquisition System (CDAS). CDAS collects only data that fulfilled certain trigger levels that are implemented in the hardware. As described in section 3.2.3 for the Surface Detector these are the trigger levels T1 and T2, which reduce noise and identify signals from more than one particle. CDAS forms the third trigger level (T3), which aims to identify compact correlated signals in more than one station. Events that meet those three trigger levels are processed in the data analysis [46].

A continuous monitoring has been established to keep track of possible hardware or software issues concerning the Surface Detector. The basic information is provided with the data set and can therefore be included in the reconstruction. More detailed information as well as the performance of the detector over time has to be obtained from the monitoring database as shown in section 3.2.4.

The general reconstruction of events is by default conducted with two different kinds of software. The CDAS provides its own reconstruction known as *Herald*. Complementary a reconstruction conducted by the software package $\overline{\text{Off}}\underline{\text{line}}$ is used, known as *Observer* [55], [56]. Both reconstructions follow similar routines and are regularly cross checked. In this thesis the $\overline{\text{Off}}\underline{\text{line}}$ is used as provided by the Karlsruhe Institute of Technology (KIT) [57].

This chapter will describe the chain of reconstruction steps with emphasis on the characteristics required for the analysis in this thesis. A complete and detailed description can be found in the $\overline{\text{Off}}\underline{\text{line}}$ Reference Manual [58].

4.1 Signal Processing

First of all, the FADC traces that are obtained from the Surface Detector have to be processed to be used as actual signals in the reconstruction. The traces have to be calibrated and cleaned from all effects that may influence the actual signals measured. Furthermore, the remaining background has to be identified.

4.1.1 Calibration

The Auger Collaboration uses a unit called Vertical Equivalent Muon (VEM) to describe the signals measured in the stations of the Surface Detector. All signals are

measured in VEM to be able to compare different stations and to have a uniform trigger condition. Therefore every station has to conduct an independent calibration of signal into VEM.

For this purpose every station records background caused by the continuous flux of atmospheric muons. Most of the atmospheric muons traverse the tank almost vertically. They provide the possibility for a continuous calibration as the Cherenkov light emitted is proportional to the track length. In detail it is known that the pulse height of the signal as well as the pulse integral is proportional to the Cherenkov light deposited. In a histogram over time both variables show a significant peak, which is closely related to 1 VEM since most of the muons traverse the same length in the station. The correlation between the pulse integral and the charge deposited is more precise than the one between pulse height and peak current, but still both enable a reasonable calibration. As the pulse integral requires more computation it can only be used in the final reconstruction. When working autonomously every station relies on the pulse height histogram [59].

4.1.2 Saturated Signals

For stations that are very close to the shower core it is more complex to measure the actual signal. Especially in case of high energetic and vertical showers the read-out electronics of stations are likely to saturate, thus only an incomplete signal is recorded. The problems are caused by two different effects; saturated FADC recordings of the anode of the PMT as well as the non-linear behavior of the PMTs at high signals.

Fortunately, in some cases a partial recovery of the actual signal is possible due to certain features of the signal. It is expected that the actual signal charge at the anode, respectively dynode, is directly proportional to the undershoot of the signal after saturation. Also, all pulses should follow a certain type of response function that can be fitted. Lastly the non-linearity of the PMTs has been studied and is expected to be invariant for all PMTs over time. These three assumptions have been combined to a method of recovery that is applied to all saturated signals [60]. In some extreme cases a recovery is not possible so only incomplete information from the signal is provided.

4.1.3 Background

As already mentioned there is a nearly continuous background of atmospheric muons, which has to be accounted for. It is quite possible for an atmospheric muon to coincide with a signal from a different air shower. If the muon occurs within the signal of a shower it only causes a fluctuation that is within the signal uncertainty. More problematic is the effect on the timing that such a muon can have since it might change the start and end time of a signal. Therefore an algorithm has been developed to reduce the influence of the muon underground by segmenting the signal and deconvolving it with a muon response function [61]. This *Trace cleaning* is applied to every signal, i.e. FADC trace, before reconstruction and improves the precise estimation of the signal start time.

4.2 Event Selection

Every event that is used has to fulfill certain additional criteria to ensure its quality. A full selection procedure is run on every event.

4.2.1 Flagging of stations

First of all, the event is checked for possible effects of lightning. Lightnings are known to cause signals in the Surface Detector that could be mistaken for an event [62]. But these signals in individual stations usually contain fluctuations below zero and baseline crossings. So entire events are not used if at least one station shows more than 3 baseline crossings in a signal no longer than 1000 FADC bins.

Furthermore, stations that are not fully functional are removed from the data set. Signals from stations from the Infill Array and from Doublets and Triplets are also not regarded for the standard reconstruction. The signals from those stations are kept for analyses especially designed for their treatment, as they are not placed in the hexagonal grid and their inclusion requires a different type of reconstruction. The events containing such stations are reconstructed with only station from the regular grid.

The second step in the selection is the exclusion of a class of stations called *Accidentals*. These are stations that somewhat coincided with the shower detected but are believed not to be causally linked to the shower. The first criteria is a check for a compatible timing. It is requested that all stations are compatible with a planar shower front propagating with the speed of light. The center of the shower front is set as the station with the highest signal measured at position $\vec{x}_1$ at the time t_1. With a first estimation of an axis $\vec{a}$ a prediction t_{pred} for every station at position $\vec{x}$ can be made.

$$t_{pred} = t_1 - \vec{a}(\vec{x} - \vec{x}_1)/c \tag{4.1}$$

It is then necessary for all stations x_i having measured a signal at the time t_i to fulfill the following criteria in order not to be flagged as accidental, in this case *Out of Time*.

$$-1000ns < t_i - t_{pred} < 2000ns \tag{4.2}$$

After having removed all stations from the event that did not meet the timing criteria it is checked whether there are stations that have no neighbors within 1800m or only one within 5000m. Those stations are considered to be too far away to be part of the shower, thus they are removed as accidentals and flagged as *Lonely*. The signals are removed from the signals used for the reconstruction of an event, but their information can still be found in the data set.

4.2.2 Quality criteria

Following the flagging of stations that could falsify the reconstruction two additional quality criteria are imposed, the so called T4 and T5 level, corresponding to T1 to T3 as first level triggers. The T4 trigger is meant to ensure a shower like configuration

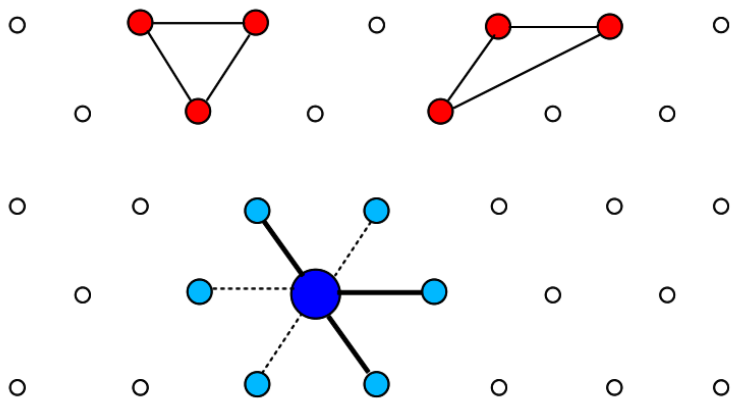

Figure 4.1: Depicted are the two different types of T4 quality trigger. The red stations (top) illustrate the 3TOT condition, requiring three non-aligned stations with a TOT type trigger. The blue dots (bottom) show the concept of the 4C1 condition. A central station (dark blue) needs to be surrounded by any three other stations (light blue) at elementary distance.

while the T5 ensures that the entire shower has been measured by the detector [46]. There are two different types of T4 levels that can be fulfilled by an event, the 3TOT and the 4C1 as shown in figure 4.1.

The 3TOT T4 was designed to be most effective for more or less vertical events with zenith angles up to 60°. It describes a compact but non-aligned configuration of three stations that have sent a TOT (time over threshold) trigger on the T2 level. The 3TOT has proven to be about 90% effective for vertical showers. The 4C1 T4 was designed to include the more horizontal showers. It requires a configuration of four stations that includes one central station and three stations at elementary distance in the so called first crown (C1).

All events that pass any T4 criteria are considered to be genuine showers. To avoid cases in which only a part of the shower has been measured, i.e. occurring at the border of the array or including stations with malfunctions, the T5 criteria is used. Prior to reconstruction it is necessary for an event to have six working stations around the station with the largest signal in order to pass T5. These stations do not necessarily need to have measured a signal. After the reconstruction the condition is loosened. The T5 posterior criteria requires the station with the highest signal to be surrounded by five working stations and the reconstructed shower core to be within a triangle of working stations. It is currently discussed within the Collaboration if the criteria can be loosened further for events of highest energies.

All events that are T3 will be reconstructed by the $\overline{\text{Off}}\underline{\text{line}}$ as far as possible. But only events that were reconstructed and fulfill T4 and T5 are considered valid events.

The next step in the reconstruction is an estimation of the essential parameters of the shower geometry. An estimated shower core is set at the weighted center of the stations with signal. The signal strengths are used as weights. According to the

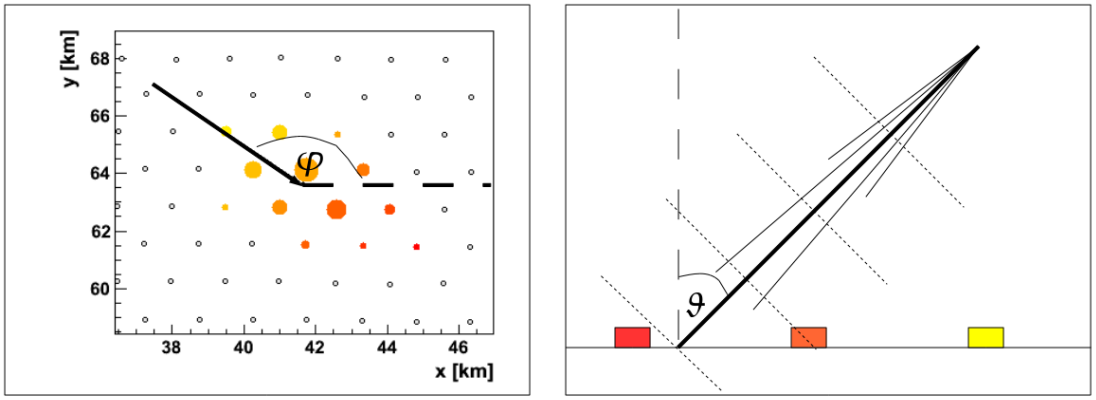

Figure 4.2: A schematic geometry of a shower. The timing is coded in colours, ranging from early stations in yellow to later stations in red. The zenith angle is referred to as ϑ, the azimuth as φ. So called vertical showers can have a ϑ up to 60°.

timing information a modeled planar shower-front is then used to calculate zenith and azimuth angle. With these values the essential reconstruction of the Lateral Distribution Function is initialized.

4.3 Lateral Distribution Function

The lateral distribution of signals from an extensive air shower measured at ground level by a detector grid is considered to follow a characteristic distribution. The strength of signal in local stations will decrease with distance to the shower. Depending on the exact spacing of detectors an individual form for this function for each experiment can be established. The lateral distribution is especially important for an energy estimation as it is the primary tool for the energy reconstruction for ground based detector grids. The exact form and parameters of such a lateral distribution function (LDF) depend on a variety of factors. Whereas particle interactions dominate the true lateral distribution, characteristics of the detector used, i.e. detection mechanism, trigger, shape of the grid, location of the detector, influence the most suitable parameterization [63]. As simulations of interactions are not yet fully reliable and the number of different types of detectors is high there is not globally valid parametrization.

4.3.1 Parameterization

For the design of the Auger Surface Detector many parameterizations were tested [64]. The most suitable form was found to be a modification of a LDF proposed by Nishimura, Kamamata and Greisen, who developed a model purely on theoretical considerations about electromagnetic extended air showers [65], [66]. This *NKG LDF* has been modified for a muonic component and a range of small subshowers by the KASCADE experiment [67]. A similar form is now used as standard in the reconstruction for SD events. The parameter that is used for the energy estimation for the Auger Observatory is the observable S_{1000}. It describes the signal at a distance

r of 1000 m to the shower core and includes an angular dependence proportional to the energy of the shower. It has been tested to be the parameter the least affected by shower-to-shower fluctuations [68]. The following parameterization is used as a default in the $\overline{\text{Off}}\underline{\text{line}}$ reconstruction.

$$S(r) = S_{1000} \cdot f_{\text{LDF}}(r) \tag{4.3}$$

$$f_{\text{LDF}}(r) = \left(\frac{r}{r_{1000}}\right)^{\beta} \left(\frac{r + r_{1000}}{r_{1700}}\right)^{\beta+\gamma} \tag{4.4}$$

Here, $r_{1000} = 1000$ m and $r_{1700} = 1700$ m respectively. The signals are given in particles per station, which can be directly derived from the measurement in VEM per station. The parameters of the LDF are set via a Maximum Likelihood approach in an iterative way. Firstly, only the S_{1000} and the shower core, thereby r as distance to the core in the plane of shower-front, are varied. Only in later stages, depending on the number of available station data further parameters are included. Thus, beta and gamma are initialized by

$$\beta_{\text{init}}(\vartheta) = 0.9 \sec\vartheta - 3.3 \tag{4.5}$$

$$\gamma_{\text{init}} = 0. \tag{4.6}$$

So far γ is not varied at all in the reconstruction, since only 7% of the events have enough information to even handle β as a free parameter. Therefore even β is given by a parameterization for most events. A more elaborate parameterization will be developed for γ [69].

4.3.2 Maximum Likelihood Function

The parameters of the LDF are fitted with a Maximum Likelihood approach. In order to set up the relevant function four different types of contributions need to be considered. There are small signals that need to be treated by means of Poisson statistics since the effective number of particles causing the signal is quite small. Above a signal from 30 particles the central limit theorem enables to use a Gaussian approximation for the contribution. Furthermore the information from saturated stations has to be included as well as the information of stations that were not triggered, known as *zero-stations*. Thus the general set-up for the Maximum Likelihood, respectively the logarithmic Maximum Likelihood, can be described by the following terms.

$$\mathrm{L} = \prod_i f_{\text{Poisson}}(n_i, \mu_i) \prod_i f_{\text{Gauss}}(n_i, \mu_i) \prod_i F_{\text{sat}}(n_i, \mu_i) \prod_i F_{\text{zero}}(n_i, \mu_i) \tag{4.7}$$

$$l = \sum_i \ln f_{\text{P}}(n_i, \mu_i) \sum_i \ln f_{\text{G}}(n_i, \mu_i) \sum_i \ln F_{\text{sat}}(n_i, \mu_i) \sum_i \ln F_{\text{zero}}(n_i, \mu_i) \tag{4.8}$$

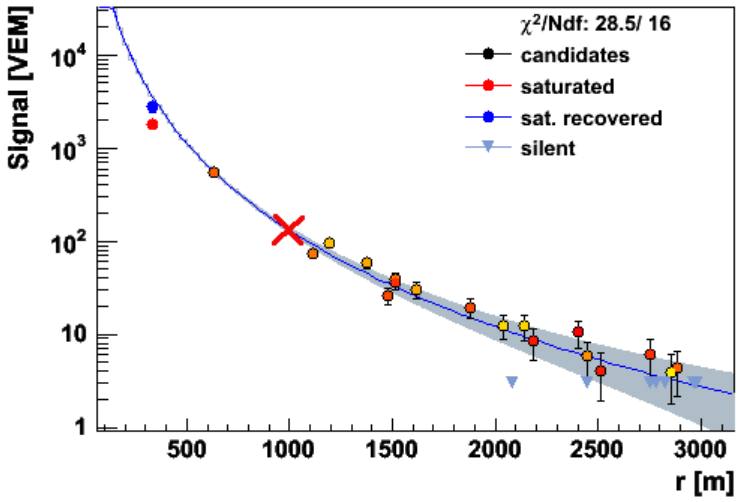

Figure 4.3: Example of a Lateral Distribution Function, Event 7035303. Different types of stations are coded in color. Colors ranging from red to yellow indicate the relevant timing. The blue station corresponds to the deep red station, which had saturated electronics and depicts the recovered signal. The triangles are those stations that were silent and did not trigger a signal, i.e. zero-stations. They could have recorded any signal between zero and about 3 VEM. The X marks the signal at 1000 m distance to the shower core, i.e. S_{1000}. This figure and all following reconstructed data samples are taken from the EventBrowser that is delivered with the Offline.

Here n_i is the effective number of particles in the tank which can be obtained from a conversion of the signal measured in VEM by the station. Respectively μ_i is the theoretical expectation of particles obtained from the LDF, as a function of the LDF parameters [70].

In detail the contribution from the small signal can be described as:

$$f_{\mathrm{P}}(n_i, \mu_i) = \frac{\mu_i^{n_i} \mathrm{e}^{-\mu_i}}{n_i!} \tag{4.9}$$

$$\ln f_{\mathrm{P}}(n_i, \mu_i) = n_i \ln \mu_i - \mu_i - \sum_{j=1}^{n_i} \ln j. \tag{4.10}$$

Gaussian signals contribute as follows:

$$f_{\mathrm{G}}(n_i, \mu_i) = \frac{1}{\sqrt{2\pi}\,\sigma_i} \exp\left(-\frac{(n_i - \mu_i)^2}{2\sigma_i^2}\right) \tag{4.11}$$

$$\ln f_{\mathrm{G}}(n_i, \mu_i) = -\frac{(n_i - \mu_i)^2}{2\sigma_i^2} - \ln \sigma_i - \tfrac{1}{2} \ln 2\pi \tag{4.12}$$

For saturated signals one has to distinguish certain cases. If the signal has been fully recovered and the rise of the LDF is in a moderate regime it is treated as

Gaussian signal. If the rise is too steep i.e. the second derivative at the position of the station is smaller than a threshold value of one, the recovered signal is, as any signal without recovery, only used as lower limit giving the following contribution. The differentiation is necessary since the true form of the LDF very close to the core is still not fully understood [68]. Thus saturated stations give the following contribution:

$$F_{\mathrm{sat}}(n_i, \mu_i) = \int_{n_i}^{\infty} f_{\mathrm{G}}(n, \mu_i)\,\mathrm{d}n = \frac{1}{2}\left(1 - \mathrm{erf}\left(\frac{n_i - \mu_i}{\sqrt{2}\,\sigma_i}\right)\right) \tag{4.13}$$

Lastly, the stations without triggered signal also give a contribution. This has proven to be effective since it stabilizes the LDF in the tail and ensures that the lateral distribution approaches zero in the outer regions. Furthermore it accounts for a possible bias on the shower parameters that the local trigger induced as it selects upward fluctuations of the signal.

$$F_{\mathrm{zero}}(n_{\mathrm{th}}, \mu_i) = \sum_{n=0}^{n_{\mathrm{th}}} f_{\mathrm{P}}(n, \mu_i) \tag{4.14}$$

$$\ln F_{\mathrm{zero}}(n_{\mathrm{th}}, \mu_i) = -\mu_i + \ln\left(\sum_{n=0}^{n_{\mathrm{th}}} \frac{\mu_i^n}{n!}\right) \tag{4.15}$$

Still not completely understood is, whether the treatment of n_{th}, i.e. the threshold value for the trigger is completely correct. As described in section 3.2 there are different types of triggers using different threshold conditions. Those conditions range from about 1.7 VEM to 3.2 VEM and are not equally effective for different types of events. So far n_{th} is set to 3 VEM for the Maximum Likelihood approach, as it is the best approximation.

4.3.3 Fitting stages

The actual fit of the LDF is executed in $\overline{\mathrm{Off}}\underline{\mathrm{line}}$ using MINUIT [71] as an iterative process. The first step is an estimation of the core using the initialized values for the angles and parameters. In a second step the core and S_{1000} are fitted, leaving all other parameters fixed. In the next stages step by step further parameters are included depending on the information available. In any of these stages the fit can be terminated if no converging solution is found. Only in the last step the contribution of the zero-stations is added. Due to the hexagonal structure of the detector there are configurations of stations possible that might bias the reconstruction. When including zero-stations this effect is minimized and the LDF will be stabilized.

After having completed the LDF reconstruction a more realistic curved model of the shower-front is used to refine the angular reconstruction as this weakly depends on the position of the core.

This entire reconstruction is based on models for air showers and the current understanding of processes within the shower. Most of the steps have been optimized

in the measurement of air showers. Therefore the quality of the reconstruction or certain difficulties within the chain of reconstruction could indicate showers that do not meet our expectations of cosmic air showers. Any shower that does not show the characteristics according to the general expectation will not be reconstructed with a good quality. Thus, this reconstruction and the results for every shower provide a handle to systematically search for anomalous events.

5. Shower Geometry

From the overall reconstructed shower geometry features can be derived that can be used as criteria when looking for showers that do not meet our expectation. Due to the current physical explanation the entire reconstruction is based on a certain expectation about the form and features of an air shower. It is therefore consequent to ensure that the model for the general appearance is met by the data before going into further detail. In this chapter general features that are worth investigating will be identified, discussed and compared with the expectation.

5.1 Overall Features

When looking for deviating features we need to identify an expectation, i.e. the properties of a regular shower. Starting at the most general point it is necessary to ask whether we detect a rate of events as it is expected and whether all parts of the array are fully functional.

The Surface Detector should be measuring events roughly uniformly from all directions in azimuth as there should be no major effect influencing the arrival direction.

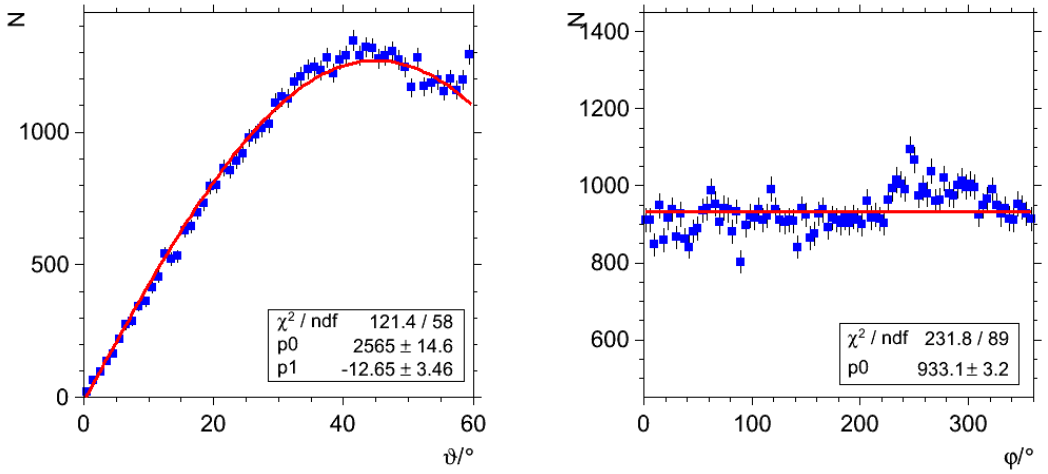

(a) Zenith Distribution, Fit $\sim \sin(\vartheta)\cos(\vartheta)$ **(b)** Azimuth Distribution

Figure 5.1: Angular distribution of mostly vertical SD Events with an energy larger than $3 \cdot 10^{18} eV$. The zenith angle is given by ϑ and the azimuth angle by φ. The azimuthal distribution is mostly flat, while the distribution of zenith angles is influenced by the curvature of the surface and the detector acceptance.

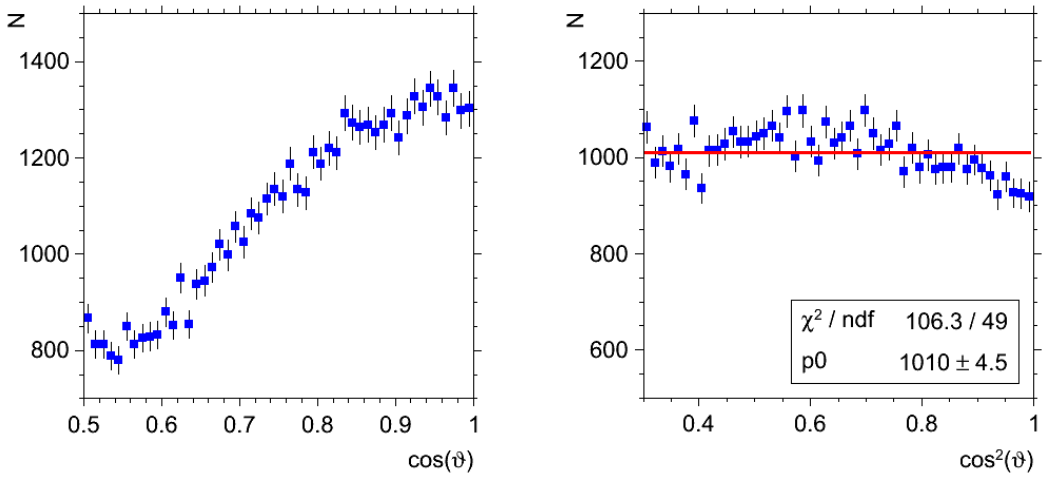

(a) Zenith Distribution in units of $\cos(\vartheta)$ **(b)** Zenith Distribution in units of $\cos^2(\vartheta)$

Figure 5.2: The zenith ϑ distribution of mostly vertical SD Events with an energy larger than $3 \cdot 10^{18} eV$ is depicted in different variants. Plotting $\cos(\vartheta)$ shows the distribution in solid angle bins, while introducing $\cos^2(\vartheta)$ flattens the distribution by abstracting from the flat detector.

We expect a distribution of zenith angles that follows a $\sin(\vartheta) \cdot \cos(\vartheta)$ distribution. If there is an isotropic flux on the surface of the earth, there should be the same number of events in every $\cos(\vartheta)$ solid angle bin, which introduces a term of $\sin(\vartheta)$ in the arrival direction of ϑ.

$$\frac{dN}{d\cos(\vartheta)} = \text{const} \qquad \Rightarrow \qquad \frac{dN}{d\vartheta} \sim \sin(\vartheta) \tag{5.1}$$

Since the SD is a flat detector the area of the detector seems largest for vertical events and decreasing for inclined events, which introduces a $\cos(\vartheta)$ dependency.

Local effects such as the geomagnetic field or an overall anisotropy might influence the distribution, but for a general overview only to a small amount. Furthermore, the detector is a hexagonal grid, which needs at least three stations to be triggered in order to detect a valid event. This leads to a different angular acceptance for certain directions. This effect is most prevalent at low energies and an energy cut as introduced should minimize the dependence. As shown in figure 5.1 the general expectations of a flat azimuthal distribution and a dependence in the zenith distribution are met. In figure 5.2 it is shown that the zenith distribution can be lead back to a flat distribution that corresponds roughly to isotropy.

Also, we expect the events measured by the SD to be uniformly distributed within the array. The location of the shower cores should not depend on any characteristics of the detector as soon as the detector is fully functional. We cannot expect fully measured high quality events in an area were only half the necessary stations are deployed.

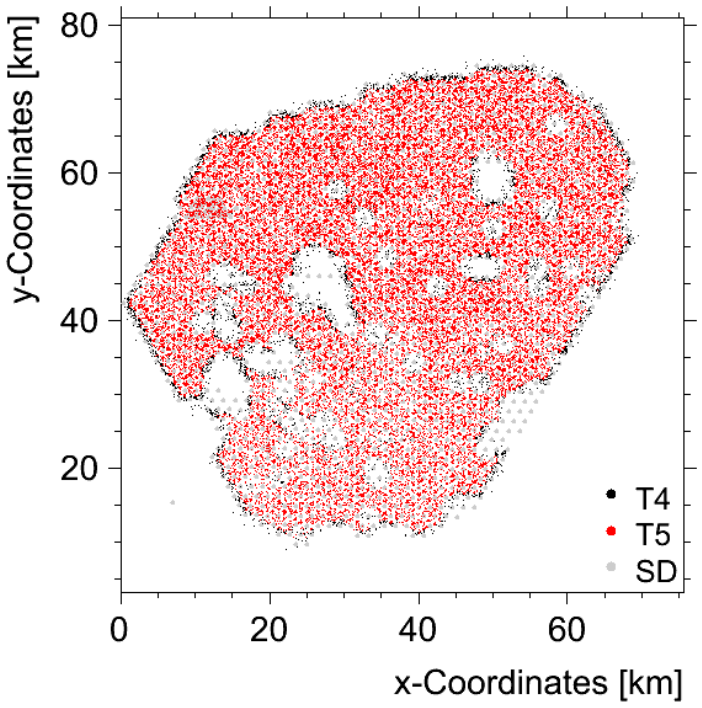

(a) All Events from January 2009

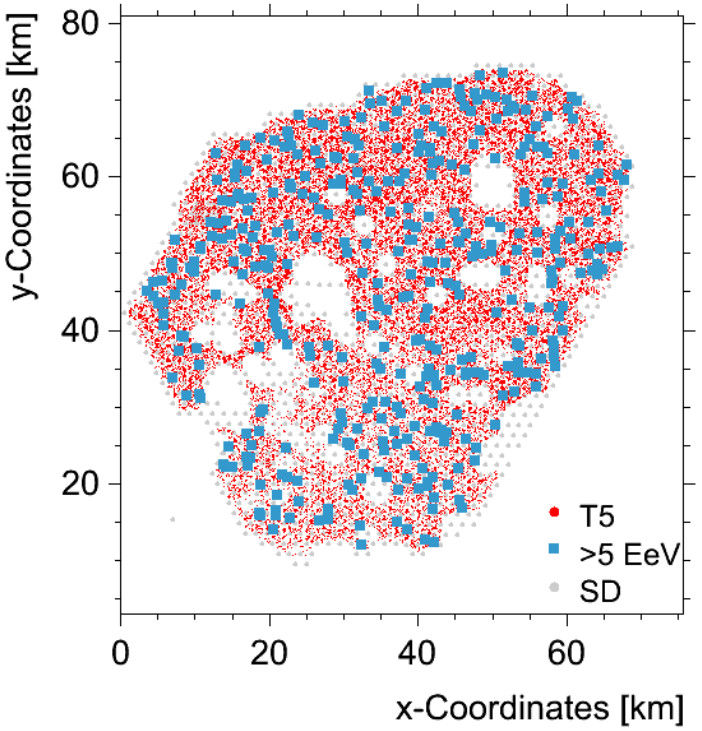

(b) Events above an energy of 5 EeV

Figure 5.3: The positions of the cores of all showers from January 2009 are marked. Different types of events are shown according to their trigger name. The T4 events are considered to be genuine showers. Adding the T5 criteria ensures that the entire shower has been measured with the detector. Therefore no T5 events can be found at the borders and along holes in the detector. The overall distribution shows more events in the northern part of the array. A cut on the energy as done in figure (b) evens the distribution.

As shown in figure 5.3 the events do not seem to be evenly distributed. First of all areas with no events should be noted. In these areas either the station was not deployed due to environmental problems such as flooding or landowning issues, or the station was out of order in the relevant time period. This is an expected effect.

The distribution of shower cores reflects the hexagonal structure of the array. This is due to the fact that the reconstruction favours core locations that are between the stations rather than on top of a station. Most events are measured by three stations, which necessarily requires the core to be in between the stations. In addition the reconstruction always introduces a weighted barycenter as provisional core in a first step thus mostly starting the optimization from somewhere in between the stations. Again this effect was foreseen in the design of the detector.

Furthermore it seems as if there are more events in the northern part than the southern part of the array. When comparing for example two areas in the array with a similar structure, the upper right corner (y $>$ 42 km, x $>$ 38 km) and the lower middle part (y $<$ 32 km, 20 km $<$ x $<$ 50 km) the effect can be quantified. In the upper corner about 32.0 ± 3.2 events were measured per station, whereas in the other part only 17.0 ± 1.7 events were measured. This is certainly unexpected in a general context. When choosing only events above an energy threshold of 5 EeV the effect becomes smaller. The values drop to 0.27 ± 0.03 and 0.22 ± 0.02 respectively, which are compatible within 2σ. The rate of events seen is restricted by the acceptance of the array. The acceptance of the array depends on the number of active hexagons at a given time. This number is influenced by the general structure and irregularities as well as failures of stations. In order to calculate the exact acceptance of parts of the array a lot of information is required that is not easily obtainable. Therefore the errors on these rate are estimated to 10%.

This effect can also be seen in a different context. When counting the number of events that a station has participated in, the effect can be correlated to the number of the station as shown in figure 5.4. Stations having a higher number contribute significantly more often in an event than those with a lower number. As the number of the station corresponds to its deployment date, it shows that older stations seem to participate less often in events. A cut on the signal strength eases this difference. As the signal strength is related to the energy of the shower, such a cut shows the same effect as a cut in energy of the events.

The effect that is described here was indeed not foreseen but it is known. It is due to a change in the PMTs used and is known as *raining PMTs*. After about station number 600 a new type of PMTs was used similar to the former PMTs as the older type was no longer being produced. It was found when inquiring this effect that the new set of PMTs had a different grounding of the base of the dynode, which causes a fluctuation of the baseline. This results in a gain for signal and consequently in an increase in the number of triggers sent. This effect was thoroughly studied and it was found that as soon as the trigger efficiency is saturated no effect on the data can be found, which is illustrated by the cut on the signal strength [72]. This effect has to be taken into consideration when defining our expectancy of the data measured

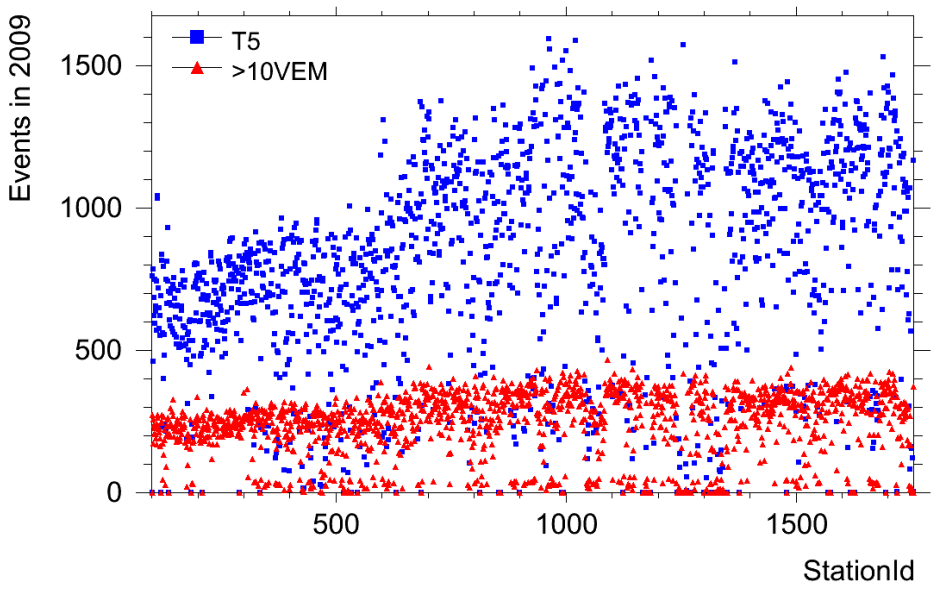

Figure 5.4: Number of T5 events that a station participated in are plotted against the ID number of the station. Only events from 2009 are shown. The lowest IDs belong to the oldest stations. The ID is not changed if parts of the station are replaced. Some stations might show lower rates if they are located near the border of the array or have been defective.

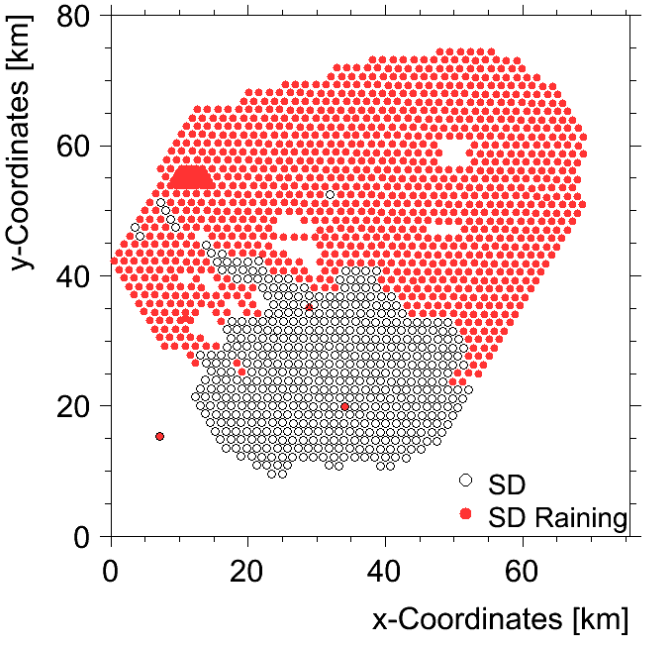

Figure 5.5: This map shows the position of stations on the array that might be affected from *raining* PMTs. Not all these stations need to show raining PMTs. In some the PMTs have been repaired, while in others the raining was never excessive.

with the Surface Detector. The position of possibly raining PMTs is shown in figure 5.5.

Concerning the overall event rate it should be noted that it is dependent on time. As the shower development in the atmosphere depends on pressure, temperature and density, one can observe a 10% yearly and 2% diurnal modulation of the event rate detected by the Surface Detector [50]. In addition studies have been conducted about possible ageing effects of the PMTs or other parts of the detector [73]. So far no general trend in time have been observed.

After having checked the overall rate of events a step towards individual events have to be taken. We expect the reconstruction to be based on a model that correctly describes the events that are detected. How well a reconstruction is conducted qualitatively should and will be discussed in chapter 7. The extreme case that the reconstruction cannot reconstruct the event at all should be a first step to verify that our expectation is met.

Another criterion that the entire set of data considered should fulfill is the expectation about background. The background rejection should be effective and remove signal according to this expectancy. Any deviations should be investigated. This will be discussed in detail in chapter 6.

5.2 Air Shower Footprints

When looking at the geometry of an individual shower one of the most prominent features of an air shower is the spatial distribution of the signals on the ground, which is known as *footprint*. As the shower is believed to be caused by one very energetic cosmic particle interacting with the atomic nuclei in the atmosphere one expects a compact footprint on the ground. The shower in general can be described as a cascade having the shape of a cone. The footprint measured on the surface can then only be a conic section if we consider the earth to be locally reasonably flat. This approximation is not true for very horizontal events since those showers will be influenced by the curvature of the earth's surface. Thus it can be concluded that the footprint of an air shower in the vertical regime has to be compact, axially symmetrical and having an ellipticity corresponding to its zenith angle. However, one has to keep in mind that due to the hexagonal spacing of the SD with its 1.5 km distance between stations the elliptic shape might be difficult to identify in small showers.

5.2.1 Identifying classes

In the search for unusual events many shapes could be discussed that are not quite elliptic. Shapes looking like a banana or a barbell are certainly unexpected but might also be caused by signal fluctuations, which are not unusual in air showers. It is also debatable what exact criteria a shower needs to fulfill in order to be categorized as for instance as a banana. The hexagonal grid makes it difficult to establish exact geometric criteria for curved shapes that can be found by an algorithm. Furthermore

most exotic physics models that predict non-symmetric shapes predict only slightly alterations that will be hard to identify with a detector that only samples the shower.

An unusual footprint which is however most unlikely and easy to identify is a shape like a conic section but with a missing station in the middle. These shapes could be caused by a non-operational station in the middle of an event. Normally those stations are tagged by the data acquisition and therefore the entire event does not meet the quality criteria. The tagging can be later controlled in the monitoring data-base. Thus events having this shape could either hint at an issue concerning the identification of non-operational stations or could indeed hint at unusual events that deserve further investigation.

In the context of this thesis an algorithm was developed that identifies events that show a missing station. This type of event will be referred to as *hexagonal events*.

According to their shape 233 events can be identified as hexagonal events. Those 233 events do not include events, in which the central station was not yet deployed. But they include events, in which the central station was in general operational but was in the time window of the event erroneous and did not participate in data taking. Removing these events from the set leaves 28 events of which an example is given in figure 5.6.

5.2.2 Occurrence of hexagonal events and cross-checks

As described above such events might be due to issues within the detector. A look at the exemplary events also suggests that a shift of the shower core towards the missing station could have resulted in a regular LDF. Therefore investigating issues within the detector are needed to exclude failures. Whenever the Central Data Acquisition System (CDAS) notes changes or unexpected behavior in the detector a *Bad Period* is called [74]. This is also true if the CDAS itself has not been fully operational. So if data is taken in such a bad period one cannot completely rely on its correct acquisition and therefore such data is not used in analyses requiring full acceptance. In analyses like this thesis that study event by event a general exclusion of bad periods is not needed. However, since the hexagonal events might be caused by the detector is it worth investigating whether those events coincide with a bad period. A complete overview of the events and bad periods is given in appendix A.3.

During a time-period in 2009 starting April 17th lasting until November 15th a number of problems referred to as *Comms Problems* occurred. Due to an error in the software update for the communications unit of the SD stations data was not transmitted correctly to the CDAS and loss of data occurred. Even though a lot of effort was put into the inquiry of this data loss the error was not found and fixed until November. Therefore the entire period should be dealt with caution even though some parts of it might be used with some limitations for analyses [75].

Eight of those 28 hexagonal events occurred during a bad period with five occurring in the period with the Comms problem. Taking into consideration that the bad periods are usually only short time periods with only a small part of the entire time in which data is taken three events are within expectation.

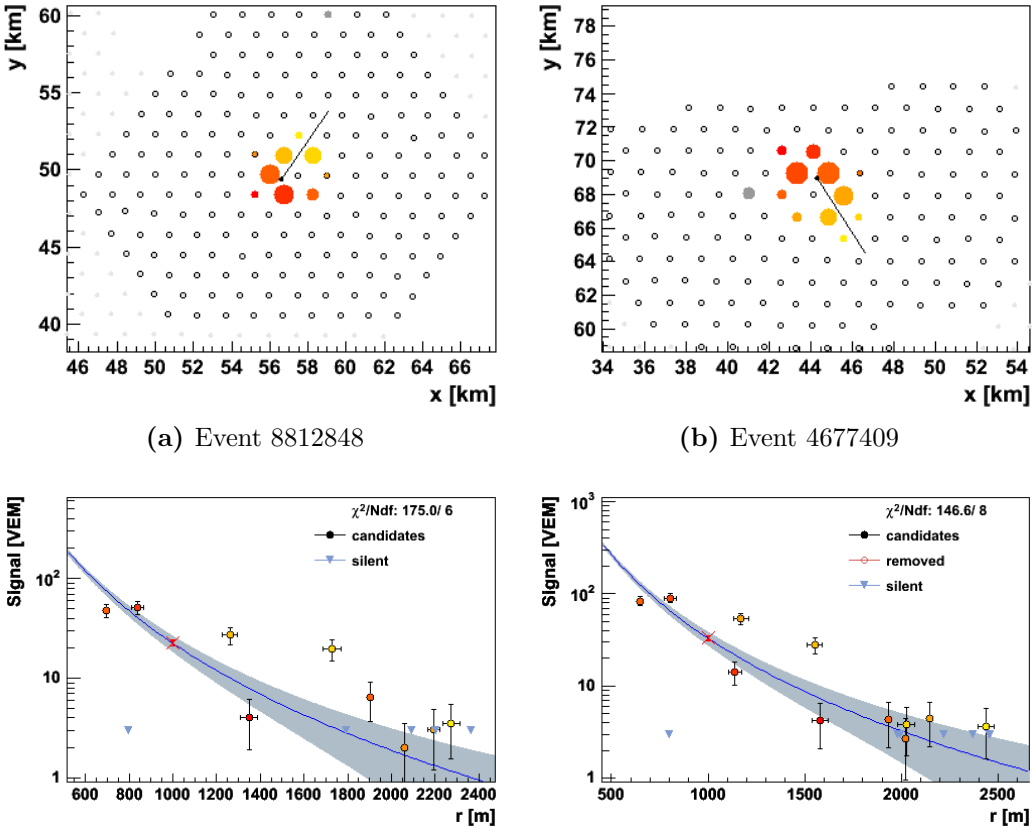

(a) Event 8812848 **(b)** Event 4677409

(c) LDF Event 8812848 **(d)** LDF Event 4677409

Figure 5.6: Exemplarily two events are shown, that did not record a signal in the central station. The fit of the lateral distribution function (LDF) treated the central station as working but having recorded no signal. Not regarding what caused this shape the fit does not seem to fit the data. Possibly, shifting the position of the core would result in a better fit as the shape suggests. If this were true it would be likely that the missing station was due to a failure in data-taking rather than due to an exotic event.

Looking further into the data of 2009 leads to some more interesting events. 12 hexagonal events were measured in 2009, of those six in December, which is not considered a bad period. Such a clustering is noticeable. Considering that in 2008 overall six events were found equally distributed among the months and that the exposure of the SD did not change too much between 2008 and 2009 even emphasizes the effect. If those types of events are actually due to issues within the detector this effect suggests that the detector is not yet back to normal even though there is very low statistics to stress this point. Indeed it was reported that the communication situation did improve as opposed to the Comms problems. But there is a not yet fully understood effect that is still affecting the data [76].

After all, not regarding what actually causes these events, it can be said that statistically this overall effect is certainly irrelevant. According to the considerations

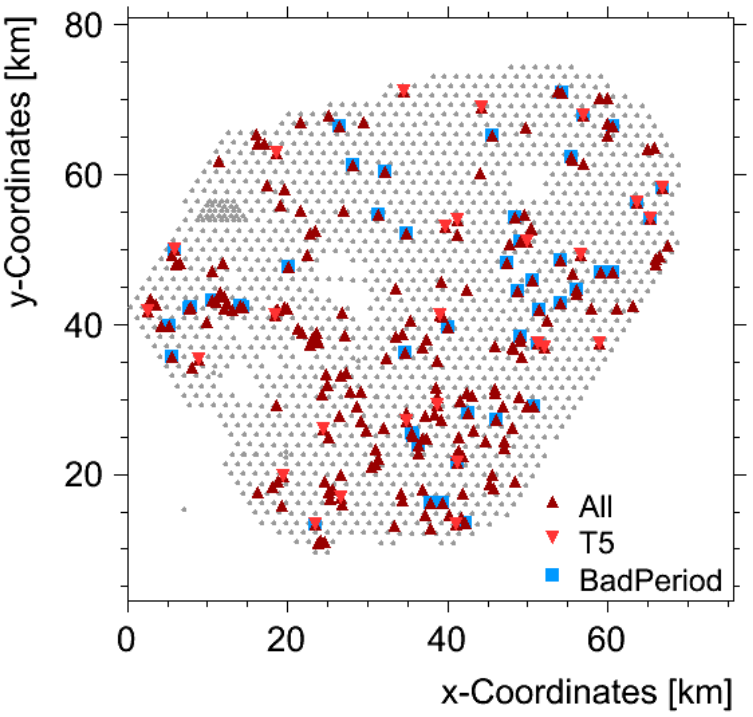

Figure 5.7: The positions of all hexagonal events in the data set are shown; they show a configuration in which a central station did not record any signal. Upward pointing triangles mark all events of this shape. Downward pointing triangles are those events that reported the central station to be operational, T5. All events that fell within a Bad Period in which the data-taking was not reliable are marked with a blue square.

made in the previous section a station participates in about 1000 events per year, depending on the exact location and age of the station. Thus, taking into account technical instabilities that might occur, a non-participation of 28 out of 1600 stations in one event is within a reasonable probability.

Looking at the involved stations in detail shows that all are different but two. Both hexagonal events seen in 2005 involved station 715. Such a coincidence would be very improbable for a purely statistic effect. The station was deployed only in 2006, according to the maintenance log. Thus, there might have been a problem flagging the station or concerning the maintenance database. One has to keep in mind that in 2005 the detector was in the early process of being built thus irregularities in the flagging might have occurred.

The other station that is involved two times is station 1687. Both events concerning this station took place within the bad period of 2009 during the Comms problem. Station 1687 is located close to the border of the communications area of the tower of Los Morados. As described in [75] the problems arriving from the flawed station software occurred preferably near the border of a communications sector. Thus, one is tempted to say that here another hint for a not reliable detector is found.

All other stations involved only participated once and are as far as the maintenance log goes treated correctly. As the station number corresponds to the time the station was deployed one can say that there is no dependence on the type of station. Numbers between 113 and 1678 occur more or less uniformly distributed as far as low statistics allows such a conclusion. The overall distribution of the events is shown in figure 5.7. The fact that there are more events in the lower half of the array than in the top half can be explained by continuous completion of the array.

As the Pierre Auger Collaboration is planning on using some data from the period of Comms problems a new tool to identify problematic events was developed. Before there were communication problems an event was considered valid, if the hexagon of stations involved in an event had been operational in the second in which the event occurred. But as a station is usually given 120 s to retransmit the data in case of an unsuccessful communication, this restriction is considered to be too loose. Especially during the Comms problems the rate of retransmitting operations dramatically increased and it is known that there are events from which singular stations were lost. Therefore it will soon be necessary for an event to be considered valid to be contained by a hexagon of stations that has been active at the time of the event and a minimum of 120 s after the event. Applying this cut during a stable period only excludes about 1% of the events, which indeed corresponds to the expected rate of events lost. During the Comms Problem about 20% of the events are excluded by this cut [77].

As a preliminary solution a web tool is provided in which the events from the Comms problems can be checked for their validity [78]. The recommendation is however only valid for events after June 6th 2009, as the first part of the bad period was too unstable to be used. It was agreed that only events fulfilling a T5 with these restrictions can be used. Therefore, two hexagonal events can be rechecked with this tool and are candidates for such an exclusion. In fact, one of these two events is meant to be excluded according to the most recent requirements. This therefore again strengthens the idea that these events might not be due to unexpected physical events, but due to issues concerning the detector.

The bottom line from this approach should definitely be that bad periods cannot be underestimated and further research is needed to identify whether the Comms problem is completely resolved. Again it stresses how important a steady and reliable monitoring is. However, no statistically significant amount of unexpected events were found.

5.3 Incomplete Reconstruction

In chapter 4 was described that the reconstruction has several steps. A first estimation is done for the location of the core according to the signals measured in the stations, i.e. the core has to be closest to the station with the highest signal. This step is possible for every kind of event. However stepping further in the reconstruction not for every kind of event a suitable solution can be found. Especially when minimizing the negative Log-Likelihood-Function to establish the lateral distribution

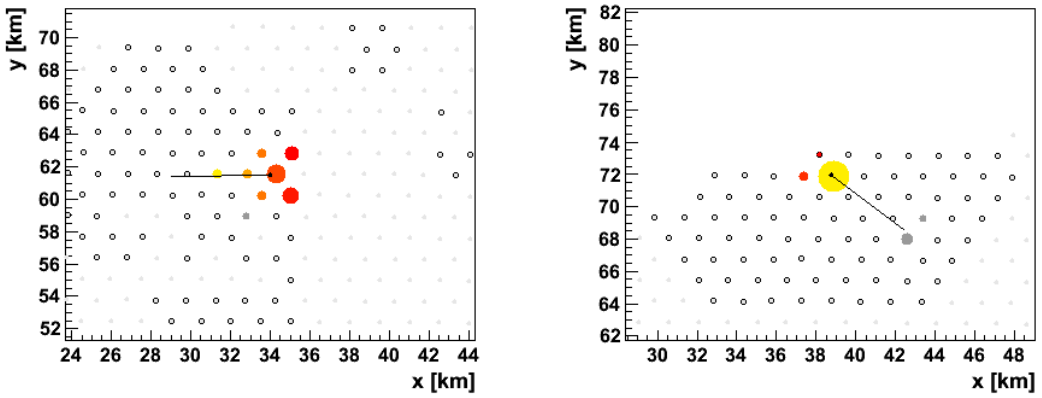

(a) Event on the Border 3083766 **(b)** Saturated Event 4744954

Figure 5.8: Exemplarily the footprints of two events are shown for which the reconstruction was not able to terminate. A shower core was only estimated. This abort in the reconstruction is probably due to the unfortunate configuration of the events.

function (LDF), problems might occur if no minimum can be found and the reconstruction is aborted. As such an abort is mostly due to an unusual configuration of stations, those events deserve to be investigated in a search for unexpected events. It has to be identified whether they are just an expected fluctuation or whether there is something significant about the event itself to be found.

Overall there are 54 events out of the data-set of T5 quality events used that were not successfully reconstructed, which equals a fraction of 0.003%. Therefore we are looking at a very small effect, which is certainly probable just to be seen by chance. Nonetheless this small group of events can be investigated to look for possible explanations. A full list of all Event IDs, the classification and the data set of which the events are taken is provided in the appendix A.3.

Even though the T5 quality criteria has been applied, which should exclude events that have fallen so close to the border of the array that the full information was not detected, 16 out of those 54 events have fallen close to the border. A visual inspection suggests that these awkward configurations prevented the reconstruction from finding a suitable solution. An example is given in figure 5.8 (a). This finding suggests that the T5 quality trigger should not be loosened any further, especially when applying a condition that relies on already reconstructed characteristics. The reconstruction will favour a core to be surrounded by stations having measured a signal, thus applying a posterior condition based on the location of the core should be used with caution, especially in events with a low multiplicity of stations.

An additional class is formed by 7 events that have a saturated central station while only very few other stations have measured a signal. These events are probably real events of low energy whose core was very close to the central station. As the LDF is not fully established by the reconstruction an exact energy of these showers cannot be given, but their estimated energy is indeed low. It is quite obvious that such

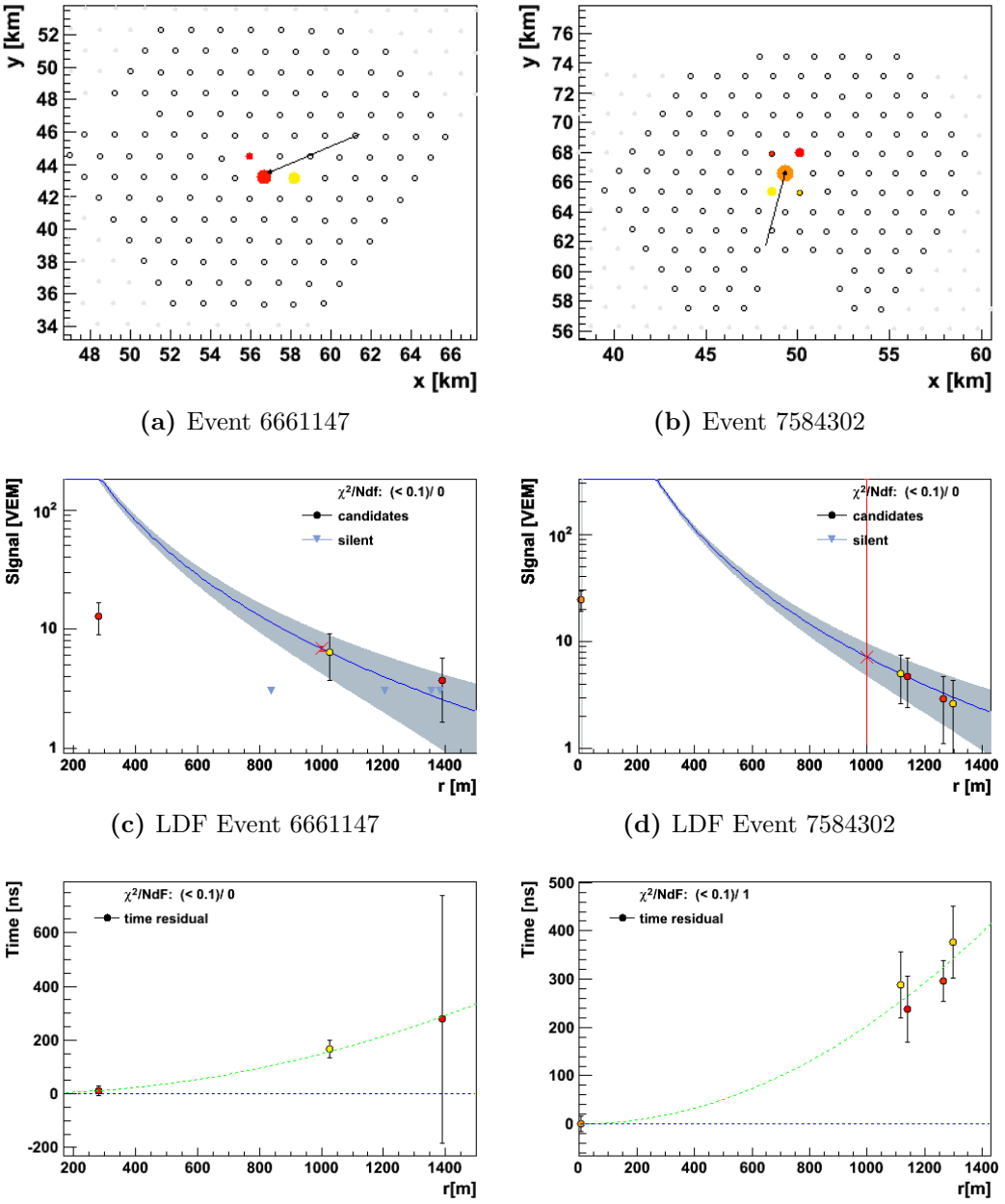

(a) Event 6661147 **(b)** Event 7584302

(c) LDF Event 6661147 **(d)** LDF Event 7584302

(e) Timing Event 6661147 **(f)** Timing Event 7584302

Figure 5.9: As another example for a incomplete reconstruction two events are shown with their estimations from the reconstruction. The timing information is also added, which seems to reasonably fit the expectation from a shower.

a type of event is difficult to reconstruct, since it is of very low multiplicity in a difficult configuration as there are saturated stations which can in some cases only be used as a lower limit. An example of such an event is shown in figure 5.8 (b).

There is one event that has a structure as described in section 5.2, having a missing station right in the center. In another singular event it seems as if the reconstruction discarded the wrong station as background, thus removing a central station from the actual shower and leaving an unreasonable geometry.

All other events could be classified as events of low multiplicity and low signals with an awkward station configuration. Either the signals measured are all about the same size, thus identifying a center proves difficult. Other events show a signal distribution that does not fit the timing distribution, i.e. the earliest signals are not in the center of the event. There is no direct physical explanation for those events. One could suggest that these events we caused by uncorrelated muons coinciding by chance. Estimating the probability, one needs the T1 rate of 100 Hz, which indicates the flux of signal in individual stations. The T3 time window that defines an event is 60 μs. For three station this gives an expected number of 0.018 triggered stations per time window. If we now consider the about 2 Million events that the SD has already recorded, a toy Monte Carlo estimates the number of cases in which all three stations are triggered to 9 ± 3. This would therefore only explain some of the 31 events. This leaves very few not fully understood events in the low energy regime. Possibly, model-dependent searches looking at events of lower energies could make a more definite statement about those events. Two examples for this type of event are given in figure 5.9.

Furthermore the reconstruction does not seem to be stable for vertical events that have one central station with a saturated signal very close to the shower core and are in general very symmetrical. As discussed in chapter 4 such saturated signals will only be used as a lower limit, as the rise of the LDF is too large and the true form of the distribution near the core not yet known. Since these stations are so close to the shower core that the next closest station is further than 1000 m away from the core there is only one lower limit to define the parameters of the LDF in the most crucial region. This will result in unreasonably high errors for the location of the core or the value for S_{1000}. The $\overline{\text{Off}}\underline{\text{line}}$-developers have rearranged the flagging of these events, therefore they will be no longer considered valid events in the newest data-set.

Some simulation studies have been carried out about failed reconstructions due to muons that disturb the air shower signal but which were not actually from the shower [79], [80]. According to those results the trigger conditions have been optimized, thus the effect of muons within the shower should have been minimized. Consequently, we expect only little disturbances from accidentals muons.

Overall, we can conclude that there are some events that look anomalously. However, there are only very few events of many different kinds. Therefore we cannot identify a class of deviating events that could not be explained by background or detector effects. So after having discussed the shower geometry in general a more detailed

look at the signals rejected as background by the reconstruction is worthwhile since we have quite certain expectations about it. It can be used as another criteria to identify unexpected events.

6. Accidentals

All non erroneous signals measured in the Surface Detector (SD) of the Pierre Auger Observatory correspond to particles crossing the water-tanks of the local stations. The average trigger threshold of 3 VEM corresponds to three muons vertically crossing the station in a time window of 325 ns. Since there is an almost continuous flux of muons in the atmosphere [81], we expect muons to randomly generate signals above the threshold in singular SD stations. The quality criteria T3 and T4 try to reduce the amount of random signals. However, with every event not only the stations that have formed the trigger but also other stations around that primary event are read out in order to exclude trigger failures and secure a broader set of data. Therefore some signals caused by muons originating not from the corresponding air shower might be in the set of data. Those stations need to be identified and cannot be used for the reconstruction. In Auger terms these stations are called *Accidentals*.

Taking a deeper look at these accidentals is worthwhile. As they are removed from an event as background due to timing or position as shown in section 4.2.1, they contain information about the background itself and can be compared to the expected background. The most basic information is their existence, i.e. their number should not exceed the expectation. A too high number could hint at a yet not correctly understood background or a faulty background removal. The same is true for too few accidentals. Furthermore there are expectations about the signal strength of the accidentals and their location in the array. Thus, many different handles will be used in this chapter to ensure that possible deviations are identified.

6.1 Number of Accidentals

In general the expected number of accidentals per event can be estimated by assuming a continuous flux of background and applying the trigger constraint T3 in its most effective specification. Since only events that are within a T3 are recorded, the T3 determines the rate of data taking, while the T1 rate corresponds to the general flux of signal recorded by SD stations. Furthermore, the number of stations read out influences the probability of detecting an accidental. Thus, the expected number of accidentals per event is given by:

$$\begin{aligned} N_{\text{accidental}} &= N_{\text{stations}} \cdot T1_{\text{rate}} \cdot T3_{\text{time-window}} \\ &= N_{\text{stations}} \cdot 100 \text{ Hz} \cdot 60 \ \mu s \\ &= N_{\text{stations}} \cdot 0.006 \end{aligned} \tag{6.1}$$

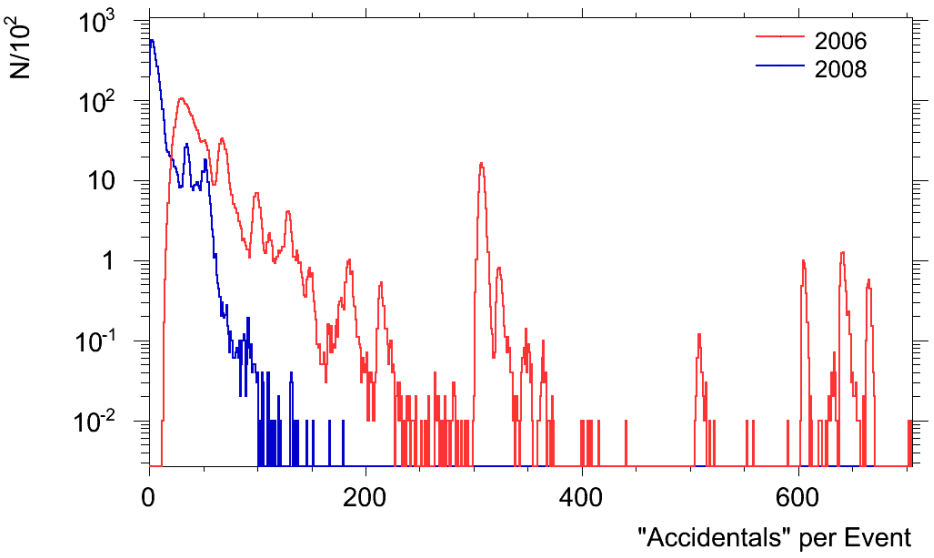

Figure 6.1: Number of stations disregarded by the reconstruction per event for the years 2006 and 2008. Shown are all stations that measured a signal, which was not used in the reconstruction. The reasons were technical as well as physical.

Consequently there is a robust estimation of the number of accidentals expected. No significant deviation form this expectation should occur.

Exemplarily, figure 6.1 shows the number of stations per event that were removed by the reconstruction for the years 2006 and 2008. All events that have a full reconstruction were used for this analysis. When looking for a removed background, there are certain unexpected aspects in this figure. The most unexpected are the different peaks at higher values in the distribution. Furthermore, in 2006 the SD was not yet complete, there were less stations installed than in 2008. Given the correctness of formula 6.1 the expectation for 2008 should therefore by higher than in 2006, as it is proportional to the number of station. Also the form of the distribution is vastly different comparing the two years.

First of all this figure does not show only removed background from muons. All stations that have been removed are shown, not regarding the individual reasons. Therefore also all stations that have been in-operational or that do not have a position on the regular SD grid are included. For example engineering stations or stations from the Infill Array as well as doublet or triplet stations that have been built for detailed analyses are by default rejected in the reconstruction. The peaks in the distribution correspond to such groups of stations. As the detector had been continuously enlarged at that time the peaks do vary in time and correspond to the different structure of the two distributions.

Still, it is obvious that there are more stations being removed in 2006 than there are in 2008, which is in contrast to a growing detector. An explanation can be found requiring additional information about the detector. The effect is mainly due to the fact that the read-out mechanism has been changed by the end of 2006. As

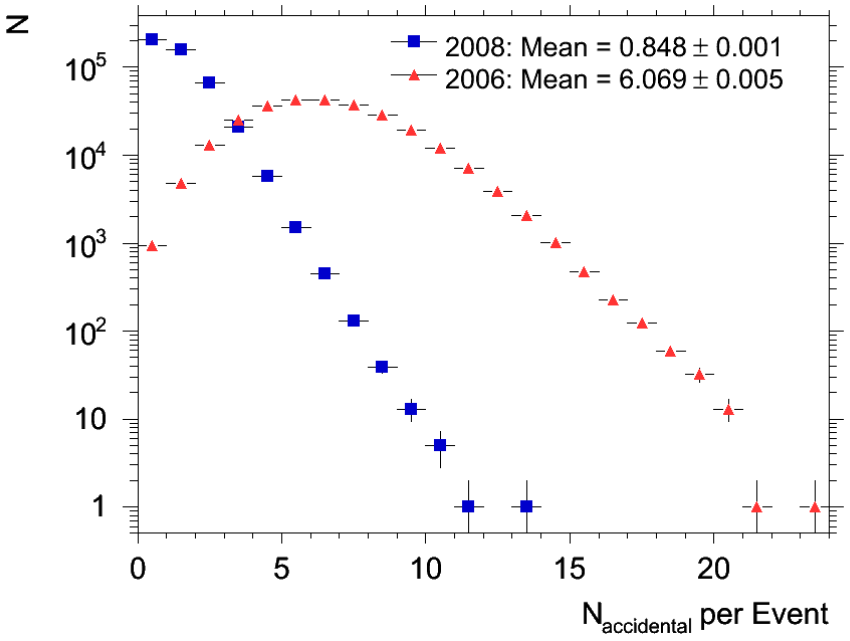

Figure 6.2: Number of stations rejected as *out of time* and *lonely* for the years 2006 and 2008. Those two criteria correspond to background rejection. The means of the distributions correspond to the expectation.

the communications system was no longer able to handle all information from all stations once an event had been triggered the number of stations that receive a read-out command has been reduced. Since the beginning of 2007 only stations that are within a radius of six detector-spacings to the stations that formed the trigger, i.e. 9 km, have been requested to send data. Before that the entire detector had been requested to provide data once an event had been triggered. This reduction of data consequently also reduces the expectation of stations removed as the expectation is proportional to the number of stations.

Therefore an identification of only those stations that have been rejected for physical reasons instead of technical reasons is needed to ensure that the expectations about the background are meet. For this purpose one can use the error flag that a station has in the reconstruction. As discussed in section 4.2.1 there are two reasons for stations to be removed that correspond to signals caused by particles not from the original air shower. Every signal that does not fit into the time window which is set by the shower is flagged as *out of time*. Also every signal that is too far away from the shower core without having additional neighbours is flagged as *lonely*. Those two criteria truly identify background. All other flags correspond to technical issues or lightning. Therefore the amount of truly accidental stations is shown in figure 6.2.

Taking into account that up to 2006 an average of about 1000 stations have been deployed and operational we could expect an estimated $N_{\text{accidentals}} \approx 6$. This number corresponds to the mean of the distribution. In 2008, after the read-out algorithm had been changed, the corresponding number of stations that were read out was

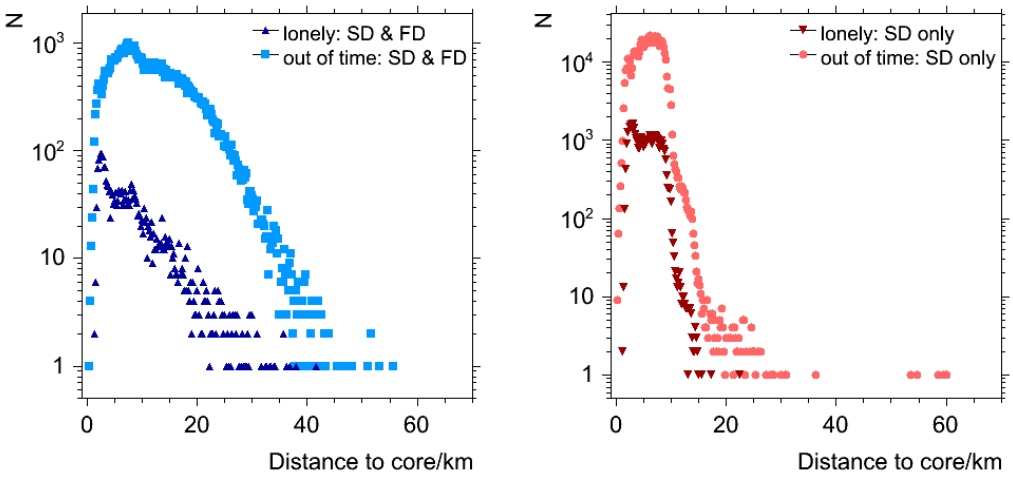

(a) Hybrid Events **(b)** SD Events

Figure 6.3: The distances of stations discarded by the reconstruction with respect to the shower core of the event from 2008 and 2009 are shown. It is distinguished between events only detected with the Surface Detector in (a) and those events also detected with the Fluorescence Detector (b). Furthermore it is distinguished between the accidental criteria *lonely* and *out of time*.

somewhere between 120 and 200. The exact number depends on the size of the shower as the read-out criteria is given in crowns of stations around the signal stations. The more stations are triggered by the shower the more stations are read out. Most showers measured with the SD are events having triggered three stations. If all stations around such an event had been operational 120 stations are read out. But this is only true for showers measured by the SD only. The Fluorescence Detector (FD) is able to trigger the read-out of a large portion of the array when it detects a shower to ensure that all necessary information for a Hybrid reconstruction is stored. In these cases up to half the array is read-out which corresponds to 800 stations. However, there are only about 10% of the events that are detected in coincidence. Taking all this into account $N_{\text{accidentals}} \lesssim 1$ seems reasonable. Again this is only a rough estimate, but the expectation is met by the analysis reproducing this value.

Nevertheless, accidentals yield more information than just their occurrence. In the following section the individual characteristics will be discussed in more detail.

6.2 Distribution of Positions

One of the first cross-checks that should be conducted is looking at the overall spatial distribution of accidentals and their distance to the shower core. If the background is removed correctly, one expects a smooth distribution in accordance with the number of stations read out and the structure of the array. The distribution obtained from the data is shown in figure 6.3.

The main effect on the distribution of distances is again due to the type of trigger applied, i.e. whether an event has been detected by FD and SD or only by SD. As accidentals can only be obtained from the data of the SD, the detection with the FD is not related to the accidentals detected but to the number of stations read out. The more stations are read out further away form the shower core the higher the probability to measure accidentals further away from the core. Every FD event triggers a read-out of about a quarter of all SD stations. An event only measured in the SD will only trigger a read-out of a certain number of stations around the actual event as discussed in section 6.1. In intervals set by the CDAS a complete read-out of the SD array is triggered. These so called *random triggers*, which are used to ensure the stability of the SD can explain the accidentals measured only by SD but very far away from the core of the shower.

One can see in figure 6.3 that the criteria according to which stations are discarded are always checked in the same order after each other, even though events might meet both criteria. First it is checked whether the timing is correct, thus most of the stations are flagged as *out of time*. In a second step it is checked whether the stations do have neighbouring signals or whether they need to be flagged as *lonely*. If a station is already discarded as *out of time* the second step will not be performed. The criteria for *lonely* as discussed in chapter 4.2.1 is a geometric one, distinguishing orders of neighbours in the hexagonal grid. Therefore the plateau near the shower core is not unexpected. Furthermore it is expected that we cannot have many accidentals very close to the core as we need actual signals neighbouring the core position in order to have an event. The rise of the distribution close to the shower core corresponds to an increase in the number of neighbouring stations.

Overall the distribution of accidentals does not look smooth but qualitatively all features can be explained by the way the Surface Detector is read out. A quantitative analysis would require more information about trigger distributions and the CDAS performance.

6.3 Distribution of Signal Strengths

The strength of the signals measured in the accidental stations yield further information that could be investigated, but again we first need an expectation for the distribution.

The signal distribution should be a mixture from uncorrelated atmospheric muonic underground and *little showers*. Little showers are those that have a lateral spread that is too small to have been measured in at least 3 stations, therefore those showers are below the trigger threshold and are only detected with a signal in one station.

From the muonic background we expect only a contribution concerning lower signals. To cause any signal in a local station we need muons that have a total energy above the Cherenkov threshold, thus for $\beta_{\text{water}} = n^{-1} \approx 1.33^{-1}$ of at least about 150 MeV. These particles need to cross the station within the time window of the trigger. The same is true for any other charged particle that has an energy above the Cherenkov threshold. If the energy of a muon is above 1.5 GeV the Cherenkov light will be

proportional to the track length. A VEM corresponds to one roughly vertical muon of at least 1.5 GeV.

The flux of muons at sea level at an energy of 1 GeV has been estimated to $\Phi = 2.24 \cdot 10^{-3} (\mathrm{m}^2 \cdot \mathrm{s} \cdot \mathrm{sr} \cdot \mathrm{GeV})^{-1}$ [81], which can be used as a lower limit for an estimation. In fact the Pierre Auger Observatory is located 1400 m above sea level, which should result in a significant increase in the muon flux. But assuming this flux as a lower limit we can at least estimate the expected number of muons in a station.

This flux can now be calculated for a local station from the SD. A local station covers an area of $10\mathrm{m}^2$ with a solid angle of

$$\Omega = \int_0^{2\pi} d\varphi \int_{\cos(\vartheta_1)}^{\cos(\vartheta_2)} d\cos\vartheta = 2\pi \int_{\cos(0°)}^{\cos(60°)} d\cos\vartheta = \pi \tag{6.2}$$

for vertical events, i.e. $\vartheta \in [0°, 60°]$.

The trigger requires a signal in a time window of 13 FADC bins, which equals to 325 ns. Thus transforming the flux into units of a local station shows that there is only a flux of $1.65 \cdot 10^{-8} (10\mathrm{m}^2 \cdot 325\ \mathrm{ns} \cdot \pi \cdot \mathrm{GeV})^{-1}$ of muons in a station. Even if adding the contribution of signals by muons of a lower energy, this flux of muons cannot be responsible for signals larger than a couple of VEM. Therefore only small signals will be caused by individual muons from the atmospheric background.

However, there is also the contribution of correlated signals from muons from showers. Most showers below the threshold energy of about 10^{18} eV will only be recorded in one station, since the lateral spread is not large enough to produce signals that are above the trigger threshold at larger distances from the shower core. Evidence for this can be found in events of an energy of $2 \cdot 10^{17}$ eV that have been detected in the SD. This was only possible, because their core had fallen right in between three stations, so the next closest stations are in about 860 m distance. Fore those events a S_{1000}, i.e. the signal that would have been detected at 1000 m from the shower core, can be calculated. For showers of this energy its value is between 1 VEM and 1.5 VEM. These values are well below the trigger threshold of each individual station. Keeping in mind that the distance between stations is not just 1000m but 1.5 km, these showers can only be detected if there is a suitable location of the core. Consequently, the SD has full trigger acceptance only at energies above $3 \cdot 10^{18}$eV.

Those showers contribute to the number of accidentals. Concerning the distribution of signals one should therefore see a decrease in the rate following the decrease of flux of air showers with a rising energy, as discussed in chapter 2. But the spectrum of the signals from accidentals does not necessarily have to have the same exponent as the decrease in flux of air showers. The signal measured will depend on the energy of the shower, but also on the exact position of the shower core with respect to the position of the station. The closer the shower core is the higher the signal will be. But if the shower core if too far from one station it might already trigger the next station. Therefore the spectrum will be a combination of decrease in flux with energy and lateral spread, also influenced by signal fluctuations as the signal strength is not strictly proportional to the energy of a shower.

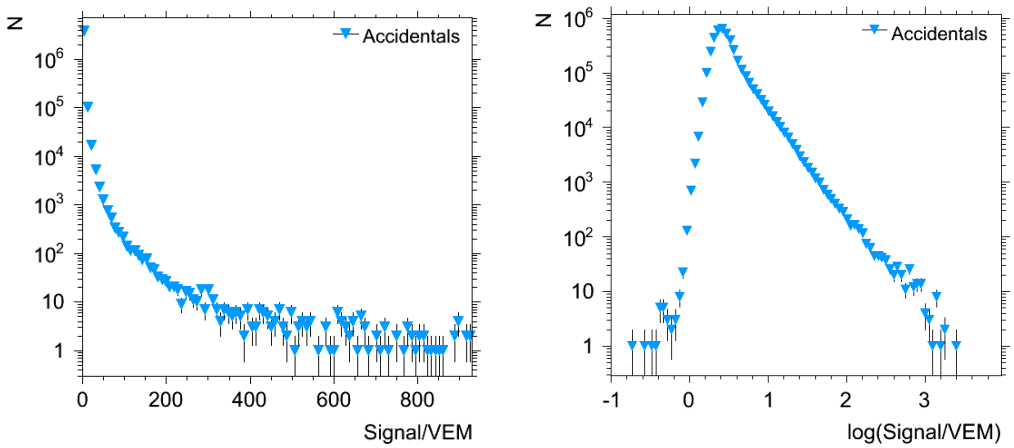

Figure 6.4: Distribution of signal in the stations discarded by the reconstruction. The left side shows the overall distribution, a steep decrease with signal strength can be seen. Only about 200 events remain with signals larger than 300 VEM. The right side shows the same distribution but with a logarithmic scaling. The number of signals decreases roughly according to a power law with an exponent of about 3.

It was found in [82] that one can roughly estimate the energy of a shower from one station. This study was done to improve the reconstruction of events measured by the FD with only one station from the SD, but the results are transferable. They show that for signals larger than 20 VEM in a station very close to the shower core there is a general relation of

$$E \approx S[\text{VEM}] \cdot 10^{15}\text{eV}. \tag{6.3}$$

Thus a shower of $10^{17.5}$ eV will correspond to a signal of about 300 VEM. The upper limit for individual accidentals should be signals of up to 1000 VEM $\approx 10^{18}$eV, as at this energy the trigger threshold will be reached in a distance of 1.5 km. It also has to be kept in mind, that at somewhere below 1000 VEM the saturation of the station electronics will set in, which will prevent the entire signal from being recorded. This study was only done for events reaching as low as $10^{17.5}$ eV. It is questionable whether the results could be completely extended further to lower energies.

Figure 6.4 shows the signals of all accidentals measured with the Surface Detector. First of all the trigger threshold is visible. Regularly signals of at least 3 VEM are needed in order to be recorded, which corresponds to the most prevalent trigger type. But since the calibration of the station and the one in the reconstruction rely on different methods, some events below this threshold are expected. Furthermore, the number of accidentals decreases with signal strength as it was expected. One can fit a power law to the right part of the distribution receiving an exponent of about -3.0 ± 0.7 depending on the range of signals included. As the flux of air showers decreases with an exponent of -2.7 up to -3.1, this is also within the expectation, if we consider the unknown effects of the location of the core, as well as the shower to shower fluctuations that are quite high close to the core.

One can see that there are about 200 events having signals larger than 300 VEM, which can only be caused by air showers if they are real signals. To gain the expected number of those events one can derive an estimation from the flux. Signals of this strength can only be caused by showers of higher energies hitting the station directly. From for example figure 2.1 one can obtain a flux of particles:

$$\frac{\Phi(E_0) \cdot E_0^{2.5}}{E_{bin}} = \Phi_0 \left[\frac{eV^{1.5}}{m^2 \cdot s \cdot sr} \right] \tag{6.4}$$

This flux has to be scaled to the effective area of the detector and the time in which this detector is read out. As the detector is only read out in case of a T3 event the detector is not continuously sensitive to accidentals. The T3 rate is about 1 event per minute. For each event a 60 μs window is read out. This reduces the time in which an accidental can be detected. At every trigger 200 stations, each having an area of 10 m^2 are read out. Furthermore, the angular acceptance is assumed to 2π.

The estimation does significantly depend on the energy bin chosen as lower limit for those showers that still induce a sufficiently large signal. Unfortunately the shower and detector simulations of the SD require a minimum of three stations to be triggered. Therefore a simulation cannot be used to estimate a lower energy bound. It is also questionable how far a shower core can be from the central station in order to have only triggered the central station with a relevant signal. If the core is too far away the signal will not be strong enough for the highest signals and the shower might already trigger the next station. This distance will determine whether the effective area of the detector is only the actual size of the SD stations or whether this factor has to be enlarged. Allowing for example shower cores up to 100 m from the position of the station already increases the expected rate by a factor 300 compared to allowing cores only within the area of the station. As all those signals are below the threshold energy of the SD no studies concerning the behavior have been conducted so far.

Using as an example an energy of 10^{15}eV with a binning of 10^{14}eV with only the 10 m^2 area of 200 stations, this estimation results in a rate of about 0.1 event/year. Adding a factor 300 for the effective area, there are already 30 expected events per year. We have shown that small changes in assumptions will influence the resulting rate. As it is also known that signals near the shower core tend to be very sensitive to signal fluctuations one cannot argue for sure that showers of this energy are needed for such kinds of signals. Also we do not know the exact form of the LDF close to the core, that is why there is no theoretical estimate for a signal.

However, we can conclude that 200 accidentals of this size, which corresponds to about 50 per year, are in the order of magnitude of our expectation. However, since all information about those accidentals and especially their true origin has to rely on very few information from a single station, one cannot make more exact conclusions. Therefore using some more cross-checks to gain insight into the matter of accidentals is certainly worthwhile.

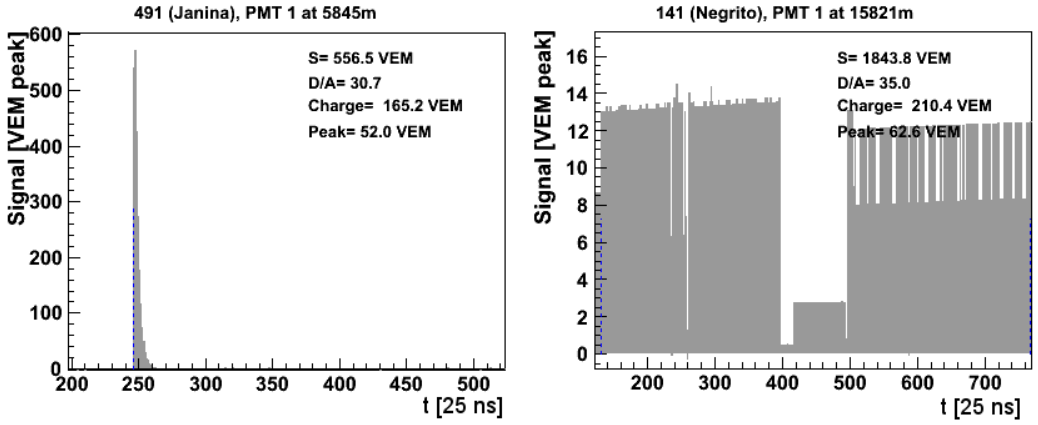

(a) Event 9325502 **(b)** Event724778

Figure 6.5: FADC signal traces of accidental stations with large signals are shown. The strength of signal in units of VEM is plotted against the time of the FADC bins. The FADC bins are numbered on the x-axis. Most signals are represented by the left figure (a), depicting a typical signal near a shower core. Only one station shows a defective signal, as shown on the right (b).

6.4 Large Accidentals

Especially the large accidentals could contain further interesting information. A subset of 230 accidentals was chosen with signals larger than 300 VEM. This cut was set on a balanced level between large signals and sufficient statics. Before establishing characteristics it is necessary to ensure that the signals are actually measured physical signals and not due to for example a failure in the electronics. Therefore a cross-check was conducted about what these signals look like. If they are small showers they should have a very common signal shape similar to the signals of showers with higher energies near the core.

In fact nearly all of the accidentals show FADC traces that look like the left trace in figure 6.5 (a). They show very high signals in a rather short time period, as one sees near shower cores. Only one accidental is different, as shown in figure 6.5 (b). Probably, when measuring this trace an error in the electronics occurred as the signal shows very sharp edges which look like artefacts from the electronics. This signal is removed from the set of large accidentals for further analysis.

Overall it is reasonably safe to say that most of the large accidentals look somewhat like small showers. As these showers occurred sometime near an actual shower a question could be whether those two events are related. As there are theories as discussed in chapter 2 that suggest that a second cascade can be caused in air showers due to exotic physics, it could be interesting to establish whether a connection between the actual shower and the large accidental could at all have been possible.

6.4.1 Test of timing compatibility

The most important restriction for a causal link is given by the timing. If we assume that a part of the original cascade has split apart due to some unknown effect and

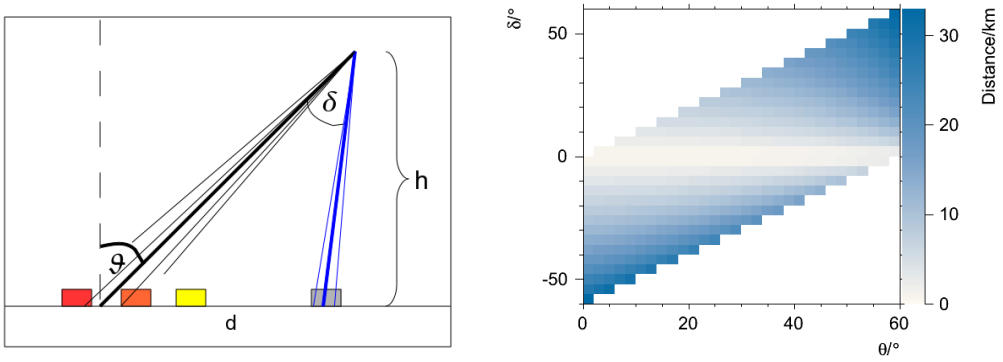

(a) Geometry of Event **(b)** Possible Distances

Figure 6.6: Shown are the geometrical restriction of accidental and shower in case of split-off. It is assumed that a second shower was created and developed independently from the original shower as shown in (a). The right side (b) shows possible distances that such a shower would have from the original shower when detected on the surface. The split-off angle δ results in different distances d of the accidental from the shower core, depending on the angle ϑ of the shower.

was detected by the SD as an accidental, this accidental should still be in a loose connection in time with the shower. In order to verify this idea a geometric approach was used. In figure 6.6 the schematics of such a split-off are shown. We assume that a part of the shower has been disconnected from the rest of the shower and developed an independent shower of its own. So possible distances of this second shower to the actual shower core can be calculated depending on the original zenith angle ϑ and the split-off angle δ. Some restrictions are made on the split-off angles to keep the resulting showers and the accidental reasonably close together. As both showers are in fact highly relativistic the split-off angle δ cannot be too large if the conservation of impulse is given. Since we do not know what might have caused this effect this criteria will be handled very loosely. Therefore a radius d of 20 km around the shower core is set as cut in order to still enable a possible causal link. With this restriction the split-off angle will then have a maximum of about 30°. This cut has the advantage that the differences between data taken in different years will be not too large. As already explained, in earlier years a larger portion of the detector was read out, so more accidentals further from the shower core were detected. By restricting ourselves to 20 km we assume a similar, yet larger cut in retrospective. From these assumptions and the geometric model a possible timing difference can be calculated.

The timing difference of the accidental and the shower depends on the height in which the split-off could have taken part. The atmospheric height of the primary interaction of a shower is usually assumed to be about 15 km. But as it depends on the energy and nature of the primary particle, as well as the zenith angle, and is influenced by atmospheric conditions, there is an uncertainty to this height. If a split-off can take part it has to be within the first interactions since possible unknown interactions could only take place at the highest energies.

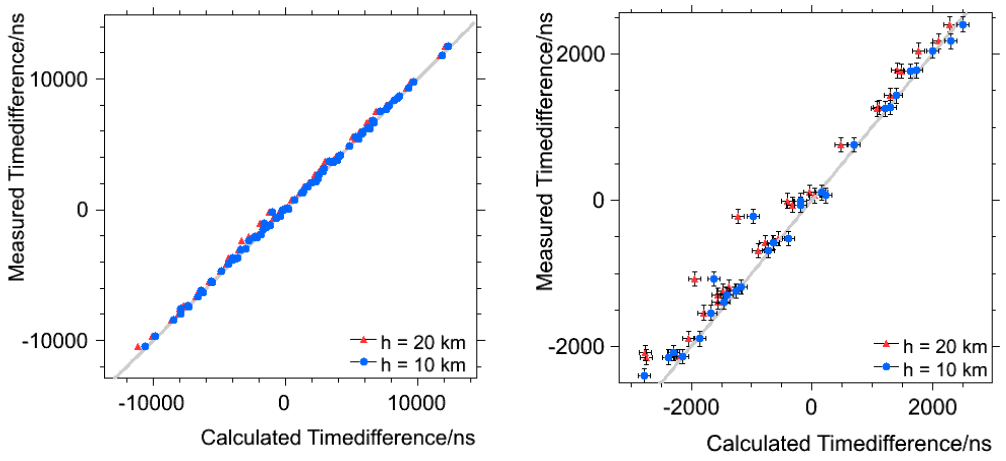

(a) Overview **(b)** Detail

Figure 6.7: Timing of regular showers measured by the Surface Detector according to a simple geometric model. From regular showers the station with the largest distance to the shower core was chosen to calculate a possible difference in time with respect to the shower core. This timing was then compared with the measured timing difference. Negative timings represent stations that should have triggered before the shower core.

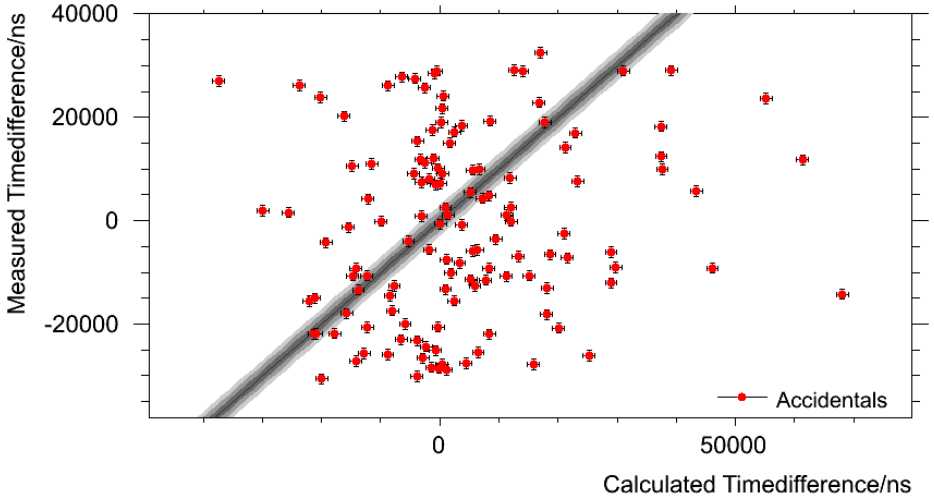

Figure 6.8: Comparison of the measured timing difference of an accidental station and station closest to the shower core with the timing difference that could be allowed for a causal link between accidental and shower. The line through the origin marks the region in which the accidental could have been linked in timing to the shower. The error bands were derived from the spread of the method, tested with regular events as shown in figure 6.7.

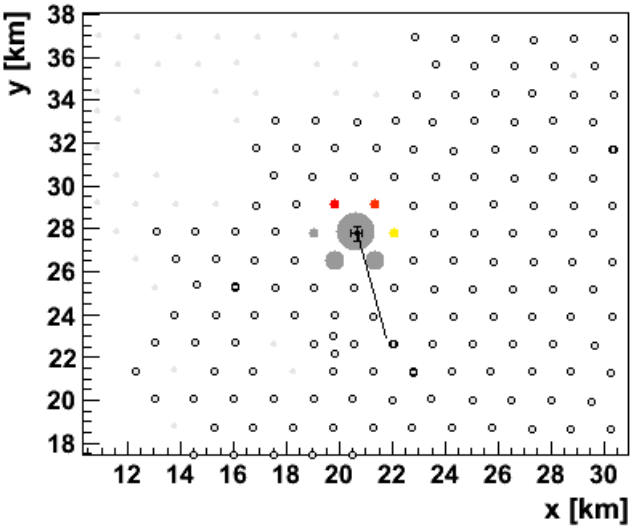

Figure 6.9: From its footprint this Event 1272553 shows a removal of the central station of the shower rather than an accidental. The gray stations were removed for out of time reasons and flagged as accidental.

The result of the application of this model to the regular events is shown in figure 6.7 and can verify the method. For regular showers the timing of the central station of the shower was compared to the timing of a station with a larger distance to the core. The general expectation is met by this simple model. All events can be found near the line through the origin, which shows that the measured difference in timing between stations equals the expected timing according to this model. Zooming in, as it is done in figure 6.7 (b), one can see that the expectation is not fully met. Furthermore one sees that the expectation from a height of 10 km produces a better result than the one from 20 km. This is due to the fact that a real shower does not split apart and that the timing of all particles is a lot more similar, especially in showers that do not have a large lateral spread. In contrast, showers having a larger lateral spread, i.e. those with larger differences in time, so for example those in the lower left corner, are better described with a height of 20 km. Overall, it can be concluded that this model is suitable to identify timing constraints within a certain uncertainty.

Figure 6.8 shows the results of the application of this method to 130 events having an accidental station with a signal larger than 300 VEM within a radius of 20 km from the shower core. From this plot one can exclude several events that have a down time, which can not at all be related to the actual shower. These are those that are not contained by the gray error bands. Therefore most of the events can be seen as truly accidental. Nevertheless there are some events that could be related to the shower, i.e. the events that are spread along the line through the origin. With respect to their errors and an estimated error on the method, 14 events can be kept as suspects for further analysis. The only exception is shown in figure 6.9. Apparently, the reconstruction disregarded stations as belonging not to the event which should be part of the shower, in fact being the actual shower core. Even

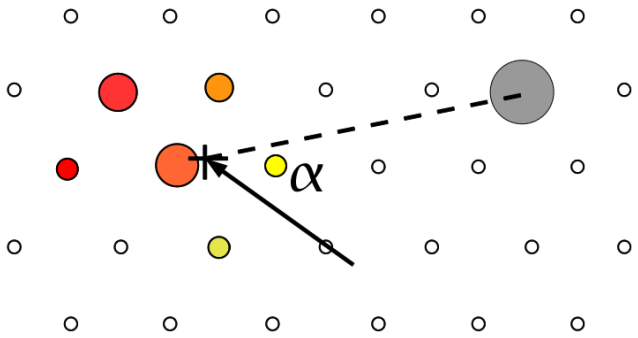

Figure 6.10: The drawing illustrates the calculation of the angle α between the azimuth of the shower and the location of the accidental station in the detector plane.

though they are removed as out of time, their timing information seems reasonable. An explanation could be that the time window that determines an exclusion was set by stations, which were later than the shower core and therefore the stations were excluded. This could have happened if no T3 had been formed by the central stations during data acquisition.

Overall it is interesting that indeed some event could have been linked to the shower assuming purely geometric constraints. These events could be investigated further, to establish whether an connection could have been possible.

6.4.2 Test of local correlation

Having checked the accidental events for the compatibility according to their timing and dependence on the zenith angle, the next step should be to take a look at the distribution with respect to the azimuth angle of the coinciding shower. Generally, all events should be found randomly around the actual shower core having no correlation to the azimuth angle of the shower itself, if they are independent from the shower. But if a second shower is caused by the same primary interaction and is detected by the SD as an accidental, we expect to see more accidentals in the area of the direction of the shower. This is only true if the zenith angle ϑ is larger than 0. For strictly vertical events the accidentals should be uniformly distributed around the event. But there are in fact only very few strictly vertical events.

A possible correlation can only be investigated without having any information about the angle of the accidental, since an angular reconstruction is only possible with at least three stations. Therefore, again a geometric approach was followed as shown in figure 6.10 An imaginary line was drawn along the azimuth of the shower as it is usually shown in shower footprints. Another line was drawn connecting the position of the accidental and the shower core. The angle α between those lines can then be used as an estimator. If the accidental arrived from the direction of the shower it is more likely to be detected with an angle α smaller than 90°. If it is detected on the other side it would have had to cover a longer distance, which would result in a less likely detection.

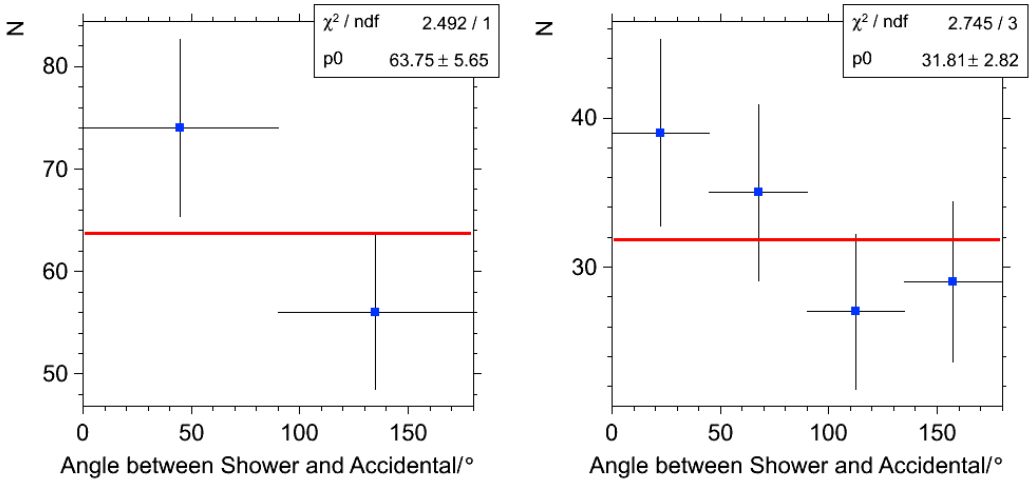

Figure 6.11: The two figures show the angle between the azimuth of the actual shower and a line connecting the position of the accidental with the shower core. The fit of a constant is also shown. As the method does not distinguish between sides, the maximum angle is 180°. Altogether there are 130 accidentals of a signal strength larger than 300 VEM, therefore 130 entries in each histogram. The left side emphasizes the difference between *in direction of the shower* and *direction opposite to the shower* by showing less bins.

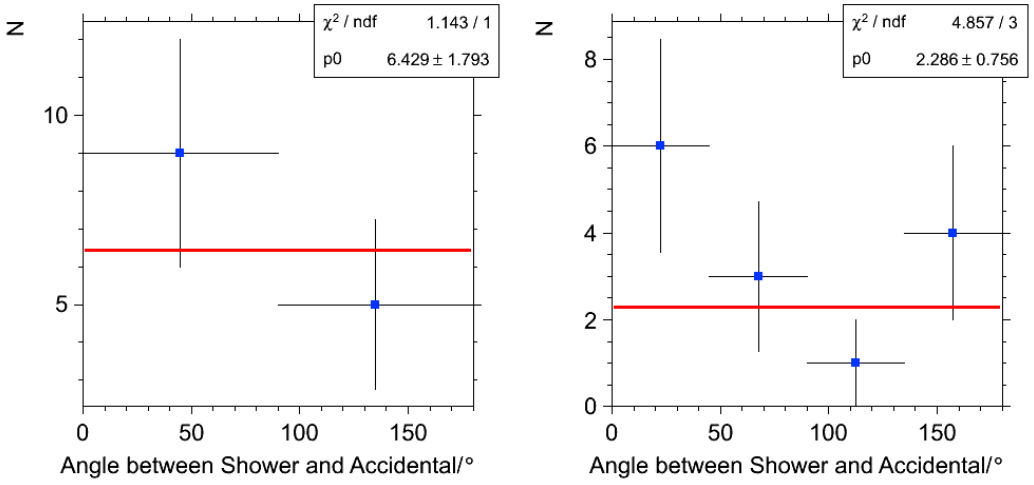

Figure 6.12: As in figure 6.11 the angle between the azimuth of the actual shower and a line connecting the position of the accidental with the shower core is shown. The number of events included is restricted to 14 accidentals with a signal larger than 300 VEM that occurred in a time window that enables a causal link to the original shower, as depicted by the gray area in figure 6.8. The selection of those events decreases the difference between the first bin *from the direction of the shower* and the second bin *direction opposite to the shower*. Still the structure of the distribution seems to stay the same.

The results from this method are shown in figure 6.11. Apparently there are more events that are within this definition from the direction of the shower than those from the opposite direction. But this effect is only 2.2σ with 130 events and therefore not statistically significant. As in the first step all accidental events are used, even those that are far out of time, it is consequent to show the same results for those 14 events that were kept as suspects for further analyses. The results of the method applied only to those selected events are shown in figure 6.12. The significance of the difference did not strengthen, but it has to be kept in mind that there are now only 14 entries in the histogram. Interestingly the structure of the distribution seems similar, which suggests that the cut on timing did not select a specific subset with different characteristics. Altogether, one cannot conclude a deviation from the expected uniformly distributed events.

Overall, the discussion of large accidentals did not yield significant evidence for events that deviate from the expectation. It was a valid cross-check for our understanding of the background, the detector and the reconstruction. However, more statistics might make revisiting those events worthwhile. A full list of all events with accidentals and their categorization is given in appendix A.3.

After having discussed features concerning the overall structure of events, one can go again further into detail. A valuable handle should be the actual reconstruction, especially the fit of the lateral distribution function. It is necessary to develop statistically and mathematically valid criteria that can be used to identify classes of regularly reconstructed events that show a deviation from the expected behavior.

7. Assessing the Quality of Reconstruction

When looking for measurements that do not meet an expectation it is a common approach to estimate the quality of the reconstruction and its parameters in order to identify those events of an insufficient quality. Still, it is not always straightforward to identify a variable that can be used as an indicator for the goodness of a fit. One of the most commonly used variables is the χ^2-value or the χ^2-probability respectively, as it is easy to calculate and yields easy to handle information. It will be discussed to what extent this estimator can be used to assess the quality of the reconstruction of the lateral distribution function (LDF). An alternative approach using the Maximum Likelihood function of the LDF will also be presented.

7.1 χ^2 -Analysis

The χ^2-test is a very common method to test whether a model is compatible to a given set of data [83]. The χ^2-value itself is related to the number of data points and can directly be converted into an estimation about the quality of a reconstruction. The χ^2 can be used for any kind of model to be tested as long as a Gaussian error model can be assumed. It is an absolute estimator for the quality of a fit and easy to be calculated and is therefore widely used.

The general approach is based on a comparison of data points with a theoretical distribution derived from a model. Given the data points $y_1, y_2 ... y_n$, which depend on a variable x_i, thus $y_i(x_i)$. The question is whether those values are compatible with the model $y_m(x_i)$. The value that can be used as an estimator for an answer to this question calculates to:

$$t = \chi^2 = \sum_{i=1}^{n} \frac{(y_i - y_m(x_i))^2}{\sigma_i^2} \tag{7.1}$$

This estimator is called χ^2 if the y_i follow a standard normal distribution and are a random sample of the theoretical model, which is usually true for measurements at high statistics. The general χ^2-distribution is therefore the sum of the squares of n independent standard normal random variables as for such a type of distribution the expected value $y_m(x_i)$ is zero and the standard deviation σ_i one. The number $k = n$ is referred to as *degrees of freedom*.

Usually a model that will be tested has also parameters p_j that are fitted to the data.

$$t = \chi^2 = \sum_{i=1}^{n} \frac{(y_i - y_m(x_i, p_j))^2}{\sigma_i^2} \tag{7.2}$$

This reduces the degrees of freedom to the difference of data points and parameters, i.e. $k = n - j$.

If the error model is not Gaussian, the χ^2 test can with restrictions also be applied. For example, a Poisson error model can always be approximated with a Gaussian error for large values of the data. Also, the χ^2 will follow the standard χ^2-distribution if the number of degrees of freedom in the fit is sufficiently large (> 10), even if the errors still have to be considered as Poisson. For other error models the validity of the χ^2 test is a-priori not given.

When testing the compatibility there are different possibilities. When only looking at one set of data it is a rule of thumb that a fit is good if the χ^2-value equals approximately the numbers of degrees of freedom. This is due to the fact that the expected value of a χ^2-distribution corresponds to the degrees of freedom.

When testing more than one set of data one could compare the distribution of χ^2 from the data sets to the expected distribution. However, this is not very intuitive since one always needs to compare to a standard χ^2-distribution, which would require an additional mathematical test. Alternatively, the χ^2-probability can be used. It denotes the probability that an observed χ^2 exceeds the value by chance, even for a correct model. It therefore corresponds to the cumulative distribution. Consequently, many of those probabilities from data sets and a correct model should follow a flat distribution. A flat distribution can easily be identified, even with the eye.

7.1.1 Application to data from the Surface Detector

It is of course possible to calculate the χ^2-probability for the data from the Surface Detector. All stations with a signal will contribute a term, where S_i is the measured signal and $S(r_i)$ is the expected signal from the LDF in dependence on its parameters.

$$\chi^2 = \sum_{i} \frac{[S_i - S(r_i)]^2}{\sigma_{S_i}^2} \tag{7.3}$$

Nevertheless, it is questionable whether this test is applicable. As discussed in chapter 4 the error models of the signals are not all Gaussian. Furthermore, stations such as the saturated stations or zero-stations are only used as upper respectively lower limit. Therefore their contribution will not lead to a regular χ^2-distribution.

Furthermore, there is an issue concerning the number of events that can be used for such an analysis. As the LDF has at least three parameters that will be fitted the number of degrees of freedom will be zero for most of the events since there is only data from three stations. Overall only about 20% of the events from the Surface Dectector contain signals in more than three stations. One can argue that

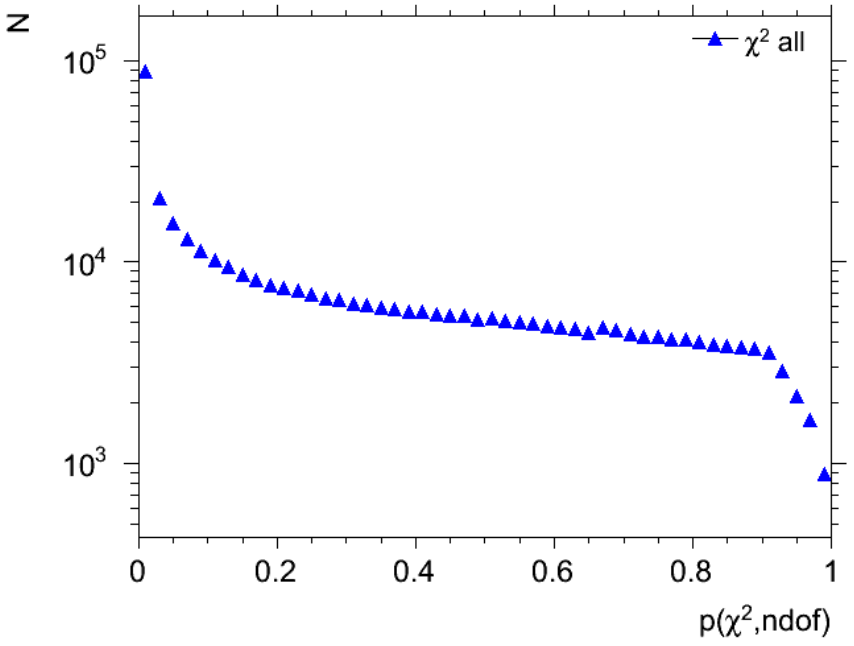

Figure 7.1: The χ^2-probability is calculated for all SD events with at least 4 stations that have measured a signal. No additional cuts are applied. The number of degrees of freedom corresponds to the difference of number of stations and parameters that are fitted. The number of parameters is usually three, only in very few cases it is four as discussed in chapter 4.3.

those low multiplicity events are the least interesting since they are below the full trigger acceptance and of low energy. Therefore they will not be used for studies of the spectrum and other prominent analyses. But in the search for exotics also those events yield valuable information. As shown in section 5.3 low multiplicty events can for example have a reconstruction that does not seem to match the data convincingly.

However, as the χ^2 is such an intuitive estimator for the quality of a fit and is widely used, it is worthwhile to test what information the χ^2 can yield about the LDF fit and whether this parameter can be used to identify special classes of events.

When looking at the distribution of the χ^2-probability for all possible SD events as it is shown in figure 7.1, there are certain interesting features. First of all the distribution is not flat. The first bins near zero have significantly more entries, while the last bins near one have less entries than the average. Without prior knowledge such a distribution would hint at a reconstruction that does not suit the data. But since we know that the mathematical approach for the calculation of χ^2 is not completely applicable in this case, a deviation was expected. Therefore it will be discussed whether the method can be refined to obtain more information.

To ensure that the distribution of χ^2-probability is not biased from characteristics of the events a cross-check on the correlation of this distribution on different event characteristics was performed. The results are shown in figure 7.2. Overall, the

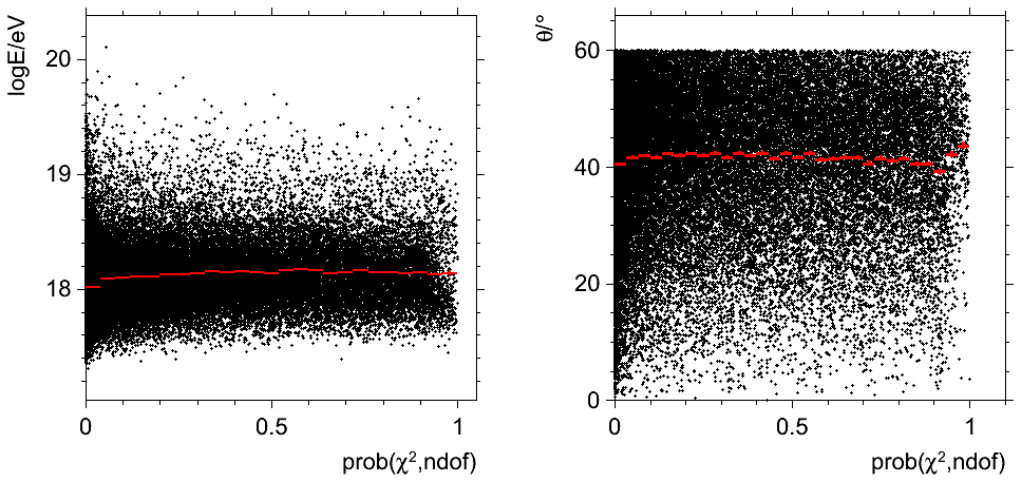

Figure 7.2: The left side shows the dependency of the χ^2-probability distribution on the reconstructed energy of the shower. The right side shows the dependency of the χ^2-probability distribution on the reconstructed zenith angle of the shower. The red marks indicate the mean energy or angle in the relevant probability bin.

means of each probability bin are fairly equal. There seems to be no large dependence on energy or angle, as there are only slight deviations. Starting with the dependency of the probability distribution on the energy, one can see that the mean energy of small probabilities is slightly lower than for other probabilities. This might be due to the fact that a lower probability relates to a too high χ^2-value. In showers with smaller energies there are less stations and therefore less data points, which results in a less reliable fit and possibly awkward station configurations.

In the dependency on zenith the mean angle at higher probabilities has the tendency to be higher than the other mean zenith angles. Here one has to keep in mind that the angular region near 60° is a transition region. Showers more inclined than 60° are reconstructed with an entirely different reconstruction, e.g. [84], as one can no longer neglect the influence of the curvature of the earth and the geomagnetic field. The differentiation at 60° is a convention, therefore showers from that transition region can already be influenced into deviating characteristics if reconstructed with the standard vertical reconstruction.

A methodically similar χ^2-study has been conducted for the reconstruction of the shower profiles of the FD events [85]. Having the advantage that the fit of a *Gaisser-Hillas-profile* is based on a Gaussian error-model for every contribution, the χ^2-probability distribution can be interpreted easily. The distribution is also in this case not flat. The first bin is again significantly enhanced. The rest of the distribution is u-shaped, showing again fuller bins near one. A structuring of the data into subclasses showed that different classes contribute differently to the χ^2-probability distribution. Thereby events that have been disturbed by atmospheric effects could be identified. As these effects can also be identified by monitoring the atmospheric conditions the χ^2-probability distribution worked as a cross-check for the detector. In the hunt for exotic physics, so far no significant class of events was found.

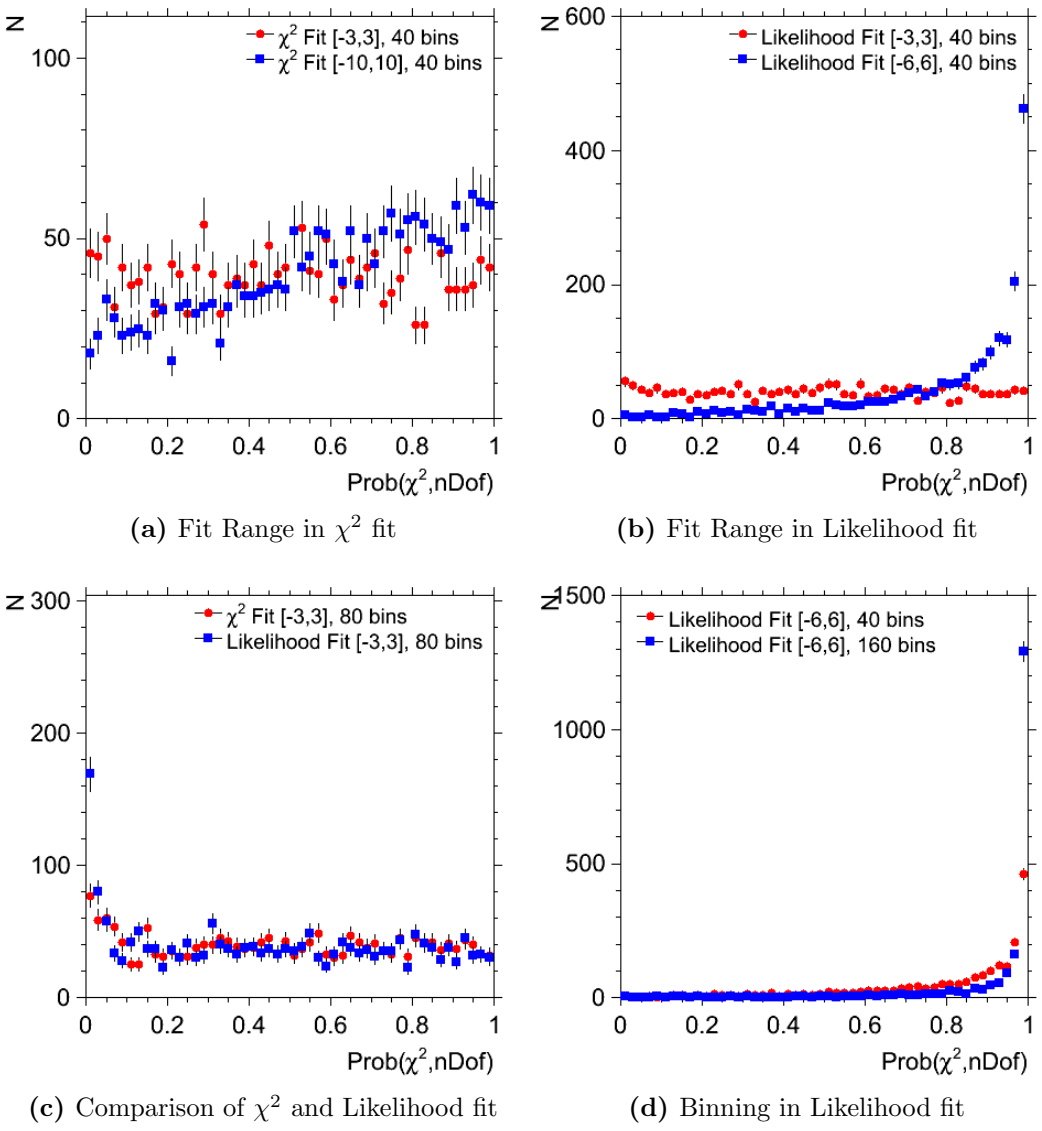

(a) Fit Range in χ^2 fit

(b) Fit Range in Likelihood fit

(c) Comparison of χ^2 and Likelihood fit

(d) Binning in Likelihood fit

Figure 7.3: In a toy Monte Carlo model the dependency of the flatness of the χ^2-distribution was tested. 2000 histograms were filled with 1000 Gaussian random numbers. A Gaussian distribution was then fitted and the χ^2-probability calculated. Various factors that influence the fit were changed as described in the individual legends.

7.1.2 Validity of χ^2 for quality tests

The general question when dealing with data is how sensitive the χ^2-probability distribution is to different components of a reconstruction. From various physical results it is known that the distribution is rarely completely flat, even if the model is in overall good agreement with the data.

To explore and illustrate the dependencies a toy Monte Carlo model was used. Random numbers according to a standard normal distribution were generated, and afterwards a Gaussian function was fitted to this data. From this function and the gene-

rated data the χ^2-probability was calculated. This was repeated several times in order to receive a probability distribution.

As each random data set was defined to follow a Gaussian distribution, which was later fitted, the resulting χ^2-probability distribution from all sets should be flat according to the model. Overall this is true. But there are dependencies on the fit routine that can already influence the distribution.

In figure 7.3 one can see different probability distributions received from the same data set but with different restrictions on the fitting process. Very influential on the shape of the χ^2-probability distribution is the fitting range as well as the binning of the data. The dependency on the binning is expected as the χ^2-contribution is calculated for every bin. Therefore the number of bins will influence the value. For real data this should not be problematic, as the data is fitted without binning. The effect that the fitting range could only be explained by analyzing the fitting routines of ROOT [86], the software with which this small model was tested. There might be a difference between the handling of Poisson and a Gaussian error, especially for low values, which could explain the dependency as a larger fitting range includes more small values.

Furthermore, there are significant differences between a fit based on a likelihood minimization as opposed to a χ^2-minimizing fit. When a likelihood minimization is used, the fit does not minimize the χ^2. The relevant value of χ^2 can only be calculated after the fit has been done. Therefore a difference between those two results is in general possible, even though a Gaussian error model for a likelihood minimization should correspond to a χ^2-minimization. Where the exact differences derive from will be due to the exact implementation of the fit routines in ROOT. Identifying these differences cannot be conducted in this thesis. But as ROOT is used in nearly all particle physics analyses as well as in Offline, one should keep in mind certain dependencies. Therefore the χ^2-distribution does not necessarily need to be completely flat, even though it should theoretically be flat for a correct model.

This toy Monte Carlo Model can be developed further by generating data with Gaussian errors from a lateral distribution function instead of a Gaussian distribution. When using only stations with a Gaussian error the χ^2-probability should be reasonably flat as shown in the simpler model. For this purpose LDFs from events with a high station multiplicity were chosen. In the range of a high signal, in which a Gaussian error model should be appropriate, station positions were chosen and data was generated from the LDF expectation. The results from this model are shown in figure 7.4 and compared to the flattest distribution derived from the simpler model using the Gaussian distribution.

The comparison shows that this Monte Carlo model is also possible for values generated from the LDF-expectation. The distribution derived from this model is reasonably flat. Therefore effects that influence the distribution might be identified according to the type of events and its stations.

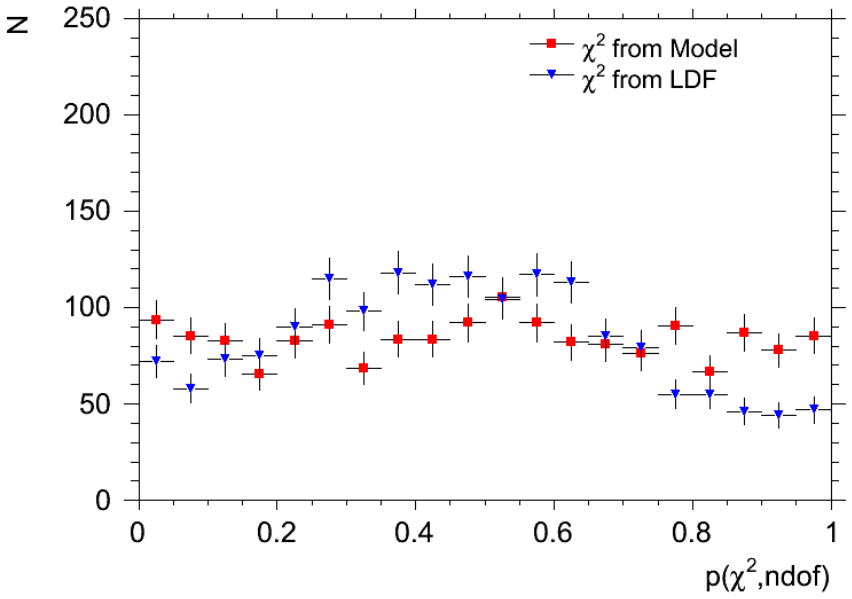

Figure 7.4: The results for a Monte Carlo model for data generated from a LDF are shown. The χ^2-probability distribution is compared to the results from generating a Gaussian distribution as done in 7.3 (a) and (b). 2000 data sets with Gaussian errors were generated from LDFs and the χ^2-probability was calculated.

7.1.3 Subclasses

All stations that have measured a signal without any saturation of the electronics should not add an unusual contribution to the χ^2. The Gaussian stations fulfill every criteria necessary, while those with small signals, i.e. Poisson statistics, can roughly be approximated in a χ^2-test. More problematic are the stations that are only used as a limit for the maximum likelihood fit, which are the zero-stations and the saturated stations. On the one hand it is questionable whether their contribution will have an effect on the number of degrees of freedom as information is added but not as restraining as from a regular station. On the other hand it is difficult to estimate what a reasonable contribution to the χ^2 could be.

In the current reconstruction in $\overline{\text{Off}}\underline{\text{line}}$ an extra contribution is added by default for zero-stations, but their information does not lead to an extra degree of freedom. In this contribution $S(r_i)$ describes the expected signal from the LDF and σ_{S_i} the expected error.

$$\chi^2_{\text{zero}} = \sum_{i}^{\text{zero-stations}} \frac{S(r_i)^2}{\sigma_{S_i}} \tag{7.4}$$

This factor is added for every station up to a predefined cut-off radius to the shower core. Therefore their χ^2-contribution adds as if there had not been a signal at all, although the known information is only that the signal must have been below the threshold. By default the cut-off radius is 10000 m, but from 1000 m there will be a soft transition that will decrease the contribution.

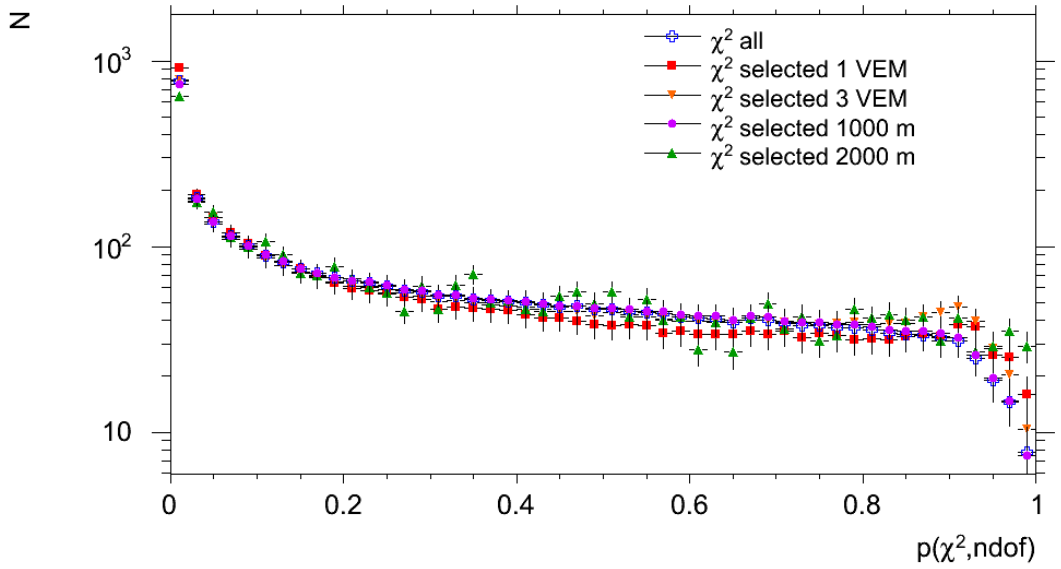

Figure 7.5: The χ^2-probability is calculated for subclasses of events. The blue crosses correspond to the χ^2-values from all events. The selection with a VEM value excludes those events that have zero-stations for which the expectation from the LDF is higher than the exclusion value. The selection according to a radius excludes events that have zero-stations within this radius. All distributions are scaled to the same number of entries.

This approach seems reasonable if a fit is conducted by minimizing the χ^2-value. But as the χ^2-minimization has proven to be less reliable it is no longer used for the default reconstruction. When calculating the χ^2-value from a Maximum Likelihood Fit this method does not seem to be mathematically correct. The same is true for the contribution to the χ^2 of the recovered saturated stations, which are handled like regular signals.

In order to check whether those factors influence the shape of the χ^2-probability distribution subclasses of events were investigated. When restricting ourselves to events that do not have stations near the core without signal, i.e. zero-stations, or saturated stations the distribution should flatten, if the model is correct and those types of stations contributed the disturbing terms.

The number of events is drastically reduced when only using subclasses. The following table shows the number of remaining events in the subclasses and their respective fraction of the entire data set. The subclass *All* corresponds to all events that have signals in more than three stations. All other classes will be explained in the following discussions.

Class	All	1 VEM	3 VEM	1000 m	2000 m	no saturation
Events	384939	71951	174912	348031	3383	366073
Fraction	21.8%	4.1%	9.9%	19.7%	0.2%	20.7%

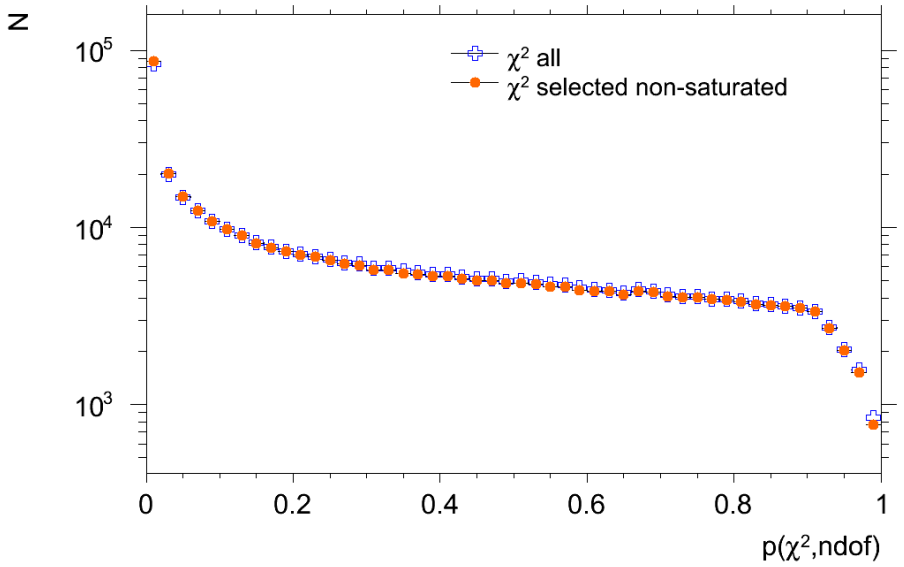

Figure 7.6: The χ^2-probability is calculated for subclasses of events. Here the distribution from all events having more than four station is compared to a subclass of events without saturation. Both distributions are scaled to the same number of entries.

When trying to exclude zero-stations there are two possible approaches. A more relaxed criteria can be that all events are excluded in which the LDF predicts values above a certain threshold (1 VEM, 3 VEM) for stations that did not measure a signal. A very strict criteria is to exclude all events that have zero-stations within a certain radius (1000 m, 2000m). The results from both approaches are shown in figure 7.5.

First of all it has to be noted that the overall shape of the distribution did not change. But details in shape vary between the subclasses. The first bin is a lot higher than the rest in every distribution. However, it has to be kept in mind that the diagram has a logarithmic scaling, which shows that the entry from the cut at 2000 m is already 30% lower than the highest value.

The cut on zero-stations within a distance of 1000 m to the shower core influences the distribution the least. This is not surprising since there are only very few events that are within this category as already discussed in chapter 5. Cutting on expectations from the LDF influences the distribution but does not flatten it. This is probably due to the effect that such a cut is an a-posteriori cut on reconstructions that have already been influenced by such stations.

The cut that flattens the distribution the most is the cut on a distance for zero-stations nearer than 2000 m. In this region the zero-stations add the largest contribution. Especially the bins close to one are higher than in the other distribution. Also the distribution is not quite flat in the middle section. This can possibly be explained by the fact that there is very low statistics for such kinds of events. Therefore an even larger cut-radius is not feasible.

Similarly to the exclusion of zero-stations saturated stations can be excluded. This results in a distribution as shown in figure 7.6. This distribution is completely compatible with the one from all events. When it comes to flattening excluding saturated stations does not contribute.

The formation of subclasses leads to the assumption that zero-stations have the largest effect on the shape of the distribution. For inclined shower, i.e. having a zenith angle of more than 60°, a special study has been conducted about the effects that zero-stations have. It shows that certain parameters derived from the reconstruction are especially sensitive to the threshold value applied for zero-stations. As the reconstruction of inclined showers differs from the one for vertical showers the results cannot be directly transferred. It is however stressed that comparable effects are expected for vertical showers and that further studies are needed [87].

7.1.4 Reconstruction using only Gaussian contributions

Developing the idea of forming subclasses further leads to the concept of recalculating the χ^2-value from only Gaussian stations. If the χ^2 is recalculated using only the contributions that are Gaussian the χ^2-value should be correct. But if the actual fit is performed with all stations the method will still include a bias. Therefore consequently a reconstruction with only Gaussian station is needed for a mathematically correct χ^2.

Overall there are 1751 events in the data set that have four or more stations in the signal range, where the signal can be considered Gaussian. These events were fitted with a maximum likelihood function that contained only the values from the Gaussian stations. Contributions from other stations were ignored. When checking the reconstruction it shows that it does not represent the data as well as the full reconstruction does, which is probably due to the fact that less information is used. Still, it seems to represent the showers fairly well, compared to the full reconstruction. As it will not be suggested to change the actual reconstruction the individual effects on events are not relevant. This method is only used for the mathematical approach. Still, one has to keep in mind that the tests in section 7.1.2 illustrated that the kind of fit does influence the form of the distribution. So a fit via the maximum likelihood even if it only contains Gaussian errors will not be as flat as a χ^2-minimizing fit. The result of such a fit on limited numbers of stations is shown in figure 7.7.

First of all it should be noted that the distribution is not as smooth as the distribution from all SD events. This is due to the low statistics. Less than 0.1% of the entire data set was suitable for this new kind of reconstruction. Furthermore the form of the distribution has changed. The content of the first bin has decreased significantly whereas the rest of the distribution is overall konvex now. One cannot state that the distribution has become flatter.

When analyzing these results, assumptions can only be based on the fact that the parameterization of the LDF itself was optimized using the data. It was optimized for events that had stations with higher and lower signal as well as zero-stations and saturated signals. Therefore the LDF is not a concept derived from purely

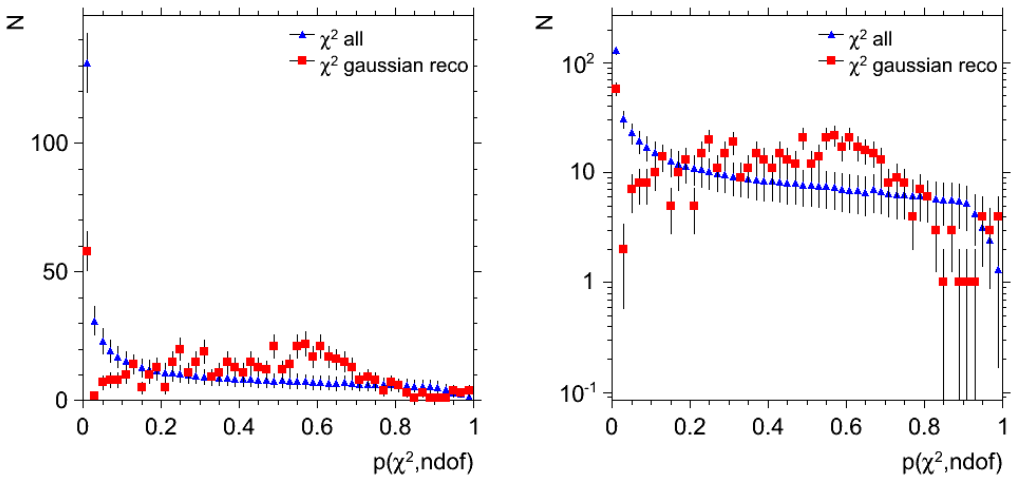

Figure 7.7: The red squares illustrate the χ^2-distribution from reconstruction with only Gaussian signals. For this reconstruction only a limited amount of events was suitable as more than four stations is the Gaussian signal range are needed. For a comparison the blue triangles show the χ^2-distribution from all events. Both distributions are scaled to the same number of entries.

theoretical expectations. It is therefore not unexpected that the LDF fit performs different once the structure of the events changes.

7.1.5 Comparison with simulated air showers

After having checked many dependencies still a definitive statement about events that disturb our probability distribution cannot be made. Overall, the shape of the χ^2-probability distribution seems to depend on the method applied. In the model-independent approach one can go a step further to compare the distribution from data to a distribution derived from simulated air showers.

When applying this, one needs to keep in mind that air shower simulations can in their exactness not be compared to full simulations for collider experiments. First of all, there is usually no background included, such as atmospheric muons. Furthermore, in this energy range the standard model reactions are not yet fully explored to be able to generate fully reliable cascades. This will show in particular in the comparison of different models of air shower simulations. There are various models for the reactions in air showers and also different approaches to the entire simulation.

For a comparison of the χ^2-probability distributions a data set of simulations is needed, that is comparable to the real data set. It has to be continuous in energy according to the spectrum and it needs to represent the angular spectrum as measured by the Surface Detector. For this analysis different complete sets of simulated showers were used that fulfill all necessary criteria. One simulation was done using CORSIKA with the low energy model FLUKA and the high energy model QGSJet-II, with a transition energy of 200 GeV. About 90000 showers were available to this

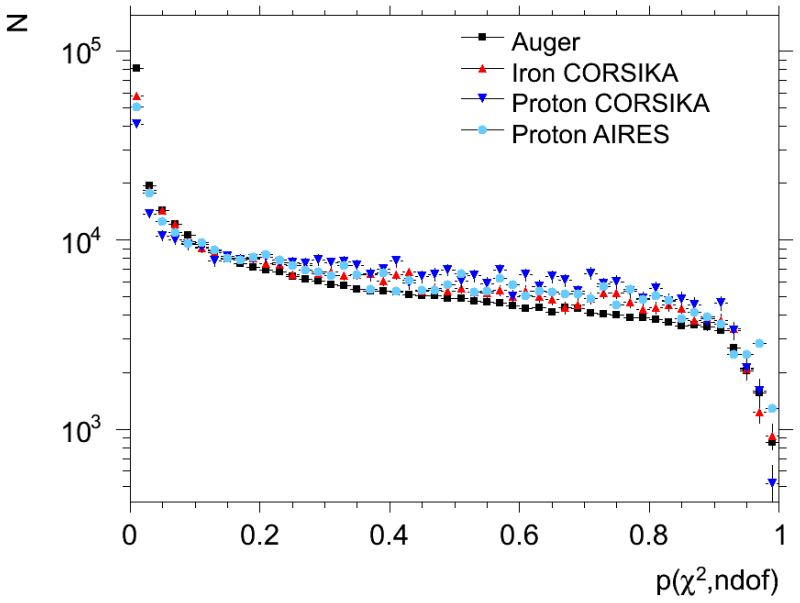

Figure 7.8: Shown is the comparison between the χ^2-probability distribution derived from actual showers and distributions derived from simulated showers. The simulated showers included iron as primary particle as well as protons as primary particle. Also two different types of simulation software were used, CORSIKA and AIRES. The simulated showers were weighted according to their energy, as compared to the real spectrum. Thereby all three histograms were scaled to the same number of entries. The angular spectrum roughly corresponds to the real spectrum.

analysis, one half being induced by protons, the other half by irons as primary particles. The showers were simulated for a thesis and were thankfully provided to the Aachen group [88]. The other simulation was done in Aachen using AIRES 2.8.4 with QGSJet-II and consists of 10000 showers according to the energy and angular spectra.

The simulated showers were reconstructed with the same software as the measured showers. As shown in figure 7.8 the form of all four χ^2-probability distributions is similar. The excess in the first bins can be found as well as the decrease in the last bins. Smaller deviations can be seen in both models and types of simulation software. As the simulations use a perfect detector with no missing stations and the saturation of electronics is only forced at a fixed value for signal strength, there are known differences between data and simulations. Taking also into account the missing background and deviations between the different models, the simulations seem to represent the data reasonably well. The main features in the χ^2-probability distribution seem to be due to the treatment in the reconstruction, rather than due to deviating events in the data set.

Overall, one can conclude that the entire distribution of χ^2-probability does not deviate significantly from our expectation. Unfortunately this analysis is not able to identify single events or classes that deviate from the expectation that will be interesting to further analyses. As the main challenge for the χ^2-analysis is that the

reconstruction is done based on a Maximum Likelihood approach a good estimator should take this into account. Therefore, a method to evaluate the quality of the reconstruction based on the likelihood function was developed.

7.2 Likelihood Analysis

The main issue concerning the validity of the χ^2-analysis is due to the individual contributions of stations. Some signals are only used as limits while others do not follow the Gaussian error model. All those effects have led to the conclusion that for the reconstruction an approach based on a χ^2-minimization will not produce the best suitable results. Therefore all error models and limits have been implemented in a Maximum Likelihood approach as introduced in chapter 4. So if the inconsistencies concerning the χ^2 should be avoided for a quality criterion, criteria based on the likelihood itself should be established in order to obtain an estimator for the quality of the reconstruction.

In contrast to the χ^2-value the likelihood value of a reconstruction does not have an absolute relation to the quality of the fit. The value depends on the different contributions, their error models and a possible normalization. Therefore the likelihood values of different events with different number of stations will vary even if the fits are of the same quality.

Well known when dealing with likelihoods is the *Likelihood Ratio Test* or *T^2-Test* [89]. All tests from this family compare the ratio of two Likelihoods and make a statement about the representation of the data by a model. But this kind of test is only suitable for the same set of data and different models. Mostly it is used to compare different parameterizations and their representation of the data. It is argued that most tests that are set to test the quality of a hypothesis using the value of the likelihood need at least implicit alternative hypotheses [90].

As this analysis is not aimed at testing different parameterizations, but at identifying events that are not well represented by the fit, a different approach is needed. The quality of the reconstruction of one event can be estimated in a method that requires generating new signal data from the fit. As shown in figure 7.9 mock data will be generated from the LDF function. For each event a new core and S_{1000} will be generated within their uncertainties from the fit. These parameters define the LDF and the distances in which stations can be found. For those stations signal is generated according to the expectation from the new LDF. For this mock data the likelihood value can be calculated with respect to the LDF from which it was generated. Repeating this variation a number of times will result in a distribution of likelihood values. If the model represents the data well, the true likelihood value will be within the distribution from the mock data. This method will be referred to as *Likelihood Monte Carlo*.

This Likelihood Monte Carlo is similar to a method known in context of bootstrap methods, as the *parametric bootstrap test* [91]. Bootstrapping in general is the practice of establishing properties of an estimator by measuring those properties by sampling from an approximating distribution. Most commonly this is done by

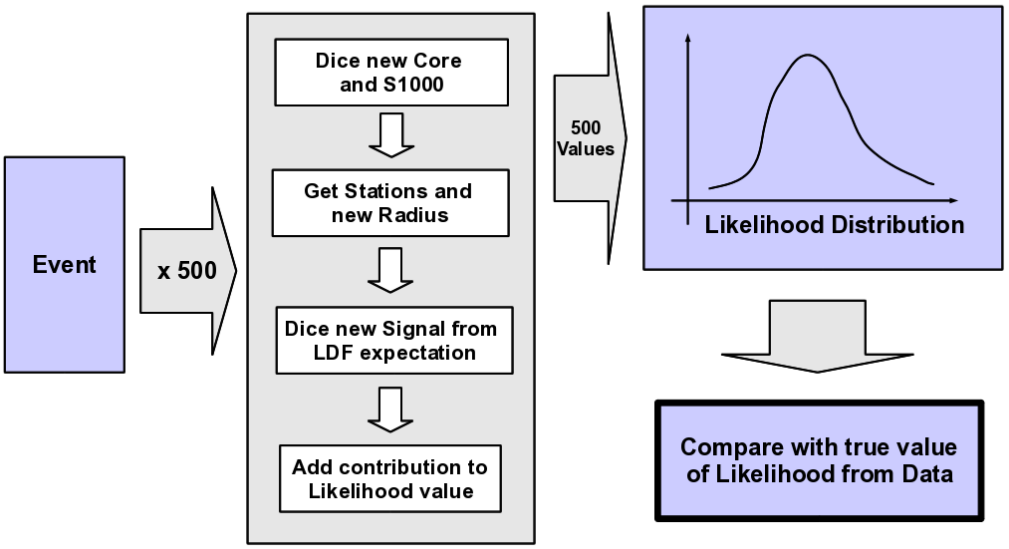

Figure 7.9: The concept of the Likelihood Monte Carlo. For each event 500 likelihood values will be generated according to this method and compared with the true value of the data from the event.

resampling an existing data set but sampling new data from a parameterization is also feasible. It should be kept in mind that this method relies on large amounts on computation and that it is sometime a little overly optimistic as it relies on a parameterization that is fitted to the data. Furthermore, mathematically significant confidence levels for the properties of an estimator can only be calculated if the fit is redone.

7.2.1 Application to the data from the Surface Detector

The Likelihood Monte Carlo has been tested on a small subset of events, using only the data from January 2009. For each event new LDF parameters were generated 500 times according to the errors returned from the reconstruction. By generating a new core a new distance to the shower core could be calculated for every station, hereby identifying those stations that should have detected a signal. For each of those station new signals were generated according to the accuracy of the signal, which is assumed in the reconstruction to $1.06 \cdot \sqrt{S}$. This empirical value is taken from an analysis about the signal accuracy [70].

When following this approach the stations could change character. A station that did not measure a signal in the real data set could become a station with a signal and vice versa. An overall threshold of 3 VEM corresponding to the most prevalent trigger was set for this distinction.

The analysis was performed on the reconstructed events provided in ADST ROOT-files. In order to ensure a certain quality only events with T4 and T5 and a zenith angle between 0° and 60° were used. When generating the new signal data all

stations were excluded that were tagged with an error flag and were removed from the reconstruction. The fit was not redone for the newly generated data, but the likelihood value was calculated with respect to the LDF from which the data was derived.

Some exemplary distributions from this approach are shown in figure 7.10. Usually the negative log(likelihood) is used in the reconstruction as algorithms for minimization used to be more effective than those for maximization and it is kept as a convention. However, these plots always show the true value of the log(likelihood) without multiplying the values with -1. The optimum values are therefore on the right side of the distributions.

Most events returned a distribution like the one that is it shown in the first row of figure 7.10 and the respective histogram. One example of a bad quality is shown in the lowest histogram. Also the respective LDFs are shown. In the one event with a bad quality, one can see that the data does not look like fitting a regular lateral distribution function.

7.2.2 Impact of shower characteristics

There is no a priori expectation about the shape of the likelihood distribution. It does not need to be neither symmetrical or centered around a certain value. The form of the likelihood distribution obtained for every event depends on the shower itself. In general, it is true to say that the more stations are involved in the calculation of a likelihood the broader the distribution gets and the smaller the mean of the distribution will be. The number of stations involved depends on the energy and the zenith angle of the shower. In figure 7.11 an illustration of this fact is shown. For the same core the values of S_{1000}, which corresponds to the energy, and ϑ were varied.

The number of stations involved does not only mean stations with a signal. Also missing or non-active stations in the detector-grid can have an influence on the shape of the distribution. If a station does not exist it does not contribute to the likelihood function, while a station with no signal does contribute as a zero-station. Therefore a shower close to a missing station will result in a different distribution than a core completely surrounded by crowns of working stations.

For most of the events the likelihood distributions derived from the Likelihood Monte Carlo are Gaussian. However, there are types of events that do not result in a Gaussian distribution. If for example an event has a saturated station very close to the core, possibly without recovery, this only contributes a lower limit to the likelihood function. If the shower is then of such a low energy that only few other stations will have signal above the trigger threshold, this constraints the LDF only very little. These types of events have already been discussed in section 5.3 and it is known that the definition of errors concerning these events proves difficult. The distributions of generated likelihood values tend to be very asymmetrical. Furthermore, there are events with a partly Gaussian structure but with longer tails. Depending on the binning and the width of this distribution it is questionable, whether a good

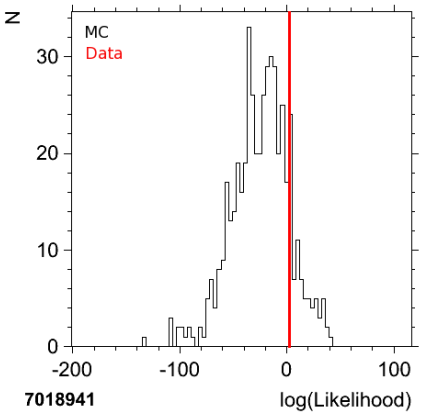

(a) Distribution Event 7018941

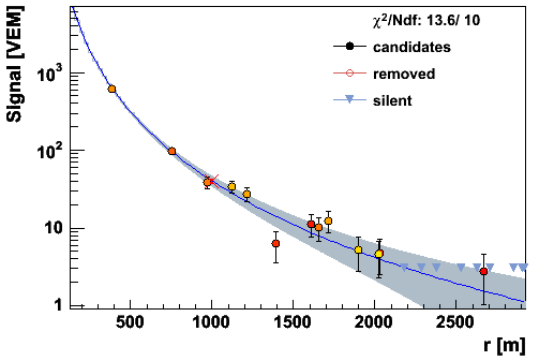

(b) LDF Event 7018941

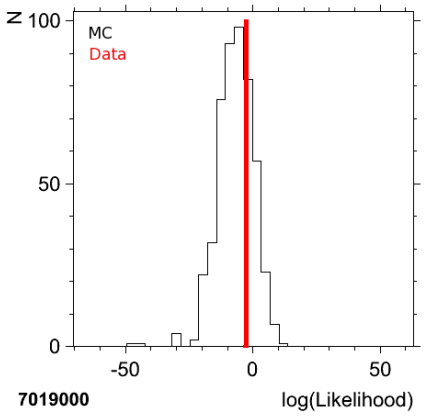

(c) Distribution Event 7019000

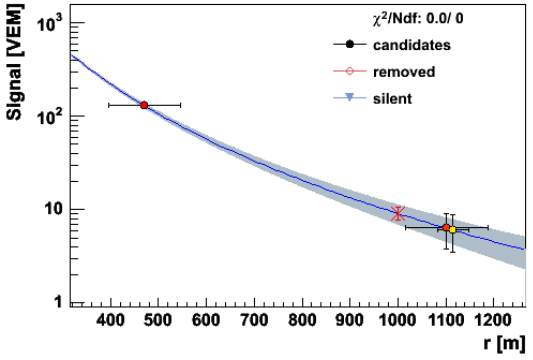

(d) LDF Event 7019000

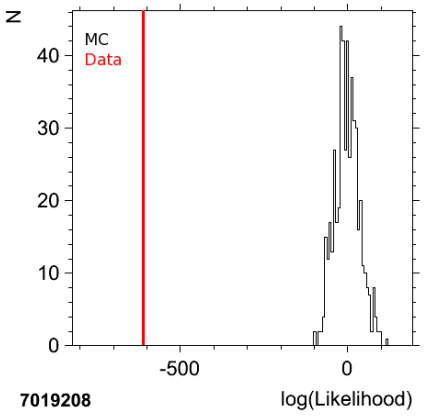

(e) Distribution Event 7019208

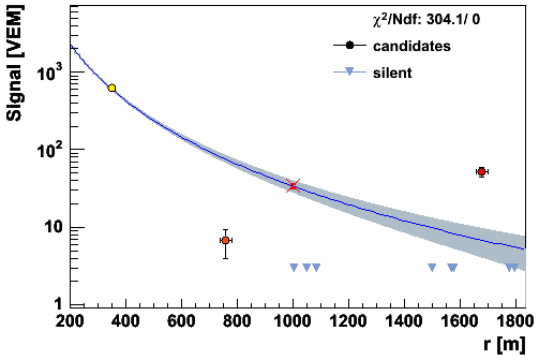

(f) LDF Event 7019208

Figure 7.10: Shown are histograms from the log(likelihood) values obtained from the Likelihood Monte Carlo generation. The red line indicates the value derived from the actual event data.

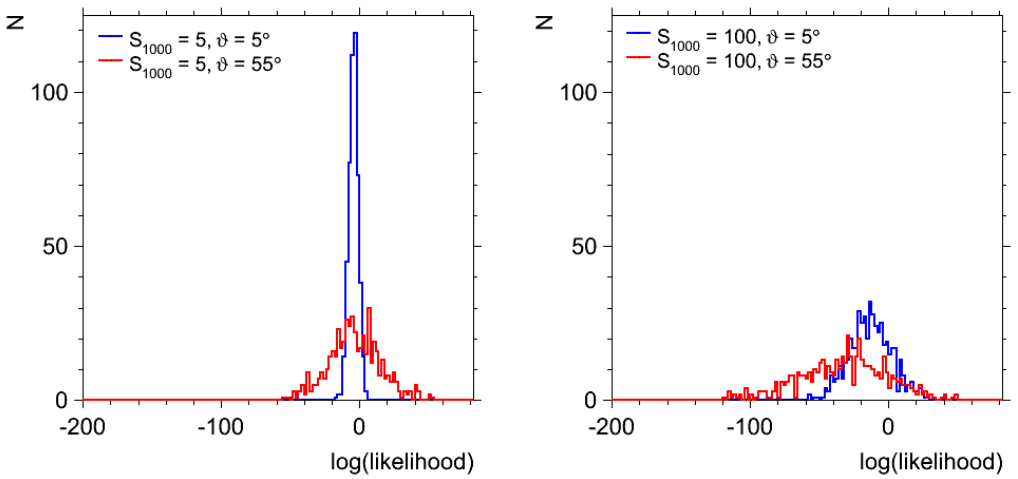

Figure 7.11: Monte Carlo Likelihood distributions for different parameters are shown. This comparison illustrates that the width and the mean of the distribution depends on the characteristics of the shower. The distributions derive from generated LDF parameters and do not rely on real events.

true value should be found in the peak only or also in part of the tails. For some events a changed range of fit in likelihood values enables to fit a Gaussian function to the distribution, whereas for others a fit did not converge. All latter events were not compared to the Gaussian events and form a subclass of events. Two typical examples are shown in figure 7.12.

Overall, the shape of the distribution is influenced by the fact that the fit was not redone. Therefore a tendency towards low values is possible. When a configuration obtains a low value for the likelihood value a maximization procedure by refitting the LDF would probably result in a higher likelihood value.

As already discussed when introducing the likelihood function the treatment of zero-stations is not completely clear. It has been estimated that the effect that a signal is not recorded below the trigger threshold has an effect on real signals up to 10 VEM. In a study comparing twin stations, i.e. two stations located at 20 m distance, it was found that the signal accuracy is distorted for signals smaller than 10 VEM [70]. This shows that the fluctuations are higher than expected for lower signals and that zero-stations are likely to be a result of an random fluctuation to lower values. For this Monte Carlo analysis a trigger cut was set at 3 VEM, which corresponds to the one implemented in the reconstruction. In real data however this trigger cut is not that strict. Due to different trigger types and the expected fluctuations of the real signal, there might be signals treated as valid that are lower than 3 VEM. Therefore the choice of this parameter will also influence the distribution obtained from the generated data.

7.2.3 Consequences

From all generated likelihood distributions and the true value of the likelihood from the event a measurable deviation can be calculated. As most likelihood distributions

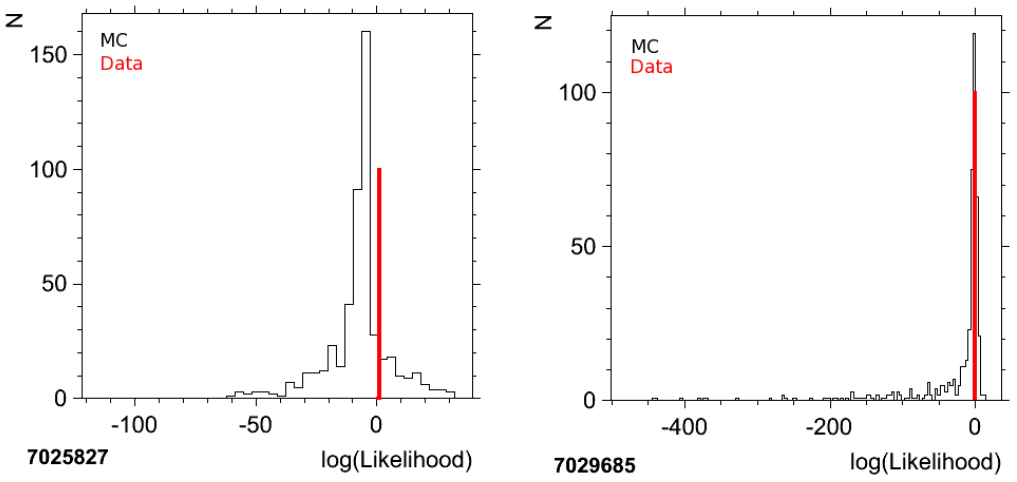

Figure 7.12: Two examples of non-Gaussian distributions of likelihood values. On the left side a very narrow distribution with small tails is shown. This structure derives typically from three stations events with small signals. On the right side an asymmetrical distribution is shown. This is typical for events with a very central saturated station and only very few other stations.

have a Gaussian shape, a Gaussian function was fitted to the distributions. From this the mean was compared to the true value obtained from the event. The deviation can be calculated in units of the σ from the Gaussian fit. The results for all events from January 2009 for are shown in figure 7.13.

Overall, this is an excellent result for the quality of the fit. Almost no event deviates further than 2σ from the mean of the likelihood distribution. This shows that the fitted LDFs are really optimized for the data.

However, two constraints on this distribution have to be given. First of all the width of each individual likelihood distribution depends on the errors allowed for the generation of new data. For example, the assumption of smaller errors of the signals results in a tighter distribution and therefore larger deviations in units of sigma. But this dependency is not strong, for example halving the errors only slightly influences the distribution.

Furthermore, as already discussed, the fit was not redone. Figure 7.14 illustrates the effect that this has caused. There is an excess of true values being higher that 50% of the generated values. This again shows that the generated values have a tendency towards lower values and that in case of a new fit the resulting distribution of generated likelihood values should be tighter around the higher values.

Thus, we can conclude that the units of sigma are not absolute and that a deviation to $+\sigma$ is more probable than a deviation to $-\sigma$. Still, if one wants to identify a class of events that shows the poorest quality of fit to use them for further model-dependent tests this method is useful. The deviation cannot be given in absolute units of sigma, but events that deviate significantly to lower likelihood values can surely be considered as candidates for a bad quality of fit.

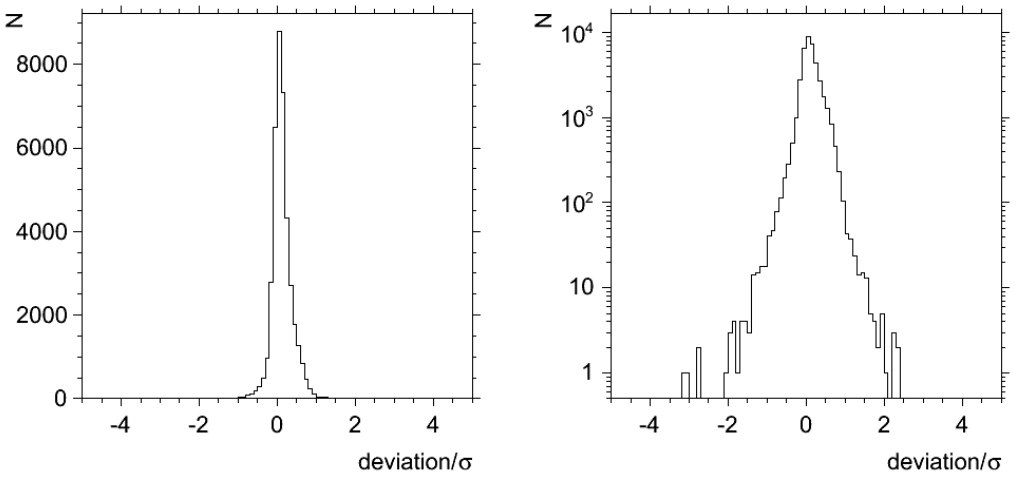

Figure 7.13: This distribution shows the deviation of the likelihood value received from actual shower data to the mean of the generated likelihood distribution in units of sigma of this distribution. The sigmas are not absolute. Only the middle section of the distribution is shown. Very few events were found outside this section, as for instance shown in figure 7.10.

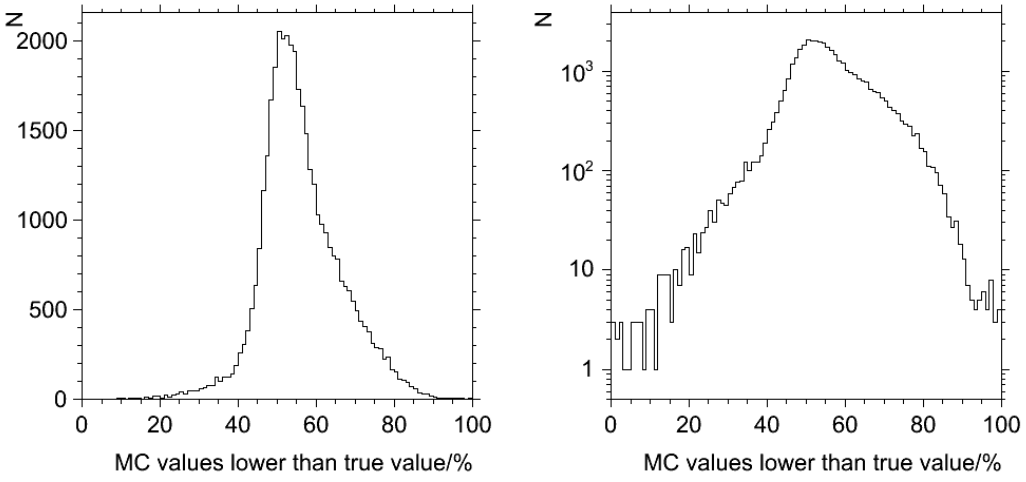

Figure 7.14: This distribution shows the number of generated Likelihood Monte Carlo events that have a likelihood value lower than the likelihood value obtained from the real event. This way of depicting the result of the deviation shows that the true values have a tendency to be higher than the generated values. Furthermore, this again shows that only very few events deviate significantly from the expectation.

The percentage of events that deviate significantly even with the restrictions given is very low with respect to the overall amount of events. In subset that was tested there are about 42000 events, of which only three events deviate significantly to lower values. One of those events is shown in figure 7.10. One other event occurred near a missing station in array and the reconstructed core looks like it does not agree with the real core, which results in a LDF shifted next to the data points. The last event is an event that shows a time structure like a real shower but the spatial distribution is very different. All signals are below 5 VEM. What causes the last and the first event remains unknown.

This analysis was a valid cross-check for the performance of the $\overline{\text{Off}}\underline{\text{line}}$ reconstruction. By rebuilding the fitting process for the Monte Carlo variation some inconsistencies in the official reconstruction could be found and clarified. Solutions to this issues have then been implemented in the official version of the reconstruction.

This analysis confirms that the overall quality of reconstruction is quite good with respect to the parameterization used. It provides a tool to identify those events that do not meet the expectations of a reasonable fit. In order to identify an absolute confidence level the method can be improved by reperforming the fit.

Most events that show a poor quality of reconstruction are those with a low multiplicity of stations. According to their station multiplicity they should also be of low energy. But as the reconstructed energy depends on the LDF reconstruction no correct range can be given. Also, some bad quality fits are influenced by the geometry of the detector, which leads to awkward station configurations. This method cannot exclude exotic physics in those deviating events, but there is no significant hint for an excessive amount deviations. Still, when looking for certain model-dependent signatures this method can be used to identify a class of interesting events.

8. Conclusions and Outlook

This thesis dealt with the search for anomalous events in the data set of the Surface Detector of the Pierre Auger Observatory. Different tools to model-independently identify such anomalous events were developed. By using the most basic assumptions about air showers criteria were established that describe a standard. Different ways to identify deviations from this standard were shown, which could identify unexpected events.

The general shower geometry was analyzed. Even though some events with unusual footprints or failed reconstructions are present, there is no evidence for a significant amount of events with an unexpected shower geometry. Most of the events could be explained by features of the detector or the possibility of coinciding muonic background. However, by looking for these characteristics it became clear that an unreliable detector, as it has happened in unstable periods of data taking, will affect the data taken. This is especially relevant for studies concerning exotic signatures.

The study of background showed that the current background cuts are effective and remove background according to the expectation. In the removed background there was no significant evidence for unusual events that were mistaken for background. As statistics increases the conclusion that the large background signals are not linked to other showers could be strengthened.

Furthermore, it was established that the χ^2-probability is not a suitable tool to identify single deviating events for this method of air shower reconstruction. Still, there is no evidence from the χ^2-study that there are classes of events that are not treated correctly or do not show signals as it is expected according to the current understanding of air showers.

Based on the results from the reconstruction a different method was developed to identify deviating events. By generating data from the reconstructed lateral distribution function likelihood values could be compared and an estimator for the quality was established. This method overcomes the fact that the likelihood value itself does not hold absolute information about the quality of the reconstruction as the χ^2 does. The results however remain the same. There is no significant evidence for large classes of deviating events as possible signals of exotic physics. On the contrary, this analysis shows that most of data is in good agreement with the reconstruction.

Overall, it has to be noted that most events that were identified as peculiar were not of the highest energies but in the energy range where the detector measures most of the events. This is in good agreement with an expectation from possible statistical

fluctuations as reason for those events. Therefore this analysis does not give evidence for all those theories that claim the highest events to be of interest for exotic models. Still, this method cannot exclude exotic physics and is able to identify events that do not show a good reconstruction. Those events could be interesting to further model-dependent studies.

In order to further develop a model-independent approach, one should lower the quality criteria for the suitable data. This analysis was a cross-check if the events that are used for the physics analysis are well understood. But if one wants to identify events that do not meet our expectation, one has to go deeper into the data that is usually discarded. For this kind of search new quality triggers need to be developed. Criteria are needed that do not discard events due to their shape or missing compactness, as the T4 does, but implement the functionality of the array similar to the currently used T5. It is necessary to only analyze data from a reliable detector but not necessarily according to assumptions about the form of air showers. Consequently, one would have to look even further into the raw data, which is currently impossible as anything that has not triggered a T3 is not recorded.

The step towards more raw data for example has been taken in model-dependent analyses. In the search for double-bangs as a possible signature for exotic physics the signal traces of stations have been analyzed and coincidences in the shape of the signals of more than one station were searched. So far analyses have not been successful in identifying more than indications [92],[93]. Even though more than the signal strength is used, this analysis is still based on fully reconstructed showers that have triggered a read-out. Eventually, in a search for exotic physics in air showers the quality criteria need to be lowered as well as the level of reconstructed data.

A successful hunt for exotic particles can only be conducted using both the Fluorescence Detector and the Surface Detector. While the FD promises more information about the shower development and exotic reactions within it, the SD ensures high statistics and a reliable cross-check. Combining independent results from both detectors as well as studying a combined set of data will ensure that even small effects will be identified. Model-independent tests of the data should always be considered in this context, as they ensure a high quality of data and minimize the chance of overlooking a signal.

A. Appendix

This appendix provides a *Zoo* with events that look peculiar, a list of abbreviations and a full listing of events that have been considered in detail for this analysis.

A.1 Zoo of Exotic Candidates

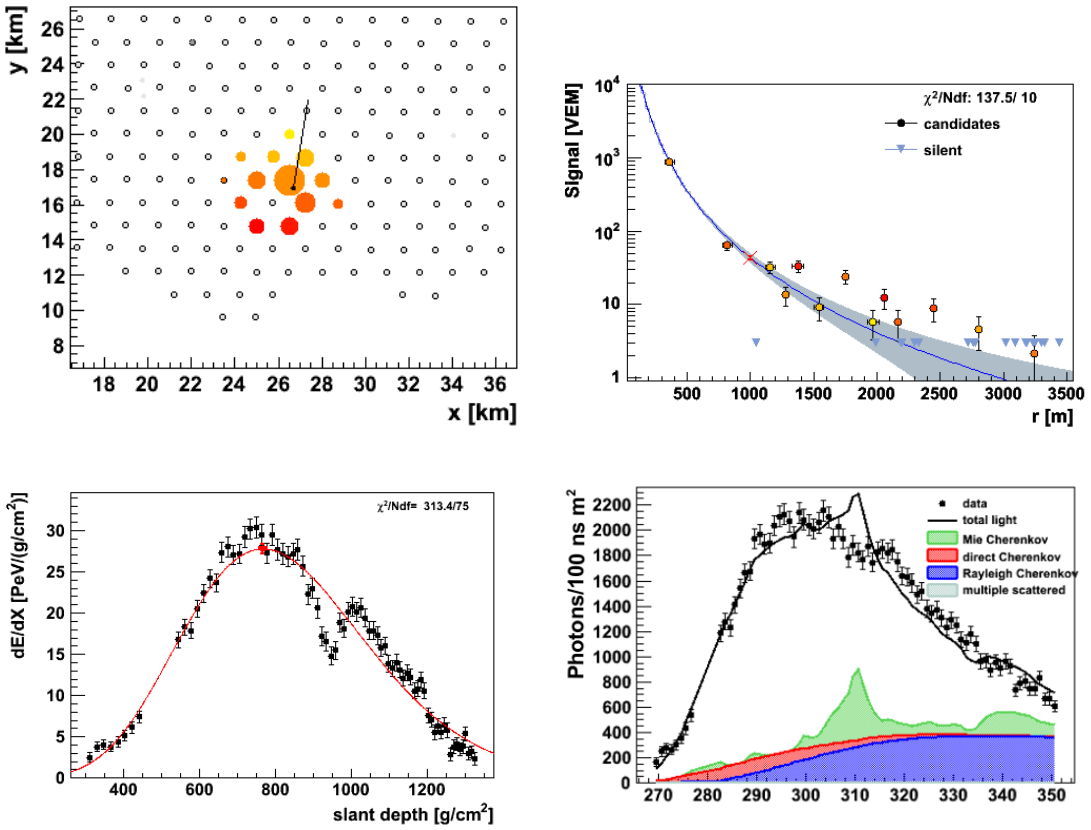

Figure A.1: Event 6652658 as measured with the Surface Detector and Los Leones

The event in figure A.1 combines two interesting features. On the one hand it has a missing station in the middle of the shower. From the fit of the LDF one can deduct that this station actually should have been present. On the other hand the profile obtained from the FD shows a significant *bump*. The contribution of light suggests that there possibly was a cloud but the subtraction of background did not remove the bump. In this event several difficulties occurring in the reconstruction are combined. These effects should be uncorrelated.

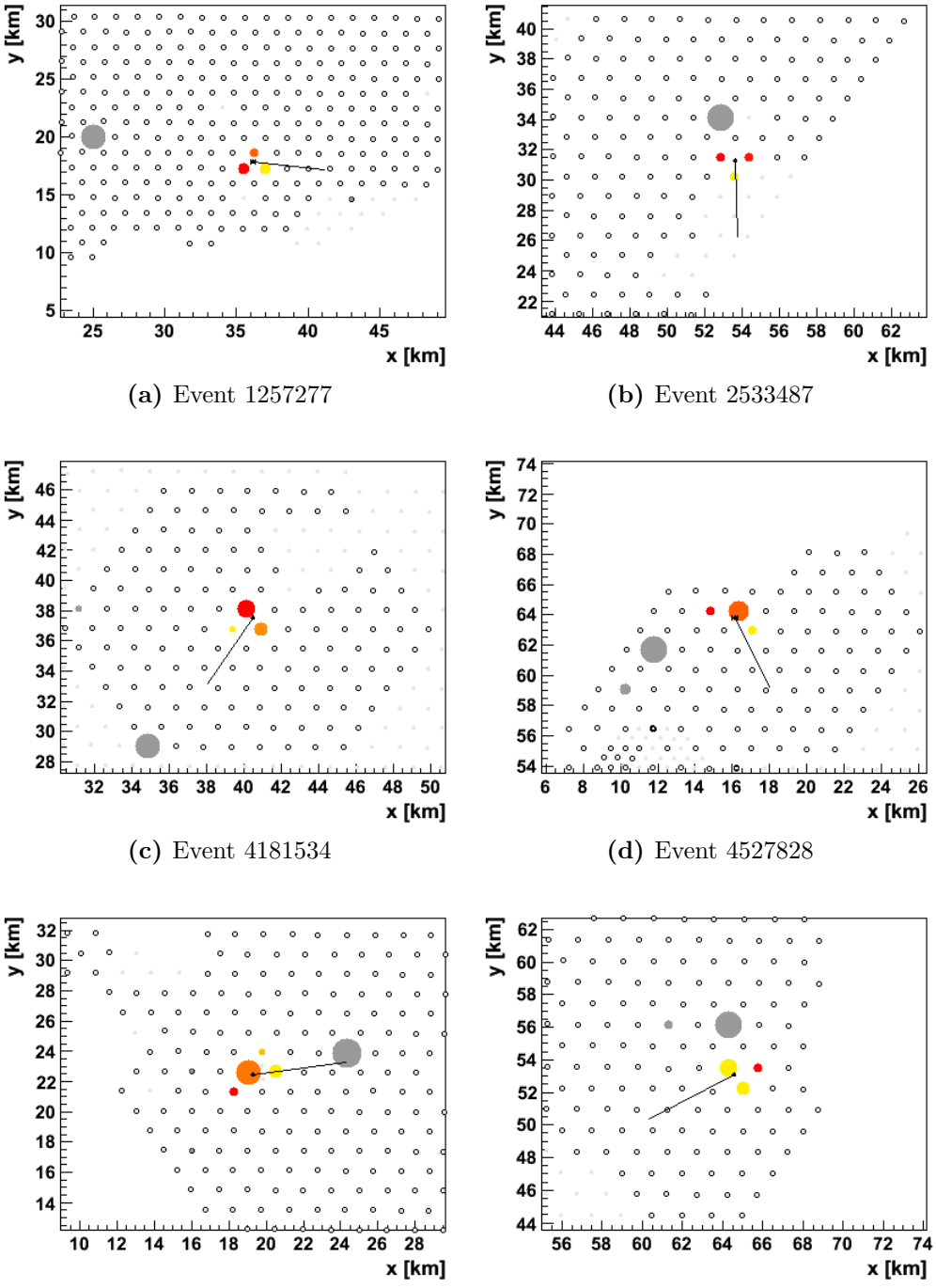

(a) Event 1257277

(b) Event 2533487

(c) Event 4181534

(d) Event 4527828

(e) Event 5138396

(f) Event 8013781

Figure A.2: Exemplary events with accidental signals larger than 300 VEM. Shown is the footprint of the corresponding event in colours. The removed accidental is coloured in gray.

A.2 List of abbreviations

AERA	Auger Engineering Radio Array
AIRES	AIRshower Extended Simulations
AMIGA	Auger Muon-detectors and Infill for the Ground Array
CDAS	Central Data Acquisition System
CMB	Cosmic Microwave Background
CMS	Compact Muon Solenoid
CORSIKA	COsmic Ray SImulation for KAskade
FADC	Flash Analog Digital Converter
FD	Fluorescence Detector
FLUKA	FLUktuierende KAskade
GPS	Global Positioning System
GRB	Gamma-Ray Burst
GZK-cutoff	Greisen-Zatsepin-Kuzmin-cutoff
HEAT	High Elevation Auger Telescope
HERA	Hadron Electron Ring Accelerator
LEP	Large Electron Positron storage ring
LDF	Lateral Distribution Function
LHC	Large Hadron Collider
MSSM	Minimal SuperSymmetric Model
PBH	Primordial Black-Hole
PMT	Photomultiplier tube
QGS-Jet	Quark-Gluon-String model with Jets
SD	Surface Detector
SHDM	Super Heavy Dark Matter
UHECR	Ultra-High Energy Cosmic Ray
VEM	Vertical Equivalent Muon

A.3 Lists of Event Ids

All events are taken from the same data set. Used is all data from the beginning of data-taking in 2004 until the end of 2009. No bad period cuts are applied as a full acceptance or a constant event rate are not relevant for this analysis. In discussions about singular events bad periods were always considered. Events were selected to be vertical, i.e. having a zenith angle of less than 60°. Also it was required for the events to fulfill quality criteria, i.e. to be T4 and any T5, as it was intended to investigate only what is considered to be a real shower. Every event is identified by its Surface Detector event number (SdId). The data was downloaded from the Mirror of the Karlsruhe Institute of Technology, thus using data reconstructed with Offline (version: v5r4) provided in ADST-ROOT-trees.

Hexagonal Events

All events listed in table A.1 show a hexagonal shape with a missing station as described in section 5.2. The listing is divided into events that show the shape but having a central station that was shortly non-operational and those events that had a fully functional station missing. The latter are marked in bold. Events that show the circular shape due to the fact that the station was not yet deployed or again disassembled are not included in the listing. Events from a bad period are shown in italics.

Incomplete Reconstruction

All events are listed in table A.2 that did not have a full reconstruction as discussed in section 5.3, determined by the LDF-status being smaller than four. They are classified from an individual analysis. It has to be noted that very few of these events were successfully reconstructed by older versions of the reconstruction even though the returned parameters and individual values do not seem very convincing.

Large Accidentals

Listed in table A.3 are the events, which include stations that have been discarded by the reconstruction as accidental, i.e. *out of time* or *lonely*. Listed are furthermore only those that have a signal larger than 300 VEM that are dealt with in section 6.4. All accidentals that are closer than 20 km to the shower core are marked in bold. All those that are within a time window that makes it possible for them to be causally linked to the shower are shown in italics.

Table A.1: Event IDs of events having a missing central station

Year	EventId					
2004	1131497	1122150	1105035	1114366	***1082848***	904348
	758175	**787469**	649481	**668387**	622158	623083
2005	1787716	1776219	1778220	1767910	1664777	1718334
	1616866	1597810	1566857	1572015	1447564	1455977
	1348451	1387820	***1277079***	1303619	1223339	1208726
	1173639					
2006	2925061	2988117	2950628	2836354	2893062	2887612
	2816491	2786742	2683523	2661310	2542187	2595338
	2437024	2437256	2445335	2479310	2459665	2469614
	2433304	**2512557**	2335731	2334506	**2358894**	2397571
	2372687	2381839	2404679	2256305	2305552	2221163
	2140573	2195732	2204918	2080151	2127734	1977302
	2029076	1944296				
2007	4357651	4274437	**4309187**	*4321711*	4229340	4170916
	4205202	4148653	4163653	4115988	4062825	3951138
	3938358	3774772	3778043	3849574	3865220	3883043
	3646729	3527997	3539684	3540628	3435152	3296694
	3335462	***3190240***	3281236	3282323	3270959	3257525
	3095461	3183015	3121382	3170019	3143926	3155829
	3076490	3076734				
2008	**4484436**	4468314	4450164	4390345	4411252	4430014
	4384741	4403756	**4518369**	4560038	4599102	4588584
	4589234	4591598	4603530	4499140	4525355	4543239
	4723632	4707706	4684666	4711818	4721741	**4677409**
	4667123	4827551	4840525	4852809	4765079	4751050
	4863748	4950277	4959594	4909891	4914194	5058167
	5028486	5047084	5127584	**6289894**	6327770	6427912
	6523719	**6652658**	6757179	6755897	6732254	**6805880**
	6878763	6715809	6716663	6873338	6899328	6901056
	6942527					
2009	**7021883**	7066613	7082640	7082640	7143602	7133984
	7097232	7249411	7199094	7266831	7257916	7180809
	7184850	7372083	7363976	7408115	7403611	7424064
	7444980	***7540078***	*7575975*	*7577973*	*7570724*	*7589258*
	7580520	*7594708*	*7524860*	***7658309***	*7623277*	*7787671*
	7790421	***7791456***	*7796825*	*7766391*	*7811488*	***7823114***
	7933517	*7861401*	*7842054*	***7941880***	*7948067*	*7960087*
	7985329	*7989837*	*8064576*	*7992344*	*8078423*	*8104795*
	8133978	*8134467*	*8150867*	*8262492*	*8160679*	*8184562*
	8221507	*8169551*	*8193243*	*8447866*	*8468461*	*8475711*
	8464374	*8552385*	*8631513*	**8809194**	**8812848**	**8826226**
	8826240	**8827662**	**8908131**	8908573	8944093	

Table A.2: Event IDs of events with an incomplete reconstruction

Year	EventId	Class	EventId	Class
2004	838816	small signals	1017163	small signals
	887116	small signals	1108879	near border
	898228	small signals		
2005	1162039	discarded	1496901	small signals
	1303077	near border	1552014	small signals
	1359762	near border		
2006	1939438	near border	2491056	small signals
	1958698	small signals	2513004	near border
	2094649	near border	2529436	small signals
	2172207	small signals	2692667	small signals
	2247556	near border	2858878	small signals
2007	3083766	near border	3354287	near border
	3091903	near border	3515222	near border
	3110300	near border	3872200	small signals
	3137725	near border	3979240	saturated signal
	3186604	near border	3994253	saturated signal
	3306109	small signals	4288019	small signal
2008	4694412	small signals	6202383	small signals
	4726268	small signals	6415077	small signals
	4744954	saturated signal	6499062	small signals
	4761522	small signals	6661147	small signals
	4896632	small signals	6850766	small signals
	5133385	near border		
2009	7036765	small signals	7584302	small signals
	7045521	small signals	7591521	saturated signal
	7155529	saturated signal	7598945	near border
	7217655	small signals	8461149	circular event
	7257423	small signals	8466700	saturated signal
	7500048	saturated signal	8934973	small signals

Table A.3: Event IDs of accidentals with signal > 300 VEM

Year	EventId					
2004	1137031	1126735	1099053	***1122204***	***1113582***	**1080148**
	1070163	**1078771**	**1080424**	**1051960**	**1055025**	**1019585**
	1015263	***911257***	934569	**935502**	**862664**	**860181**
	908345	**819226**	***724778***	**732992**		
2005	**1855670**	***1854675***	**1873966**	1874739	**1870596**	**1877460**
	1828149	**1787917**	1790453	1785111	1767531	**1797802**
	1806584	1744783	1697368	1715413	1716756	**1732073**
	1662935	1616924	1643019	1591559	**1641764**	**1646340**
	1645280	**1557434**	1558670	**1577662**	**1578526**	**1588692**
	1573239	1581750	**1551880**	1547412	**1582172**	1587030
	1541446	**1520391**	1443664	**1463274**	1463692	**1463696**
	1428997	**1378280**	**1381537**	1383009	**1388378**	**1331160**
	1292566	**1265456**	***1272553***	***1257277***	**1228315**	**1220484**
	1194862	**1188561**	***1181346***	**1174171**		
2006	2922235	3000563	3000755	2972279	2958054	2965018
	2977115	2970044	2980672	2821302	2842211	2836148
	2836444	2873310	**2878887**	2725798	2750724	2785971
	2757254	2630158	2644304	**2645506**	2722491	**2674483**
	2674656	2692065	**2696230**	***2533487***	2538587	2531348
	2542459	2536722	2547085	**2548855**	**2550674**	***2615086***
	2619863	2552014	**2436924**	**2451662**	2437630	**2439473**
	2425932	2426081	2426186	2482389	2489122	**2498403**
	2464726	2504480	**2511657**	2350411	2345775	2346812
	2338490	2355920	**2396317**	2367780	2369193	**2364513**
	2248815	2270829	2268494	2243908	2244816	2273109
	2306818	2301967	2289767	2162120	2173082	2173102
	2176685	2156459	2220027	2084072	**2091351**	2064898
	2067473	2112139	**2134615**	**2129377**	2139126	2105558
	2109222	1989161	**2004047**	2002152	2026505	**2012713**
	1942539	**1908168**	1950800	**1915819**		
2007	**4376682**	**4298733**	**4300270**	**4316568**	**4234309**	**4181534**
	4138309	**4158925**	**4136915**	**3887627**	**3641339**	**3540162**
	3364189	**3322157**	**3185766**	**3092722**		
2008	**4458117**	**4562935**	***4566149***	***4527828***	**4838494**	**4818297**
	4739366	**4911090**	**5106969**	**5138396**	**5246186**	**6243340**
	6324736	**6511210**	**6787872**	**6740682**	**6813367**	**6828754**
	6932722	**6986788**	**7015177**			
2009	**7042072**	**7063564**	**7246456**	**7261453**	**7287998**	**7377198**
	7357954	**7746948**	7876106	**7940430**	**8039617**	**8013781**
	8121598	**8151012**	**8292292**	**8461496**	**8705309**	**8770481**
	8910718					

References

[1] B. Abbott *et al.*, D0 Collaboration, *Search for new physics in eμX data at D0 using SLEUTH: A quasi-model-independent search strategy for new physics*, Phys. Rev. D., 62 (2000).

[2] T. Aaltonen *et al.*, CDF Collaboration, *Model-independent and quasi-model-independent search for new physics at CDF*, Phys. Rev. D, 78 (2008).

[3] A. Aktas *et al.*, H1 Collaboration, *A general search for new phenomena in ep scattering at HERA* , Phys. Lett. B., 602 (2004), pp. 14–30.

[4] T. Hebbeker, *A Global Comparison between L3 Data and Standard Model Monte Carlo*. L3 internal note, 1998.

[5] J. Ferrando, Zeus and H1 Collaborations, *Search for New Physics at HERA*, in Proc. PHENO Symposium, 2006.

[6] P. Biallas *et al.*, CMS Collaboration, *MUSiC - A general search for Deviations from Monte Carlo Predictions in CMS*, Journal of Phys.: Conference Series, 171 (2009).

[7] T. Stanev, *High Energy Cosmic Rays*, Springer-Verlag, Berlin, 2 ed., 2009.

[8] J. Blümer, R. Engel, and J. R. Hörandel, *Cosmic Rays from the Knee to the Highest Energies*, Prog. Part. Nucl. Phys., 63 (2009), pp. 293–338.

[9] M. Nagano and A. A. Watson, *Observations and implications of the ultra-high-energy cosmic rays*, Rev. Mod. Phys., 72 (2000), pp. 689–732.

[10] T. Stanev, P. Bierman, and T. Gaisser, *Cosmic rays. IV. The spectrum and chemical composition above 10 GeV*, Astronomy and Astrophysics, 274 (1993), p. 902.

[11] E. Fermi, *On the origin of the cosmic radiation*, Phys. Rev., 75 (1949), pp. 1169–117.

[12] A. M. Hillas, *The origin of ultra-high-energy cosmic rays*, Ann. Rev. Astron. Astrophys., 22 (1984), pp. 425–444.

[13] J. Blümer and K. H. Kampert. Physikalische Blätter, 2000.

[14] K. Greisen, *End to the cosmic-ray spectrum?*, Phys. Rev. Lett., 16 (1966), pp. 748–750.

[15] G. T. Zatsepin and V. A. Kuz'min, *Upper Limit of the Spectrum of Cosmic Rays*, Sov. J. Exp. Theor. Phys. Lett., 4 (1966), p. 78.

[16] P. Bhattacharjee and G. Sigl, *Origin and propagation of extremely high energy cosmic rays*, Physics Reports, 327 (2000), pp. 109–247.

[17] R. Beck, *Galactic and Extra-galactic Magnetic Fields*, in Proc. 4th int. meeting of High Energy Gamma-Ray Astronomy, API Conference, vol. 1085, 2008, pp. 83–96.

[18] G. Gelmini, G. Varieschi, and T. Weiler, *Bounds on relic neutrino masses in the Z-burst model*, Phys. Rev. D, 70 (2004).

[19] N. Jarosik *et al.*, *Seven-Year Wilkinson Microwave Anisotropy Probe (WMAP) Observations: Sky Maps, Systematic Errors, and Basic Results*, submitted to Astrophys. Journal Suppl. Series, (2010).

[20] D. S. Gorbunov, G. G. Raffelt, and D. V. Semikoz, *Axionlike particles as ultrahigh energy cosmic rays?*, Phys. Rev. D, 64 (2001), p. 096005.

[21] P. Bhattacharjee, C. T. Hill, and D. N. Schramm, *Grand unified theories, topological defects, and ultrahigh-energy cosmic rays*, Phys. Rev. Lett., 69 (1992), pp. 567–570.

[22] T. Kephart and T. Weiler, *Magnetic monopoles as the highest energy cosmic ray primaries*, Astropart. Phys., 4 (1996), pp. 271–279.

[23] A. Barau, *Primordial black holes as a source of extremely high energy cosmic rays*, Astropart. Phys., 12 (2000), pp. 269–275.

[24] S. Dimopoulos and H. Georgi, *Softly broken supersymmetry and SU(5)*, Nucl. Phys. B, 193 (1981), pp. 150 – 162.

[25] D. J. H. Chung, G. R. Farrar, and E. W. Kolb, *Are ultrahigh energy cosmic rays a signal for supersymmetry?*, Phys. Rev. D, 57 (1998), pp. 4606–4613.

[26] I. F. M. Albuquerque, G. R. Farrar, and E. W. Kolb, *Exotic massive hadrons and ultrahigh energy cosmic rays*, Phys. Rev. D, 59 (1998), p. 015021.

[27] L. Gonzalez-Mestres, *AUGER-HiRes results and models of Lorentz symmetry violation*, in Proc. CRIS (Cosmic Ray International Seminar), 2008.

[28] C. Wileman, *The Spread in the Arrival Times of Particles in Air-Showers for Photon and Anisotropy Searches above 10 EeV.* Auger internal note GAP-2008-160, 2008.

[29] W. Heitler, *The Quantum Theory of Radiation*, Oxford University Press, Oxford, third ed. ed., 1954.

[30] J. Matthews, *A heitler model of extensive air showers*, Astropart. Phys., 22 (2005), pp. 387–397.

[31] A. Haungs *et al.*, KASCADE Grande Collaboration, *The Cosmic Ray Energy Spectrum Measured with KASCADE-Grande*, in Proc. of 31th Int. Cosmic Ray Conf., 2009.

[32] E.-J. Ahn and M. Cavaglià, *Simulations of black hole air showers in cosmic ray detectors*, Phys. Rev. D, 73 (2006), p. 042002.

[33] J. L. Feng and A. D. Shapere, *Black hole production by cosmic rays*, Phys. Rev. Lett., 88 (2001), p. 021303.

[34] J. Hague *et al.*, Pierre Auger Collaboration, *Correlation of the Highest Energy Cosmic Rays with Nearby Extragalactic Objects in Pierre Auger Observatory Data*, in Proc. 31st Int. Cosm. Ray Conf., Lódź, Poland, 2009.

[35] J. Abraham *et al.*, Pierre Auger Collaboration, *Observation of the suppression of the flux of cosmic rays above* 4×10^{19} *eV*, Phys. Rev. Lett., 101 (2008), p. 061101.

[36] J. Abraham *et al.*, Pierre Auger Collaboration, *Measurement of the energy spectrum of cosmic rays above* 10^{18} *eV using the Pierre Auger Observatory*, Phys. Lett. B, 685 (2010), p. 293.

[37] J. Abraham *et al.*, Pierre Auger Collaboration, *Measurement of the Depth of Maximum of Extensive Air Showers above* 10^{18} *eV*, Phys. Rev. Lett., 104 (2010).

[38] M. Véron-Cetty and P. Véron, *A catalogue of quasars and active nuclei*, Astron. & Astrophys., 455 (2006), pp. 773–777.

[39] J. Abraham *et al.*, Pierre Auger Collaboration, *Upper limit on the cosmic-ray photon flux above* 10^{19} *eV using the Surface Detector of the Pierre Auger Observatory*, Astroparticle Physics, 29 (2008), pp. 243 – 256.

[40] J. Abraham *et al.*, Pierre Auger Collaboration, *Upper limit on the diffuse flux of UHE tau neutrinos from the Pierre Auger Observatory*, Phys. Rev. Lett., 100 (2008), p. 211101.

[41] D. Semikoz *et al.*, Pierre Auger Collaboration, *Constraints on top-down models for the origin of UHECRs from the Pierre Auger Observatory data*, in Proc. 30th Int. Cosmic Ray Conf., Merida, Mexico, 2007.

[42] J. Řídký *et al.*, Pierre Auger Collaboration, *The Fluorescence Detector of the Pierre Auger Observatory.* to appear in Nucl. Instrum. Meth. A, 2010.

[43] C. Amsler *et al.*, The Particle Data Group, *The Review of Particle Physics*, Physics Letters, B 667 (2008), p. 1.

[44] B. Dawson *et al.* (Pierre Auger Collab.), Pierre Auger Collaboration, *Hybrid performance of the pierre auger observatory*, in Proc. 30th Int. Cosmic Ray Conf., Mérida, Mexico, 2007.

[45] I. Allekotte *et al.*, Pierre Auger Collaboration, *The Surface Detector System of the Pierre Auger Observatory*, Nucl. Instr. and Meth. A, A586 (2007), pp. 409–420.

[46] D. Allard *et al.*, Pierre Auger Collaboration, *The trigger system of the Pierre Auger Surface Detector: operation, efficiency and stability*, in Proc. 29th Int. Cosmic Ray Conf., Pune, India, 2005.

[47] F. Schüssler *et al.*, Pierre Auger Collaboration, *Measurement of the cosmic ray energy spectrum above* 10^{18} *eV using the Pierre Auger Observatory*, in Proc. 31st Int. Cosmic Ray Conf., Lódź, Poland, 2009.

[48] The Auger Monitoring. http://paomon.physik.uni-wuppertal.de.

[49] M. Avenier, C. Berat, F. Melot, and A. Stutz, *Auger Online Monitoring SD Maintenance Task.* Auger internal note GAP-2008-148, 2008.

[50] J. Abraham *et al.*, Pierre Auger Collaboration, *Atmospheric effects on extensive air showers observed with the Surface Detector of the Pierre Auger Observatory*, Astropart. Phys., 32 (2009), pp. 89–99.

[51] D. Ravignani *et al.*, *Infill Event Reconstruction.* Auger internal note GAP-2009-116, 2009.

[52] M. Platino *et al.*, Pierre Auger Collaboration, *AMIGA - Auger Muons and Infill for the Ground Array of the Pierre Auger Observatory*, in Proc. 31st Int. Cosmic Ray Conf., Lódź, Poland, 2009.

[53] M. Kleifges *et al.*, Pierre Auger Collaboration, *Extension of the Pierre Auger Observatory using high elevation fluorescence telescopes (HEAT)*, in Proc. 31st Int. Cosmic Ray Conf., Lódź, Poland, 2009.

[54] The AERA Group, *AERA Proposal for the construction of the* 20^2 *km Auger Engineering Radio Array.* Auger internal note GAP-2009-172, 2009.

[55] S. Argiro *et al.*, *The Offline Software Framework of the Pierre Auger Observatory*, Nucl. Instrum. Meth., A580 (2007), pp. 1485–1496.

[56] The Auger Observer. http://augerobserver.fzk.de/.

[57] The Auger Offline Software. https://devel-ik.fzk.de/svn/auger/Offline/trunk.

[58] D. Veberič and M. Roth, *Offline Reference Manual: SD Reconstruction.* Auger internal note GAP-2005-035, 2005. an updated version is shipped with the Offline software distribution.

[59] X. Bertou *et al.*, Pierre Auger Collaboration, *Calibration of the surface array of the Pierre Auger Observatory*, Nucl. Instrum. Meth., A568 (2006), pp. 839 – 846.

[60] M. Aglietta *et al.*, *Recovery of Saturated Signals of the Surface Detector.* Auger internal note GAP-2008-030, 2008.

[61] P. Billoir, *FADC trace cleaning in Surface Detector through a segmentation procedure.* Auger internal note GAP-2005-074, 2005.

[62] I. C. Mariş and M. Roth, *65 Stations in One Shot. Is this lightning?* Auger internal note GAP-2006-079, 2006.

[63] H.-J. Drescher and G. Farrar, *Dominant Contributions to Lateral Distribution Functions in Ultra-High Energy Cosmic Ray Air Showers*, Astropart. Phys., 19 (2003), pp. 235–244.

[64] D. Barnhill *et al.*, Pierre Auger Collaboration, *Measurement of the lateral distribution function of UHECR air showers with the Auger Observatory*, in Proc. 29th Int. Cosmic Ray Conf., Pune, India, 2005.

[65] K. Greisen, *Progress in elementary particle and cosmic ray physics*, vol. 3, North-Holland Publishing, Amsterdam, 1956.

[66] K. Kamata and J. Nishimura, *The Lateral and the Angular Structure Functions of Electron Showers*, Prog. Theoret. Phys. Suppl., 6 (1958), pp. 93–155.

[67] T. Antoni *et al.*, *Test of high-energy interaction models using the hadronic core of EAS*, J. Phys. G: Nucl. Part. Phys., 25 (1999), pp. 2161–2175.

[68] D. Newton, J. Knapp, and A. A. Watson, *The Optimum Distance at which to Determine the Size of a Giant Air Shower*, Astropart. Phys., 26 (2007), pp. 414–419.

[69] T. Schmidt, I. Maris, and M. Roth, *Fine Tuning of the LDF parameterisation and the Influence on S1000.* Auger internal note GAP-2007-106, 2007.

[70] M. Ave *et al.*, Pierre Auger Collaboration, *The accuracy of signal measurement of the water Cherenkov detectors of the Pierre Auger Observatory*, Nucl. Instr. & Meth. in Phys. Research A, 578 (2007), pp. 180 – 184.

[71] F. James, *Minuit Reference Manual*, CERN Program Library Office CERN-IT Division CH-1211 Geneva 23 Switzerland, 1998.

[72] W. Fulgione, *About raining PMTs.* Auger internal note GAP-2007-081, 2007.

[73] B. M. Baughman, J. J. Beatty, and E. Grashorn, *Temporal Variations of SD vs FD Energy Estimators.* Auger internal note GAP-2009-144, 2009.

[74] C. Bonifazi and P. L. Ghia, *Selection of data periods and calculation of the SD geometrical acceptance.* Auger internal note GAP-2006-101, 2006.

[75] C. Bonifazi, P. L. Ghia, and I. Lhenry-Yvon, *On the unstable period of data-taking in 2009.* Auger internal note GAP-2010-002, 2010.

[76] C. Covault, *Status of Comms.* Talk at the Auger Collaboration Meeting, March 2010.

[77] P. Ghia, *Quality of the data.* Talk at the Auger Collaboration Meeting, March 2010.

[78] Exposure Calculator. http://ipnweb.in2p3.fr/~auger/AugerProtected/ExpoCalc.html.

[79] O. B. Bigas, *Accidental μ in selected stations.* Auger internal note GAP-2006-008, 2006.

[80] J. Blumer, D. Gora, M. Haag, and A. Tamburro, *On the influence of accidental muons on air shower detection.* Auger internal note GAP-2008-110, 2008.

[81] P. Lipari, *Lepton spectra in the earth's atmosphere*, Astropart. Phys., 1 (1993), pp. 195–227.

[82] J. A. Bellido, *Estimating the shower energy using the information of a single tank (recommended for brass hybrids).* Auger internal note GAP-2008-019, 2008.

[83] V. Blobel and E. Lohrmann, *Statistische und numerische Methoden der Datenanalyse*, Teubner Verlag, Wiesbaden, Germany, 1998.

[84] H. Dembinski, *Measurement of the Ultra High Energy Cosmic Ray Flux from Data of very inclined showers at the Pierre Auger Observatory*, PhD thesis, RWTH Aachen University, 2009.

[85] G. Ciaccio, R. Mussa, and A. Tonachini, *Study on exotic profiles and their selection criteria in auger data.* Talk at Auger Workshop on Exotic Physics, Lisbon 2009.

[86] ROOT - A data analysis framework. http://root.cern.ch.

[87] V. M. Olmos-Gilbaja *et al.*, *Effects of no-signal stations in inclined shower reconstruction.* Auger internal note: GAP-2009-152, 2009.

[88] I. C. Mariş, *Measurement of the Ultra High Energy Cosmic Ray Flux using Data of the Pierre Auger Observatory*, PhD thesis, Universität Karlsruhe, 2008.

[89] R. A. Johnson and D. Wichern, *Applied Multivariate Statistical Analysis*, Prentice-Hall Inc., 1982.

[90] A. Edwards, *Likelihood*, Cambridge University Press, Cambridge, 1984.

[91] A. C. Davison and D. Hinkley, *Bootstrap Methods and their Application*, Cambridge Series in Statistical and Probabilistic Mathematics, 8 ed., 2006.

[92] B. Moralez and L. Nellen, *Multiple Shower Fronts*. Talk at the Auger Collaboration Meeting, November 2008.

[93] E. Dos Santos, *Sensitivity to double shell events using the MPD*. Talk at the Auger Collaboration Meeting, March 2010.

Acknowledgements

At the end of this thesis it is time to thank all those who helped making this possible.

I would like to thank my supervisor Prof. Dr. Thomas Hebbeker for offering me this thesis and always asking those question that were the hardest to answer. The thanks need to be extended to Prof. Dr. Martin Erdmann who acts as co-corrector for this thesis.

The entire Auger group from Aachen earns my thanks. As there cannot be a fair order, I need to stick to the alphabetical listing of Stefan Fliescher, Christoph Genreith, Marius Grigat, Dr. Christine Meurer, Gero Müller, Nils Scharf, Peter Schiffer, Stephan Schulte, Oliver Seeger, Maurice Stephan, David Walz, Klaus Weidenhaupt and Tobias Winchen. The preparation of this thesis would have been less enjoyable without the unique atmosphere in the Aachen Auger group. I would like to thank everybody for contributing to this by discussing, arguing, scribbling on white-boards, helping, supporting or just drinking coffee and throwing in bad jokes.

Special thanks deserve however Stefan for the template from which this thesis was created, Marius for simulating the air showers used in this thesis and Christine, Nils, Peter, Maurice and Tobias for reading parts of the draft.

Even though he is no longer part of the Aachen group, Dr. Hans Dembinski highly influenced this work. I would like to thank him for having an idea for a topic that stirred my interest, introducing me to python and helping with all physics and software related issues.

Furthermore, I need to thank the developers of $\overline{\text{Off}}\underline{\text{line}}$ and the EventBrowser for promptly answering to all my questions and remarks about the reconstruction and providing such a beautiful tool to view the events and data.

I would like to thank the *Exotics Task Force* for enlightening me about all those exotic particles and the fun of hunting them, especially David Schuster, who provided me with an overview about current literature concerning exotic physics in air showers.

Finally, I thank my parents for taking so much interest in "real" science and providing all the support that I could have asked for. Also a huge thank you to all my friends and family for the love and support and who took my mind of physics whenever it was urgent and necessary.

Lastly, I would like to express my gratitude to my university. In a spirit of open discussions and respect for valid critique this university provided me with a lot more than just education.

Erklärung

Hiermit versichere ich, dass ich diese Arbeit einschließlich beigefügter Zeichnungen, Darstellungen und Tabellen selbstständig angefertigt und keine anderen als die angegebenen Hilfsmittel und Quellen verwendet habe. Alle Stellen, die dem Wortlaut oder dem Sinn nach anderen Werken entnommen sind, habe ich in jedem einzelnen Fall unter genauer Angabe der Quelle deutlich als Entlehnung kenntlich gemacht.

Aachen, den 8. April 2010

Anna Friederike Nelles